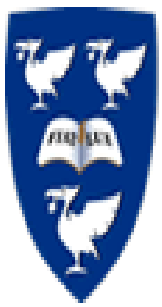

UNIVERSITY OF LIVERPOOL

Detection of Low Residual Current Flow through Gas during the Arcing Period

Thesis submitted in accordance with the requirements of the University of Liverpool for the degree of Master in Philosophy

By

Harry, Inye Hamilton

November 2013

Acknowledgements

Foremost, I would give thanks to God Almighty for sparing my life during my post-herpetic neuralgia as well as to the medical doctors, especially Dr Frank Bernard the neurologist at the Walton Neurologist Centre, Fazakerley, and Dr Chesney Rosemary, NHS Brownlow Group Practice in Liverpool for their continuous management of the ailment.

I would like to thank my supervisor, Prof Spencer J. W. for his advice and directives and Mr Jim Humphries for his technical support during the research. I am grateful to Dr Deakin Anthony and Dr Smith Duncan, both in room G03, for their valuable discussions.

Finally, I am sincerely grateful and indebted to my wife Stella, my daughter Nimiteinbo-ofri, my parents Rosaline and Hamilton, and my brothers and sisters for their patience, support and encouragement which helped me to complete this research.

Abstract

Within the switching technology and switchgear industry, the insulation properties of gases are extensively utilized as excellent methods of arc quenching. To optimize the efficiency and effectiveness of switchgear performance in interruption of the fault current through extinguishing the arc as well as to withstand the rate of rise of recovery voltage (rrrv) after current zero, the properties of these gases have been utilized. The present research is to develop a technique to identify the probe current flow during the weakened dielectric strength of the gases. Through the probe current flow during the weakened dielectric strength of the gases, the behaviour of the gases are described and compared since gases are most used in the circuit breaker for fault current extinction.

In particular, the properties of sulphur hexafluoride (SF_6) gas have been widely utilized due to its outstanding properties, but, given the connection of SF_6 with global warming, there is a drive to find alternatives (National Electrical Manufacturers Association). Although the exposed SF_6 gas is recycled back into the cylinder after exposure, there may be some leakages into the atmosphere. More so, the decomposed SF_6 gas into sulphur-fluoride and metal fluoride powdery substances when exposed to the environment after the gas might have been recycled may contribute to global warming at a later period. Hence, this research is focused to develop a technique used to determine the behavior of alternative gases which are potential candidates to replace SF_6. The work is an experimental assessment of gases and their reaction to the presence of an arc discharge and recovery from that exposure. The investigation of these gases is achieved by using a negative DC voltage-biased dielectric probe and monitoring small current flow

through this probe. The primary gases considered are dry air, nitrogen (N_2) and sulphur hexafluoride (SF_6) as a comparison.

The probe current flowing through these gases are investigated and identified respectively. The research identifies the variation in leakage current in compressed dry air in a changing electric field and pressure rise, typical examples of gas behaviour in an electric field. The search indicates that nitrogen gas is more susceptible to the fault current as compared to dry air, followed by sulphur hexafluoride SF_6 gas. These gases were examined from the probe current flow responses obtained from the negative DC voltage-biased dielectric probe when the fault current was passed in the gases' respective vicinity. Consequently, the research identified that a SF_6 dielectric medium has better insulation property regarding the fault current as compared to dry air and N_2 gas mediums under the same experimental conditions. The probe current flow in N_2 gas was experimentally determined and calculated, and the direction of current flow before and during the arcing period of the arc discharge was also identified. The direction of current depended on the circuit condition; in this case, the dielectric probe operates below its breakdown voltage in the gas, meaning the probe tips and the surrounding gas may have with positive ions, thus applying the positive half cycle of fault current will repel the positive ions while recombining with the negative ions and electrons. Moreover, the polarities of the probe voltages (input V1 and output V2) may also influence the direction of the probe current flow during the arcing period, since current flow is conventionally from negative to positive. The probe current flowing during the arc was identified as more when compared to no arc discharge. The gap resistance for nitrogen gas at various increases in pressure before and during the arcing era were

also calculated. The result demonstrates that the gap resistance of nitrogen gas is greater when no arc was present, though both show some forms of variation over time.

Table of Contents

Chapter 1 Introduction

Short line fault and short circuit fault current flow are most prevalent characteristics in electrical power transmission and distribution systems. Short line fault, a fault on an overhead line a short distance from the breaker [1], constitutes the most onerous transient recovery voltage while the short circuit fault close to the circuit breaker consists of the re-strike voltage of a high-frequency oscillation determined by the inductance, capacitance and resistance of the system [2, 3]. These fault currents impose the most serious general hazard to the electrical power network components and are the prime concerns in developing and applying protection systems. The circuit breaker or switchgear withstands the transient voltage for short periods after the electrical power has been interrupted [4],[5]. The optimisation of the circuit breaker is to effectively interrupt the fault current through extinguishing the arc and to withstand the rate of rise of recovery voltage (rrrv) after current zero. In this, SF_6 has been in use since 1960 as an alternative method to oil and air insulation. It is also been used as an arc-quenching arc medium in high-voltage switchgear. This has been due to the favourable electro-technical, chemical and physical properties characterised by SF_6, [6], but since SF_6 has been shown to contribute to global warming, there is an environmental drive to find an alternative for the purpose of interrupting fault currents and dealing with the rate of rise of recovering voltage (rrrv) [7]. During the interruption process, the arc discharge forms a conducting path between the electrodes which must become a non-conducting path after current interruption in a short period of time (μs). This recovery period can be split into two periods: thermal recovery and dielectric recovery. The thermal recovery phase, which depends on the energy loss from the previously conducting arc channel, can last for a few μs, and this is followed by the dielectric recovery period. The dielectric recovery period can last 10's of μs and is characterised by the cooling of gas and by a

recombination process as it cools. The end of the dielectric recovery period is characterised by achieving maximum dielectric withstand.

The present research is focused on the behaviour of alternative gases which are potential candidates to replace SF_6. The work is an experimental assessment of gases and their reactions to the presence of an arc discharge and the recovery from that exposure. This investigation uses a negative voltage DC-biased dielectric probe monitoring small current flow in the probe. The primary gases considered are dry air, nitrogen and sulphur hexafluoride.

1.1 Aims and Objectives

The research aim is to investigate the behaviour of gases when a positive half-cycle of fault current is passed through a circuit breaker producing an arc discharge. This is interrupted by the breaker. The negatively biased DC voltage dielectric probe is positioned near the arc and interrogates the dielectric property of the gas. The behaviour of the gases is described from the dielectric probe response by the small current flow detected when dielectrically weakened gas is between the electrodes of the dielectric probe.

To achieve the primary objectives of the research, the following investigations were carried out and reported in this thesis:

- Optimise the operational performance of the dielectric probe by varying the limiting resistor to obtain the leakage current in the milliampere range and to confirm its operation.
- Design and build a dielectric probe circuit capable of detecting small currents flowing through dielectrically weakened gas.

- Analyse the output from the probe and relate it to the condition of the gas.
- Develop a simple model to explain the events detected by the dielectric probe.
- Compare other gases with SF_6.

The objectives of the project are discussed within six chapters, beginning with an introduction in chapter 1. Each subsequent chapter is outlined below.

Chapter 2 presents the literature review and theoretical background on small current measurement techniques, advantages, disadvantages and applications. In addition, descriptions of dielectric probe module at zero input response, electrical insulation mediums, ionization and decay processes in gas, as well as electrical discharges measurements, peak current and current zero measurement are also outlined.

Chapter 3 describes the equipment and apparatus used for the research. These include dielectric probing circuit, arcing current circuit, voltage probes, test circuit breaker components and experimental earth.

Chapter 4 presents the experimental setup and preliminary tests carried out, including descriptions of pressure gauge calibration, preliminary check of oscilloscope, and high voltage probe verification. Operations of dielectric probing circuit and setup for weakened dielectrically gas detection technique in nitrogen gas, dry air and sulphur hexafluoride gases are presented.

Chapter 5 presents the experimental results, while the analysis and discussions of the results from the research are reported in **chapter 6**.

Chapter 7 provides the conclusion drawn from chapters 4, 5 and 6, alongside recommendations for future research in this area.

Chapter 2 Theoretical Background

2.1 Introduction

This chapter presents a review of the techniques for small alternating current (AC) measurement as well as an overview of how low current is acquired, comprising the principles/methods, advantages, disadvantages and some of their applications. The techniques considered include current transformer, optical current sensor, optical current transformer, Rogowski coil, Hall Effect and shunt resistor current. The chapter also discusses components of current which include electrical insulation mediums, ionization and decay processes, type of arc and electric arc, post-arc current, and electric discharge measurement, peak current and current zero measurement.

2.2 Types of Current Measurement Techniques

2.2.1 Current Transformer (CT)

CT, together with voltage transformer (VT) (or potential transformer [PT]), is known as an instrument transformer**.** CT is one of the most basic measuring elements in electric power systems. When the current in a circuit is too high to be applied directly to measurement instruments, a current transformer reduces the current accurately proportional to the current in the circuit to be measured. This can then be connected conveniently to measurement and recording instruments. A current transformer also isolates the measuring instruments from what may be very high current in the monitoring circuits.

2.2.1.1 Background Current Transformer

Power quality assessment relies on the accurate measurement of current and voltage. Current transformers exhibit good frequency response under distorted conditions, although this is only valid for a low impedance load on the secondary of the current transformer. Moreover, measuring accuracy of electromagnetic CT is high in steady state [8], so, after long-term applied research, the accuracy of measuring steady-state current is able to reach several ten thousandths. The primary objective of current transformer design is to ensure that the primary and secondary circuits are efficiently coupled, so that the secondary current bears an accurate relationship to the primary current. The primary winding is connected in series with the source current to be measured, and the secondary winding is normally connected to a meter, relay, or a burden resistor to develop a low-level voltage that is amplified for control purposes.

2.2.1.2 Theory of Current Transformer

Current transformers operate on the same principles as other transformers with magnetic cores. A transformer consists of a primary and one or more secondary windings around a closed magnetic path formed by the magnetic core. Current in the primary winding sets up a change of flux in the core. Ignoring losses, the secondary winding sets up a change of flux, equal in magnitude but reversed in direction to oppose this change in flux. This simplified and ideal description can be refined to account for secondary effects due the materials and construction methods used [8, 9]. The voltages are proportional to the numbers of turns in the coils: the coils with more turns have the higher voltage [10]. High permeability and low core loss materials in toroidal shapes are recommended to reduce errors due to leakage flux and high magnetizing currents. Materials selected for a current transformer depend on the operating frequency, accuracy and cost [11].

High permeability materials in toroidal shapes afford close core coupling and link both windings to minimize leakage flux. Such coupling is increased if the primary winding has several turns; however, satisfactory results can be obtained with only a single turn. For best results, the secondary winding should be evenly spaced completely around the core. The exciting current determines the maximum accuracy that can be achieved with a current transformer.

2.2.1.3 Advantages of Current Transformers

The main purpose of the current transformer is to produce, from the primary current, a proportional secondary current which can be measured easily or used to control various circuits. Current transformers can be used in a synthetic circuit to measure the fault current, facilitating the safe measurement of large currents, often in the presence of high voltages. The primary winding is connected in series with the source current to be measured, while the secondary winding is normally connected to a meter, relay, or a burden resistor to develop a low level voltage that is amplified for control purposes [9]. Commonly, cores with high effective permeability are used in current transformers in order to minimize magnetizing current and reduce errors [11].

2.2.1.4 Disadvantages of Current Transformers

In short circuit fault occasions, serious magnetic saturation occurs, resulting to secondary current output waveform distortion; hence, the CT is not able to reflect the transition process accurately, which may bring about protection mistake actions through not allowing the measurement of DC signals. Isolation between primary and secondary sides is implicitly given with limited frequency range problem. The main error in a current transformer is magnetizing current that causes ratio

and phase displacement errors. [12]. Though metering accuracy has been attainable using conventional CTs, there has always been a concern about the low-end meter accuracy. Considering the discussed issues above, the application of CT may not be realistic as a primary sensor for this research.

2.2.1.5 Applications of Current Transformers

Current transformers do not allow the measurement of DC signals, so they cannot be suitable for dielectric discharge detection; however they can be used in the measurements of inductive currents and voltage waveforms with secondary load impedance. Isolation between primary and secondary sides is implicitly given with limited frequency range problem. The main error in a measurement type current transformer (CT) is magnetizing current that causes ratio and phase displacement errors[11]. Current transformer is best performed in steady state AC current measurement.

2.2.2 Optical Current Sensor

Optical current sensors (OCS), also known as magneto-optic current transducers (MOCTs), are increasingly accepted in measuring of high voltage due to their superior accuracy, bandwidth, dynamic range and inherent isolation. Once deemed specialized devices intended for novel applications, optical sensors have risen to a performance level exceeding conventional magnetic devices. With this new technology (i.e., magneto-optical current transducers based on the Faraday Effect), there is enthusiasm about how the development will revolutionize older technology [13].

2.2.2.1 Background of Optical Current Sensor

The Magneto-optic or Faraday Effect was first reported by Michael Faraday in 1845. Serious research into implementing the Faraday Effect into highly accurate current measuring applications began in the late 1970s. These efforts resulted in a number of successful field trials using optical current sensor-based metering systems that date back to 1986. The installations utilized porcelain columns with data-acquisition capabilities. However, as reported by Maffetone [14], such earlier data-acquisition systems did not lend themselves to the analysis of waveform quality and performance as required for the present installation. Since Faraday's early discovery, this phenomenon has been observed in many solids, liquids, and gases.

2.2.2.2 Theory of Optical Current Sensor

Optical-based current measurement devices, known as magneto-optic current transducer, are based on the Faraday Effect, which states that, when polarised light passed through a glass material (Faraday material) that is parallel to a strong magnetic field, the plane of the light rotates. Figure 2.1 illustrates the polarized light. The amount of rotation α for the given material is proportional to the strength of the applied magnetic field and the distance travelled by the light through the medium. The rotation α is mathematically expressed as:

$$\alpha = \mu_o V n I \qquad 1$$

where I is the current in amperes, n is the number of loops around the conductor, μ_o is the constant of permeability which is equals unity in air, and V is the Verdet constant (0.31×10^{-5} rad/amp-turn), which is defined as the rotation per unit path per unit field strength and α is the angle of rotation in radian [15].

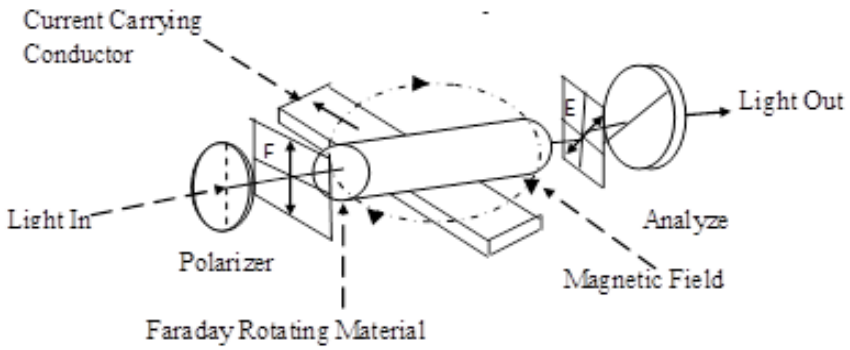

Figure 2.1. The rotation of the plane of polarization of the light path, Gondge [16].

To examine this principle closer, the following definitions are offered. The rotation θ of the plane of polarization of the light path with respect to the length L of that path is proportional to the magnetic field intensity H and can be expressed as:

$$\frac{\Delta\theta}{\Delta L} \approx \vec{H} \qquad 2$$

Therefore,

$$\frac{\Delta\theta}{\Delta L} = \mu_o V \overrightarrow{nH} \qquad 3$$

From Ampere's law

$$\oint \vec{H} dL = I \qquad 4$$

It follows that,

$$\theta = \mu_o V n I \qquad 5$$

Solving for single loop for bulk glass, then n = 1 and μ_o=1,
We have,

$$\theta = VI \qquad 6$$

Electronic signal processing circuitry is then utilized to precisely evaluate this low level 60 Hz intensity variation, and calculate a calibrated signal that is exactly in phase with respect to the primary current sine wave.

2.2.2.3 Advantages of Optical Current Sensors

The major benefit of an optical current sensor is immunity to geomagnetic effects and electromagnetic induction EMI. Magneto-optic current transducers (MOCTs) are utilised to improve performance and reliability and to solve problems in electrical power and transient recording. Each one of these areas has several difficulties that engineers have endured with conventional current transformers measurement. MOCTs will not saturate under heavy fault current and eliminate burden concerns, offering increased frequency response and an entirely optical power interface; hence, it affords total isolation which increases the safety for both personnel and equipment. It has metering accuracy and eliminates the low-end meter accuracy. MOCT has very high bandwidth and extremely wide dynamic range, freedom from saturation effects and DC operation. With temperature-compensating controls incorporated into the MOCT electronics, the long-term seasonal performance of the device will be attained.

2.2.2.4 Disadvantages of Optical Current Sensors

The problem with this approach is the relative movement between the core and the glass. The conductor encircled by a number of glass blocks, forming a closed path; this method renders the sensor insensitive to interfering magnetic fields [17]. This method has complex optical sensor assembly resulting in inadequate sensitivity. Although the glass block sensor offers some significant advantages compared with the coiled fibre sensor, the additional problems included in most designs include the sensors being sensitive to interfering magnetic fields, as closed optical paths are not normally formed round the conductors. Secondly, in common with the coiled fibre type, these sensors are sensitive to fibre down lead vibration. Pilling [18] noted that mechanical perturbations of the optical fibres connecting the sensor to the optoelectronic processing system

result in optical intensity changes, which are manifest as noise. Moreover, as Faraday rotation depends on the Verdet coefficient of the optical sensing material, materials with high Verdet coefficients have temperature and stress dependent birefringence properties, since the Verdet constant of dielectric material varies with temperature and wavelength of the optical source. In addition, the measurement may be affected by environmental perturbations such as temperature fluctuations and wavelength noise of the light source [19, 20].

2.2.2.5 Applications of Optical Current Sensors

The Optical Current Sensor (OCS) Method cannot be applied in this research due to its complexity which includes relative movement between the core and the glass, mechanical perturbations of the optical fibres; nonetheless, this method has many applications in the power distribution industry, as both absolute and differential AC and DC measurements up to very high currents are possible.

2.2.3 Optical Current Transformers

Optical current transformers (OCT) are gaining credibility in power engineering given their advantages of high resistance to electro-magnetic interference, magnetic-saturation-free and hysteresis-free performance and lack of need for extra power supply in the primary side. Furthermore, as one type of electric current transformers (ECT), OCT can interface with digital relay protection devices easily and meet the real-time demands of current automation [21, 22].

2.2.3.1 Background of Optical Current Transformers

As the name implies, the optical current transformer (OCT) is a combination of optical sensor and current transformers made of optical fibre; hence, it utilizes the Faraday Effect in current

measurement [23]. In electrical industries, OCT is commonly employed for high accuracy in the steady state applications.

2.2.3.2 Theory of Optical Current Transformers

On the high voltage side, a high current signal is changed to a small electric signal, converted to data electric signal by electronic circuit, and then changed to a data optical signal. The signal is transmitted to the low voltage side by optical fibre and is demodulated to a weak electric signal which is proportional with heavy current at high voltage side. The amplitude value and phase information of heavy current are thus obtained [24, 25]. OCT is also utilized to measure the primary current.

2.2.3.3 Advantages of Optical Current Transformers

The OCT is used in protection and metering systems with currents flowing in high voltage conductors. It utilizes the Faraday Effect to measure primary current, exhibits excellent electrical isolation and comes in small sizes. OCT has high resistance to electro-magnetic interference. It is magnetic-saturation-free and hysteresis-free and has no need for extra power supply in primary side as in CT. It can interface with digital protection device easily and meet the real-time demands of current measurement. The optical electric current transformer is light in weight and costs little. Based on virtual instrument and digital signal processing technology, error measuring system is designed by using Lab View software and DAQ-2006 data acquisition card to obtain real-time current. Also, in terms of virtual instruments, an optical electric current transformer error measuring system could be designed easily. OCT is, in principle, a suitable replacement for a conventional device for power system protection purposes without loss of system quality or reliability. It adopts high precision iron core coil and has outstanding insulation.

2.2.3.4 Disadvantages of Optical Current Transformers

The OCT is subject to the problem of linear birefringence (i.e., double refraction—the decomposition of a ray of light into two rays when it passes through certain anisotropic materials such as crystals of calcite or boron nitride) due to stress of bending fibres and change of temperature. These problems are solved by using double-coated twisted fibres.

2.2.3.5 Applications of Optical Current Transformers

Due to OCT complexity and linear birefringence resulting from temperatures, this method of current measurement cannot be applied in this work. OCT is best used for the high-voltage, high-current signal measurement as compared to currents in milliampere. OCT is used to measure exact amplitude value and phase information of analogue signals of power systems. It is able to measure phase errors and ratio errors of optical electric current transformers. In most applications, OCT is employed for its high accuracy in steady state while a Rogowski coil is employed for high accuracy in transient state applications [15, 21].

2.2.4 Rogowski Coil

Rogowski coils perform passive current measurements and are used in testing, measurement devices and power-monitoring activities, although calibration is required to account for manufacturing variations in the coil and to provide uniform device-to-device sensitivity. Traditionally, coils are compensated with an amplifier, making both the coil and the amplifier a matched pair. Rejustors provide a passive compensation solution for Rogowski coils, enabling

coil manufacturers to produce devices with uniform performance increasing interchange ability while reducing manufacturing complexity [26, 27].

2.2.4.1 Background of the Rogowski Coil

A Rogowski coil, named after Walter Rogowski, is an electrical device for measuring alternating current (AC) or high-speed current pulses. The device use a helical coil sensor which is uniformly wound onto a relatively long non-magnetic circular or rectangular strip, usually flexible (figure 2.2) [28]. The helical coil of wire has the lead from one end returning through the centre of the coil to the other end, so that both terminals are at the same end of the coil. The whole assembly is then wrapped around the straight conductor whose current is to be measured. The first description was given by Rogowski and Steinhaus in 1912 [29]. Sometimes this coil arrangement is called a Chattock coil (or Rogowski–Chattock potentiometer). Indeed, the operating principle of such a coil sensor was first described by Chattock in 1887 (it is not clear if Rogowski knew of the disclosure by Chattock, because in Rogowski's article Chattock was not cited)[30]. However, Chattock used it to measure magnetic fields rather than currents [31, 32].

2.2.4.2 Theory of the Rogowski Coil

The principle of operation of this sensor is based on Ampere's law rather than Faraday's law. If the coil of length l is inserted into a magnetic field, then the output voltage v is the sum of voltages induced in each turn (all turns are connected in series). The output signal of the Rogowski coil depends on the number of turns per unit length N/l and the cross section area A of the coil (see figure 2.3) [33]. Since the voltage that is induced in the coil is proportional to the rate of change of current i in the straight conductor, the output of the Rogowski coil is usually

connected to an electronic integrator circuit in order to provide an output signal that is proportional to the current.

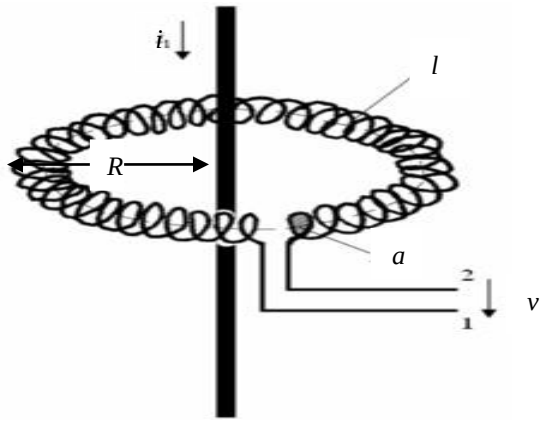

Figure 2.3 shows a Rogowski coil wrapped around a current-carrying conductor [34].

The voltage drop across the Rogowski coil is expressed as

$$v = \frac{-AN\mu_o}{l}\frac{di}{dt}$$

$$= M\frac{di}{dt} \qquad 7$$

where μ_o= 4π x 10^{-7} is the magnetic constant, A = πR^2 is the cross sectional area of the toroidal, N is the number of turns, $l = 2\pi R$ is the length of the winding, $\frac{di}{dt}$ the rate of change of the current threading the loop, M is mutual inductance of a Rogowski coil. This formula assumes the turns are evenly spaced and that these turns are small relative to the radius of the coil itself. At high frequencies, the impedance of a Rogowski coil's inductance will increase and so decrease the output. The inductance L of a toroidal coil is expressed as:

$$L = \mu_o N^2\left(R - \sqrt{(R^2 - a^2)}\right) \qquad 8$$

where R is the major radius of the toroidal, and *a* is its minor radius.

Several methods in measuring the low amplitude current by a Rogowski coil are discussed in 'Studies of Rogowski coil current transducer for low amplitude current (100A) measurement', in which the mutual inductance M of a Rogowski coil need to be improved on [35].

2.2.4.3 Advantages of Rogowski Coils

A Rogowski coil may have many features which give it advantages over other methods of current measurement (including current transformers) in this application. These advantages include flexibility in usage, for a Rogowski coil is made open-ended, allowing it to be wrapped around a live conductor without disturbing current from the capacitor bank and during breakdown voltage. Secondly, unlike conventional transformers that have an iron core, the transformer in a Rogowski coil uses an air core which provides low impedance so there is no danger of saturating the core (as can occur in iron core transformers). A Rogowski coil does not suffer from magnetic saturation under transient condition, and, therefore, it has high measuring accuracy in a transient state. It is linear, meaning that the same transducer can be used to measure a wide range of currents. For example, a breakdown voltage test and protection functions could be combined. This feature is also very useful in installations where there is some uncertainty as to the level of current which will flow, as the sensitivity of the measuring system can be adjusted after the measuring coil has been installed without the need to change the coil. Rogowski coil transducers are highly suitable for protection applications because they do not saturate in the early stages of transiency even when asymmetric components (DC offsets) are present. It has wide bandwidth, ranging from less than 1 Hz to several hundred kHz depending on the coil type. It is useful for harmonic analysis for it does not create harmonics. The systems can be made with an uncertainty better than 0.1%., and this accuracy can be maintained even

with a split coil. A Rogowski coil is compacted, lightweight and can be fitted in confined space. It is light enough to be suspended on cabling if necessary. A Rogowski coil is typically made from an air core coil, so, in theory, there is no hysteresis, saturation, or non-linearity.

2.2.4.4 Disadvantages of Rogowski Coils

One disadvantage of the coil is that the Rogowski coil produces output voltage proportional to d*i*/dt. Therefore, by connecting or disconnecting moments, the emf goes "infinite". Transient voltage suppressors (TVS) or other protections have to be considered to prevent overloading the downstream electronics. Voltage drop is only generated when there are changes in the magnetic field; therefore, a Rogowski coil cannot be used to measure the DC component in the current as in an RC circuit of dielectric probe. A Rogowski coil relies on measuring magnetic field, thus making this type of current sensor susceptible to external magnetic field interference compared to shunt resistor sensors and current transformer core coil [36].

2.2.4.5 Applications of Rogowski Coils

Considering the measurement technique and the features of the coil, a Rogowski coil cannot be applied to measure the output current from Brandenburg high voltage DC power supply since the principle is based on a time-varying magnetic field. However, the technique could be used to measure the arc current from the synthetic AC power supply system that has a time-varying component (e.g., a magnetic field). With the f coil flexibility, it is possible to make a direct measurement of the current flowing down the capacitor bank circuit and hence obtain a reliable measurement. Since the coils are linear, the same equipment can cope with any current level. In terms of protection, Rogowski coils are useful because of their good transient performance and

high-current capability. As the coils are compact, they are easier to fit on existing installations without the need for expensive modifications. Finally, Rogowski coil current transducers offer a useful contribution to the art of measuring electric currents under difficult or unusual circumstances, as well as for more normal situations. Dickinson [37] observed that a wider understanding of what the coil is and what it can do is obviously essential if its full potential is to be exploited.

2.2.5 Hall Effect Current Sensor

In power systems, safety and reliability are the most important considerations. To meet safety and reliability requirements, appropriate current monitoring devices are sought for measuring currents for metering and fault protection. The Hall effect, entirely integrated on a single silicon chip, is becoming popularly in use. This has resulted a in low-cost, high-volume application of the Hall effect as obtained in Kun-Long[38] and Honeywell[39].

2.2.5.1 Background of the Hall Effect Current Sensor

In his paper, Kun-Long [38] wrote that the Hall effect was discovered by Dr Edwin Hall in 1879 while he was a doctoral candidate at Johns Hopkins University in Baltimore. Hall was attempting to verify the theory of electron flow proposed by Kelvin some 30 years earlier. Dr Hall found that, when a magnet was placed so that its field was perpendicular to one face of a thin rectangle of gold through which current was flowing, a difference in potential appeared at the opposite edges. Moreover, he found that this voltage was proportional to the current flowing through the conductor and the flux density or magnetic induction perpendicular to the conductor. Although Hall's experiments were successful and well received at the time, no applications outside of the

realm of theoretical physics were found for over 70 years. With the advent of semiconducting materials in the 1950s, the Hall effect found its first applications, although severely limited by costs. In 1965, Everett Vorthmann and Joe Maupin, MICRO SWITCH Sensing and Control senior development engineers, teamed up to find a practical, low-cost solid state sensor. Many different concepts were examined, but they choose the Hall effect for the basic reason that it could be entirely integrated on a single silicon chip. This breakthrough resulted in the first low-cost, high-volume application of the Hall effect in solid state current monitoring devices and other applications [39].

2.2.5.2 Theory of the Hall Effect Current Sensor

When a current-carrying conductor is placed into a magnetic field, a voltage will be generated perpendicular to both the current and the field. This principle is known as the Hall effect. Figures 2.4 and 2.5 illustrate the basic principle of the Hall effect. It shows a thin sheet of semiconducting material (Hall element) through which a current is passed.

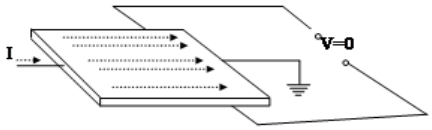

Figure 2.4 shows Hall Effect principle with no magnetic field

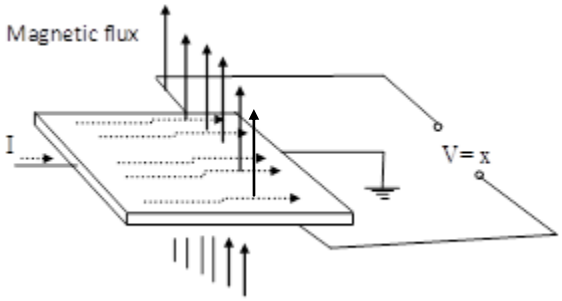

Figure 2.5 shows Hall Effect principle under a magnetic field influence

The output connections are perpendicular to the direction of current. When no magnetic field is present as shown in figure 2.4, current distribution is uniform and no potential difference is seen across the output. When a perpendicular magnetic field is present, as shown in figure 2.5, a Lorentz force is exerted on the current. This force disturbs the current distribution, resulting in a potential difference (voltage) across the output. This voltage is called the Hall voltage (V_H). The interaction of the magnetic field (B) and the current (I) is shown in equation form as equation 9.

$$V_H \propto I \times B \qquad 9$$

Hall effect sensors can be applied in many types of sensing devices. If the quantity to be sensed is incorporated with a magnetic field, a Hall sensor will perform the task.

2.2.5.3 Advantages of a Hall Effect Current Sensor

A Hall effect sensor can totally be isolated from another high-voltage electrical system which eliminates many safety concerns. The resolution can be improved by looping the wire through the current clamp as many times as to double, triple, or quadruple the sensitivity or resolution of the sensor. The Hall effect current sensor does not get hot when in use and has inherent voltage isolation from the current path, as reported in Kun-Long[38]. It can be integrated into the Hall element and interface electronics on single silicon chip [40]. The use of a Hall Effect device increases the accuracy of current in both 'high current path and a low current path' measurements and provides more signal than the shunt solution over current measurement range. Hall Effect devices are readily apparent with the low insertion loss. The device improves current measurement accuracy over a wider current range, reducing power consumption by significantly reducing the 1^2R loss. The obvious benefit for a small form-factor Hall effect solution is that the volume required is a fraction of the equivalent CT solution, and, in addition, there is an

elimination of gain and additional protection components. It has a nice advantage over safeguards in protecting data acquisitions [41].

2.2.5.4 Disadvantages of a Hall Effect Current Sensor

The drawback of this technology is that the output from a Hall Effect sensor has a large temperature drift, and it usually requires a stable external current source. Hall effect sensors are somewhat less common compared to the CT [36]. The device output voltage is very small, requiring high amplification. The sensitivity is temperature dependent and requires adequate compensation. There is an inevitable offset, i.e., a small DC voltage at zero current; the offset amplitude and temperature coefficient are subject to significant fluctuations. Also noted is sensitivity to short current peaks in the circuit: according to the hysteresis properties of the core material, these peaks can cause a static magnetization in the core that results in a permanent reminisce, and finally in an offset alteration of the Hall element

2.2.5.5 Applications of a Hall Effect Current Sensor

In terms of this research, the Hall Effect method might not suitable since it requires an external power source as compared to the shunt resistor method in use. The current detected will require amplification before it can be used. Although a Hall Effect magnetic detector has inherent voltage isolation from the current, the device sensitivity is temperature dependant which needs to be compensated before the current can be used. The use of a Hall effect device increases the accuracy of current in both ‘high current path and a low current path’ measurements and provides more signal than the shunt solution over the measurement range, yet the Hall effect

device has an inherent small DC voltage at zero current; this offsets amplitude and temperature coefficient which are subject to significant fluctuations.

2.2.6 Shunt Resistor Current Sensor

Shunt current measurement techniques are in wider use since they were the first possible method for current detection, monitoring and measurement. Measuring current requires careful consideration when setting up measurement system. It should be understood that two factors needed to be consider in ensuring accurate measurement, i.e., the device measurement method and impact of measurement on the circuit [42].

2.2.6.1 Background of the Shunt Resistor Current Sensor

With its importance in electric power control and stability, many studies and implementations have been carried out to improve techniques of shunt resistor current measurement methods [43]. This method was applied and used in post-arc detection and measurements by Michel [5].

2.2.6.2 Theory of the Shunt Resistor Current Sensor

The shunt resistor current measurement method adopts the Ohms law principle of current measurement. A known resistance of shunt is placed in series with the load so that all of the current to be measured will flow through it. The voltage drop across the shunt is proportional to the current flowing through it, since its resistance is known. A milli-voltmeter connected across the shunt can be scaled to directly display the current value (see figure 2.6) [34].

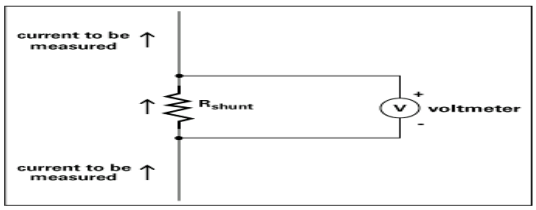

Figure 2.6 shows a Voltmeter measuring a voltage drop across a resistor.

In the shunt method, a low value of R_{shunt} is chosen to minimize the power dissipation of the shunt. If the shunt resistor of the device is too large as opposed to the resistance of the circuit under test, the voltage burden will cause large errors [42, 44]. In order not to disrupt the circuit characteristics, the resistance of the shunt is normally very small. Shunts are rated by maximum current and voltage drop at that current. All shunts have a derating factor for continuous use, 66% being the most common. Current shunt measurement techniques have two methods of measurements: low-side current sensing and high-side current sensing. The low-side refers to the return path from the load and the low-side is usually at a low voltage to ground (see figure 2.6). Similarly, the high-side refers to the supply path to the load, and the high-side is usually at a high voltage to ground (see figure 2.7). The decision to place a current shunt in either position has advantages and disadvantages.

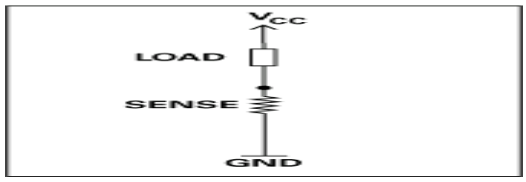

Figure 2.6 shows low-side current sensing, sense resistor between load and ground.

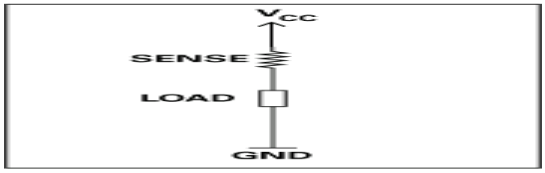

Figure 2.7 shows high-side current, sense resistor between supply and load current shunt monitor

2.2.6.3 Advantages

Current shunts are considered more accurate and cheaper due to current shunt low-side advantages, including shunt resistor current measurement low input common mode voltage, ground referenced output voltage, easy single-supply design, straight forward design which rarely requires more than an operational amplify to implement, inexpensive and precise. Other are high-side advantages such as load is grounded, load not activated by accidental short at power connection, high-load current caused by short circuit can be detected, it is easy to use, provides a ground-referenced current- or voltage-source output that is proportional to the current of interest, provides high common-mode rejection without the difficulty of resistor matching, can sense high-side currents in the presence of common-mode voltages and can have a pair of differential inputs that can be connected to shunts which are at voltages well in excess of the voltage that the amplifier is powered from and power management.

2.2.6.4 Disadvantages

Some alternatives to shunts can provide isolation from the high voltage by not directly connecting the meter (Hall effect current sensors and current transformers) to the high voltage circuit [45]. Although the voltage drop is small, this can have a negative impact on the circuit under test and the measurement. This voltage is known as the voltage burden and is a series voltage errors introduced by the device. There are thermal limits where a shunt will no longer operate correctly. At 80 °C, thermal drift begins to occur; at 120 °C thermal drift is a significant problem, depending on the design of the shunt; and, at 140 °C, the resistor (usually manganin alloy) used becomes permanently damaged due to annealing resulting in the resistance value drifting up or down. National Instruments [42] suggested that, if the current being measured is at

a high voltage, this voltage will be present in the connecting leads to and in the reading from instrument itself. Sometimes, the shunt is inserted in the return leg (i.e., grounded side) to avoid this problem. Low-side disadvantages are enumerated as follows: The load is lifted from direct ground connection and can be activated by accidental short at ground end load switch; high-load current caused by a short is not detected, adds undesirable resistance in the ground path and may require an additional wire to the load that could otherwise be omitted. High-side disadvantages are also listed as the high-input common mode voltage is often very high, and the output needs to be level-shifted down to system operating voltage levels. It requires very careful resistor matching in order to obtain an acceptable common-mode rejection ratio (CMMR). The high-side needs to withstand very high common-mode voltages, often outside the limits of the supply rails of the amplifier [44].

2.2.6.5 Applications

Shunt resistor current device and low-side current sensing are used in this research for over current-protection and controlling circuits, could measure as much as 4-20mA system current, used for programmable current sources. Linear and switch-mode power supplies, used in proportional solenoid control, create linear systems. A current shunt is considered accurate and cheaper when within the thermal limit despite the voltage burden and series voltage error introduced by the device which error is not significant

2.3 Spark Plug Sensor (Dielectric Probe)

2.3.1 Dielectric Probe Capability

The behaviour and characteristic of electrical insulation gas could be studied and obtained with a dielectric probe. This is achieved when the probe is electrically biased in the vicinity of ionised gas. During passing of a pulse current or arcing current in the circuit breaker filled with test gas, an arc produced. This will heat up the gas and its surroundings causing the atoms/molecule of the gas to dissociate into ions (positive ions and negative ions) and electrons. These discharges are either attracted or repelled to the biased dielectric probe connected to resistance and capacitor (RC) circuit. The dielectric-withstand capability of the contact gas is determined by the thermal characteristic of the gas. And, to a large extent, the dielectric probe response is influenced by the interrupter, the arcing and interrupted current, and the thermal behaviour of the arc voltage in the gas. If the gas in the arcing area is very hot following current zero due to the arc's stored thermal energy, and the arc energy exceeds removal of the energy by the interrupter gas , the dielectric-withstand capability of the gas will be quite low resulting in increase conductivity in the gas. The rising transient recovery voltage following current zero may cause reigniting of the arc and may result in fault current to flow again. The dielectric probe detects this residual discharge during these periods.

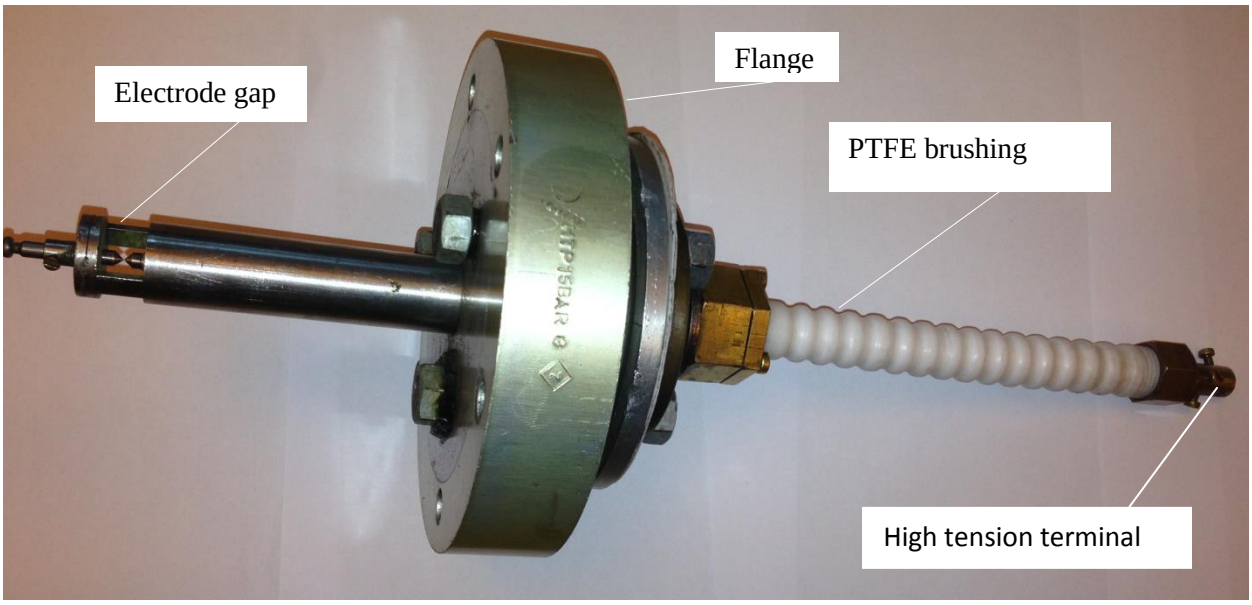

Figure 3.4a shows dielectric probe.

The dielectric probe has the capability to detect and measure low residual current before, during and post current zero periods of the arcing current in gas. Researchers have investigated the behaviour of gas in circuit breakers following current interruption using dielectric probes to examine the intrinsic properties of gas temperature and mass density [46] [47]. In this research, a negative DC voltage applied dielectric probe will be used to investigate and detect probe currents during an arcing fault current periods in some insulation gases including dry air, nitrogen and sulphur hexafluoride. The dielectric probe as shown in figure3.4a comprises two electrode tips made of 20% copper and 80% tungsten that will withstand repetitive discharge and minimum wear. The gap length will be adjusted to fit the research purposes for various insulation gases.

2.3.2 Spark Plug Sensor Module at Zero Input Response

Spark plug sensor (dielectric probe) module at zero input response tends to illustrate the fundamental operational process and parameters of a spark plug as a sensor. It shows the researcher how the spark plug works as a dielectric probe. Below is the theory of a dielectric probe at zero input response. Figure 2.8 shows circuit diagram of RC circuit at zero response: when an initial condition is present but no independent source, also known as ZERO INPUT CASE [48].

Considering figure 2.8, the diameter d of the spark plug tips surfaces were obtained using micrometre screw gauge as 8.5 x 10^{-4}meter and the gap distance D was obtained using the feeler gauge as 1 x10^{-3}meter, so the spark plug capacitance C_a between the two tips in Farad could be determined using the expression 10.

$$C_a = \frac{\varepsilon K_1 A}{D} \qquad 10$$

Where A is the area of either of the tip in square meter the spark plug sensor, $\boldsymbol{\varepsilon}$ is permittivity of free space equal's 8.85x10^{-12} F/m in air. K_1 is the dielectric constant of the space between the electrodes (it is the ratio of the permittivity of dielectric in use to the permittivity of free space, dimensionless). In this case K_1 = 1 in air [48].

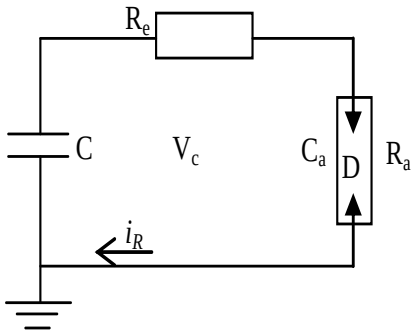

Figure 2.8 shows dielectric probe circuit

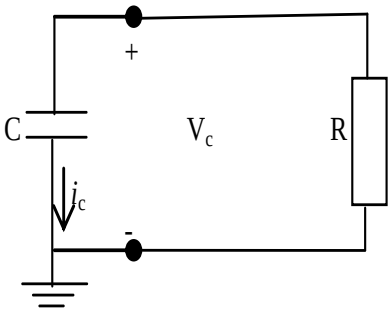

Figure 2.9 shows equivaler dielectric probe circuit

With this, the capacitance reactance R_a in ohms of the spark plug could be obtained with expression shown below.

$$R_a = \frac{1}{2\pi f Ca} \qquad 11$$

Where *f* is the frequency; the equivalent resistance R is obtained as shown in figure 2.9, since R_e and R_a are in series, then

$$R = R_e + R_a \qquad 12$$

Let the current i_R drained into the resistor R and capacitor C current i_c

And the voltage across the capacitor C be $v_c(o)$ for time $t = 0$

Let the voltage across the capacitor C be $v_c(t)$ for time $t \geq 0$

And current flowing through the capacitor and resistor be i_C and i_R respectively

Then from Kirchhoff current law KCL, total current in the RC circuit in figure 2.9 is expressed as:

$$i_R = -i_c, \qquad i_c + i_R = 0 \qquad 13$$

Defining currents in terms of voltages, we have

$$C\frac{dv_c}{dt} + \frac{v_c}{R} = 0 \qquad 14$$

Equation (14) above is a first order differential equation (ODE) and figure 2.9 is called a first order circuit since the variable v_c and its derivative are of first order. Equation (14) is a homogeneous equation since the right hand side equation is zero. The coefficient of v_c and its derivative are constant. Therefore, v_c *(t)* could be determined as the solution of equation (14) which satisfies the first-order differential equation with boundary condition $v_c(o)$.

Re-arranging equation (14), we have

$$\frac{1}{v_c}\frac{dv_c}{dt} + \frac{1}{RC} = 0 \qquad 15$$

Separating the variables in equation (15), we have

$$\frac{1}{v_c}\frac{dv_c}{dt} = -\frac{1}{RC} \qquad 16$$

Integrating equation (16) both sides with respect to time *t*

$$\int_o^{v_c(t)} \frac{dv_c}{v_c} = -\frac{1}{RC}\int_0^t dt$$

$$in\, v_c]_0^{v_c(t)} = -\frac{1}{RC}t + K$$

$$in\,[v_c(t) - 0] = -\frac{1}{RC}t + K \qquad 17$$

Taking the power of *e* of equation (17) results in:

$$v_c(t) = e^{-\frac{t}{RC} + K} = e^{-\frac{t}{RC}}.e^{K} \qquad 18$$

Where K is constant of integration, the power of *e* is dimension less and RC = τ is the time constant of the circuit and expressed in seconds, i.e.,

$$\tau = RC = \frac{v}{i} \cdot \frac{q}{v} = \frac{s}{q} \cdot q = s\ (second).$$

When *t =0, $v_c(t)$ becomes $v_c(0)$*

Hence, equation (18) becomes,

$$v_c(0) = e^{K} \qquad 19$$

Placing equation (9) into equation (18), we have:

$$v_c(t) = e^{-\frac{t}{RC} + K} = e^{-\frac{t}{RC}} . e^{K} = v_c(0)e^{-\frac{t}{RC}}, \quad \text{for, } t \geq 0 \qquad 20$$

Equation (20) is the solution of the differential equation of equation (16) subject to the initial condition that voltage across the capacitor at *t = 0* is $v_c(0)$

Current drained into the resistor R is obtained as

$$i_R(t) = \frac{v_c(t)}{R} = \frac{v_c(0)e^{-\frac{t}{RC}}}{R}, \qquad \text{for all } t \geq 0 \qquad 21$$

Capacitor current for, $t \geq 0$

$$i_c = C\frac{dv_c(t)}{dt} = C\frac{dv_c(0)e^{-\frac{t}{RC}}}{dt} = Cv_c(0)\left(-\frac{1}{RC}\right)e^{-\frac{t}{RC}}$$

$$= -\frac{1}{R}v_c(0)e^{-\frac{t}{RC}}, \qquad \text{for, } t \geq 0 \qquad 22$$

Sketching the function $v_c(t)$ versus *t* for t ≥ 0 is shown in figure 2.10, using table 2.1:

$v_c(t) = v_c(0)e^{-\frac{t}{RC}}$	1	0.367879	0.135335	0.049787	0.018316	0.006738
t	0	RC	2RC	3RC	4RC	5RC

Table 2.1 shows $v_c(t)$ for time $t \geq 0$ and *t*

The result shows that

Initially the capacitor discharges to $v_c(0)$ at *t = 0.*

The capacitor start discharging through resistor R exponentially when *t > 0*

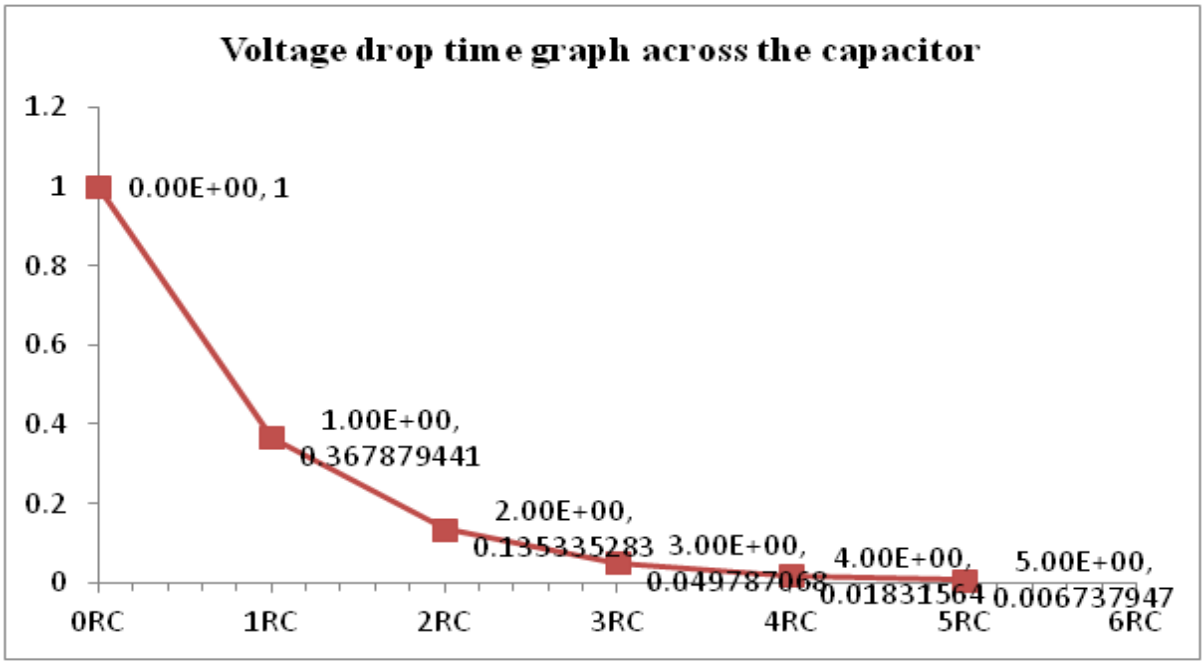

Figure 2.10 shows decay voltage across the capacitor

The energy store in the capacitor is

$$w_c(0) = \frac{1}{2} C v_c^2(0) \text{ , when } \quad t = 0 \qquad 23$$

And

$$w_c(t) = \frac{1}{2} C v_c^2(t) \text{ , when } \quad t \geq 0 \qquad 24$$

The voltage goes to zero as time goes to infinity. Also, the energy stored in the capacitor goes to zero as time goes to infinity [49, 50].

The power absorbed by the resistor R is

$$P_R(t) = R i_R^2(t) = R \left(\frac{v_c(0) e^{-\frac{t}{RC}}}{R} \right)^2 = \frac{1}{R} v_c^2(0) e^{-\frac{2t}{RC}}$$

The total energy absorbed by the resistor is,

$$w_R = \int_0^\infty P_R(t) dt = \int_0^\infty \frac{1}{R} v_c^2(0) e^{-\frac{2t}{RC}} dt = -\frac{RC}{2} \frac{1}{R} v_c^2(0) e^{-\frac{2t}{RC}} \Big]_0^\infty$$

$$= -\frac{C}{2}v_c^2(0)[0-1] = \frac{C}{2}v_c^2(0) = w_c(0) \qquad 25$$

2.4 Electrical Insulation Mediums

Insulation mediums may be classed as solid, liquid, vacuum and gas. This research will focus on vacuum and gases which includes air, nitrogen N_2, and sulphur hexafluoride SF_6.

Characteristic	*Unit of measurement*	*Air*	*N_2*	*SF_6*
Molecular weight	g/mol	28.95	28.0134	146.05
Temperature	°C	-140.5	-147	45.5
Pressure	Bar	37.71	33.999	37.59
Specific gravity (at 1.013 bar and 21 °C)	-	1	0.967	5.114

Table 2.2: Typical characteristics of insulating gases, Air Liquid [51].

Gases and vacuum insulation systems can suffer failure when a sufficiently large voltage is applied. This voltage increases the electric field within the gas/vacuum insulation. In gases, this leads to ionisation, a separation of electrons from neutral atoms or molecules leaving positively charged ions. These ions and electrons are accelerated by the electric field reaching the point where the voltage is applied. Once this happens and with continuing ionisation, current will flow and the insulation of the medium will fails [52, 53]. Under the influence of electrical field electrons, the ions accelerate to the anode and cathode respectively. Townsend and Streamer theories explain the initial breakdown mechanism. Physical conditions in a gas between the anode and cathode such as pressure, temperature, nature of electrode (material and geometry configuration) and number of the initial ionisation products govern the breakdown process [52-55]. The mechanism in a vacuum is different than in gas. The principal breakdown mechanism is the emission of electrons from the cathode (field emission). These electrons are accelerated by

the electric field between the anode and cathode. The impact of the electron on the anode may induce the emission of a positive ion. If sufficient electrons traverse the gap between the anode and cathode, then current will flow and the insulation of the medium fails. The voltage at which this happen is the breakdown voltage of the medium; with this, under high vacuum condition below 0.133μbar (10^{-4} tor), a vacuum has high breakdown strength [55]. Some properties and characteristics of insulating gas are illustrated in Table 2.2. SF_6 gas has higher molecular weight and specific gravity as compared to nitrogen gas and air, thus higher ionisation energy than the air and the N_2 gas. This a peculiar advantage SF_6 has over other insulation gases [51].

2.5 Ionization Processes in Gases

The method of dislodging an electron from an atom or molecule of a gas in its normal state, making a positive, ion is known as ionization process. This process can be achieved when high voltage is applied to two electrodes immersed in the gaseous medium. The processes of breakdown in gases could be by a single process or a combination of the processes like ionization by collision, photo-ionization, secondary ionization, electron attachment and detachment, excitation, photoionization, photo-absorption, ionization by metastable thermal ionization and recombination processes [52-54].

2.6 Types of Arcs

An arc in circuit breakers could be classed as high (or atmospheric) pressure arcs in gases and vacuum arcs in vacuum. High pressure arcs are within the pressure range of 1.01325 bars to some 101.325 bars while vacuum arcs form with ambient pressure below 0.133μbar [52, 53].

2.7 Electric Arc

Electric arcs or discharges are encountered in electrical apparatuses in electrical networks when the insulation apparatus is overstressed. As shown figure 2.11, the effect of high current density toward a narrow path leads to strong heating, contact material melting and evaporation. The discharges are due to electrical flashover and short circuits in the systems. The electric arcs in some cases are unwelcome results of lightning strikes or insulation failures [57].

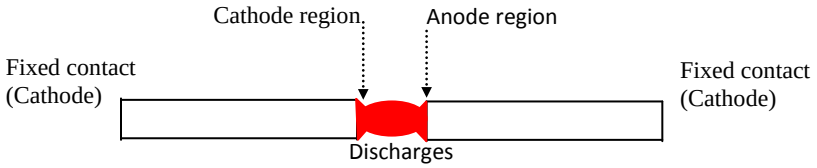

Figure 2.11 shows effect high-current density toward a narrow path

Electric arcs are created when the contacts of the switch or circuit breaker are opened in order to interrupt current. This allows the current to continue to flow until a natural current zero of AC current is reached, and the arc is extinguished. An electric arc is initiated either by an electric flashover between two electrodes or by separation of two contacts from each other carrying a current. An electric flashover may start as a Townsend avalanche or as a streamer process (see figure 2.12). The Townsend discharge is a gas ionization process where an initially very small amount of free electrons, accelerated by a sufficiently strong electric field, gives rise to electrical conduction through a gas by avalanche multiplication leading a breakdown voltage. When the number of free charges drops or the electric field weakens, the phenomenon ceases. It is a process characterized by very low current densities. In common gases like noble gas (argon, neon etc.) filled tubes, typical magnitude of currents flowing during this process range from about 10^{-18} A to about 10^{-5}A, while applied voltage is almost constant [57].

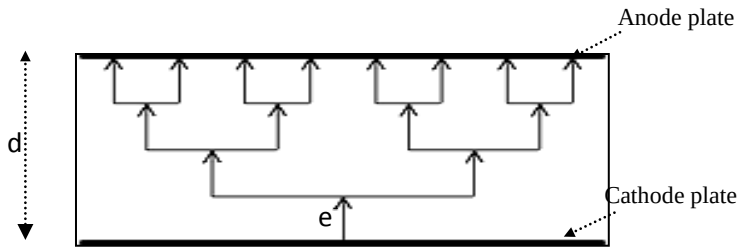

Figure 2.12 Avalanche effect between two electrodes

The breakdown voltage of an insulator is the minimum voltage that causes a portion of an insulator to become electrically conductive. Breakdown voltage is also sometimes called the "striking voltage or sparking voltage" in gases [58]. Properties of electric arcs between the anode and cathode are described in terms of region of an arc channel (as in a cathode region, an anode region and an arc column) shown in figure 2.13.

Breakdown voltage is often encountered in insulators and might be seen as the maximum voltage difference that can be applied across the insulator before collapse and conducts; it is the minimum voltage that causes a portion of an insulator to become electrically conductive [59, 60]. The temperature in the arc column was mentioned to be around 5000K to 20000K, according to Solver [57], at which point gas molecules are largely dissociated into free atoms.

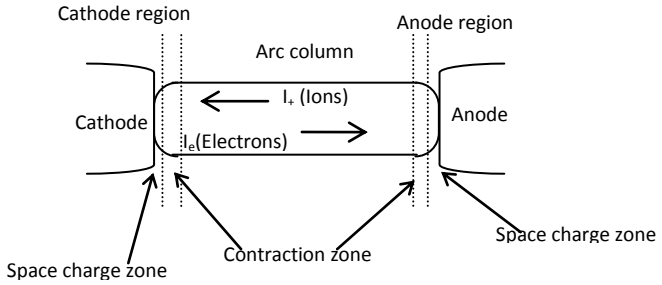

Figure 2.13 shows regions of an arc channels

At such temperature, the travel velocities of the electrons, ions and atoms are so high that ionization takes place when they collide; also, a recombination process takes place where electrons, negatively charged ions and positively charged ions form neutral atoms.

At thermal equilibrium, the gas in a plasma state occurs where high amount of free electrons, negative ions and positive ions are at balanced rate of ionization and recombination. The fraction *f* of the atoms that ionized in oxygen and nitrogen was calculated by means of Saha's equation 29:

$$\frac{f^2}{1-f^2}\ x\ P = 3.16\ x\ 10^{-7} x\ T^{5}/_{2}\ x\ e^{-eV_i/_{kT}} \qquad 29$$

where e =1.6 x 10^{-19}, the charge of electron, V_i = ionization potential of the gaseous medium, k = 1.38 x 10^{-23}, Boltzmann constant, P = the gas pressure in bars and T = the ionisation temperature in Kelvin, [57]Solver [59].

The electrons and negative ions have much higher mobility than the positive ions. Therefore, almost the entire current flow is due to the electrons. The total arc voltage, as well as the voltage gradient along the arc, depends on the current magnitude, the type of gas and the pressure.

Figure 2.14 shows typical potential distributions along an arc channel

When the arc is in thermal balance, the arc column adjusts itself in such a way that the power supplied to the column (the Ohmic heating) attains a minimum value. If there is a disturbance from this situation, which tends to increase the resistance of the arc, the Ohmic heating would increase. Consequently, the temperature and diameter of the arc would increase, and automatically counteract the disturbance. If, on the other hand, there is a disturbance which tends to increase the temperature or diameter of the arc, then the power losses would increase and tend to bring the arc back to the original situation. The current that flows in the arc channel is associated with magnetic forces, which leads to an internal overpressure P in the arc channels. This phenomenon is known as the pinch effect. The resulting overpressure in the centre of the arc column is expressed as

$$P = \frac{\mu_0 I^2}{4\pi^2 \, x \, R^2} \qquad 30$$

As P is close to the electrodes, the arc diameter is often smaller than further away from the electrodes. This means that there will be a gradient in current density, and therefore also a gradient in the internal pressure. This pressure gradient will contribute to a transport of plasma and metal vapour from the electrode into the arc column. Close to the cathode there will be an accumulation of positive ions, arriving from the arc column, as shown in figure 2.14 between $V_{cathode}$ and V_{anode}. Due to these space charges or spatial current, there will be high electric field strength close to the cathode surface (the cathode drop). This high field strength is essential for efficient field emission of electrons into the arc. The anode mainly serves as a collector of electrons, arriving from the cathode having been influenced by the electric field and current density in the anode region. The electrons will arrive at a high speed and deliver all their energies

to the anode. The energies may include thermal, kinetic, photonic etc. The anode surface will therefore keep at a higher potential with the aid of the applied voltage [5, 59, 60].

2.8 Post-Arc Current

Post-arc currents or transient currents widely are known phenomena that appear in electrical power circuits after current interruption. In electrical systems-rated voltages where circuit breakers are used to interrupt the current in medium voltage (<69kV), high voltage (100-287kV) and extra-high voltage (>500kV) systems after the electrical power has been interrupted [4, 5] experience trouble associated with such discharges after current zero is common to the distribution and transmission circuits. Methods of current detection and measurement have been explained in [61-68].

2.9 Electrical Discharge Measurement Methods

With the advancements in electrical and optical measurement technologies had deep the physical understanding of electrical discharge at atmospheric pressure discharges. Among such technological methods are biased probe, electro-optic sensors, electrostatic sensors, laser wave-front sensors and laser-induced fluorescence methods. A biased probe is a static device solely suitable for steady state discharges, as the majority of polarity ions generated in ionization region drift between the electrodes and finally to the passive collector electrode. In electro-optic sensors method, birefringence occurs in some materials when the electric field is applied across them. Birefringence causes orthogonal components of polarisation of light to travel at different velocities. Electrostatic sensors methods include an electrostatic probe using the measure of surface charge distribution on solid insulation such as insulating spacers and insulating plates accompanied by the occurrence of partial discharge. In laser-induced fluorescence methods,

charged particles and various chemical species such as radicals and metastable are in discharged. In laser wave-front sensor, the distribution measurement of a laser wave front is used to know electron density by using a single optical path: a laser beam is expanded to match the size of measurement region and transmit through the discharge region. These measurement methods are applied to physical parameters such as steady-state corona, Steamer development, long gap discharge, surface discharge and barrier discharge under atmospheric condition.

2.10 Peak-Current Measurement

Peak-current measurement as to arc current measurement is important to obtain real time information. Types of coaxial current shunt have been in used for peak current measurement. For instance, a coaxial current shunt of 0.178mΩ resistance in band width of 750 kHz and a pulse current rating of 100kA was used and designed by Grundy [16, 64]. This current shunt has a four-terminal device connected in series with the power circuit and has two connections across its resistive element for measuring purposes. The potential difference between the measurement terminals of a low-value Ohmic shunt is expressed in equation 31 as

$$v(t) = Ri(t) + L\frac{di(t)}{dt} \pm M\frac{di(t)}{dt} \qquad 31$$

This shunt has been used by investigations by various other experimentalists [64, 67, 68]. The shunt design has a good low mutual inductance and low inductance. During the peak current period, the $\frac{di(t)}{dt}$ is not large. Therefore, the second and the third terms on the right hand side (RHS) of equation (32) were negligible and the whole equation approximated to

$$v(t) = Ri(t) \qquad 32$$

The Ohmic value of this shunt was chosen on the basis of giving a good signal-to-noise ratio and to minimise heating. A current shunt between 0.5mΩ and 10mΩ was recommended as ideal for such investigations, [69]. A 2m length of coaxial cable fitted with BNC connectors connected the measuring terminal of the shunt to an oscilloscope; it was advised that when connecting a low-output impedance (1.038mΩ) measuring apparatus to high-input impedance (10MΩ) monitoring equipment, one should insert a 50Ω termination onto the input to the oscilloscope. This matching impedance stops the formation of reflected waves in the cable. Using a mismatched termination can cause an appreciable error (33% with a 75Ω terminator). Since the bandwidth of this amplifier was DC of 50 MHz and has a rise time of 7ns, the amplifier saturation will not be a problem because the peak voltage is approximately 20 volts, well within the normal operating range of the Tektronix 1A1 pre-amplifier used [69].

2.11 Measurement of Current Zero

During one half cycle of arc current measurement, current zero and small post-arc current were investigated. A 19.83mΩ current shunt with 2MHz bandwidth and a rise time of 170ns was used for the current zero investigation arcs. A diode clipper (figure 2.15) eliminates current level from 400 volt that would be applied to the pre-amplifier of the oscilloscope, which would not only cause saturation of the amplifier but also cause permanent damage.

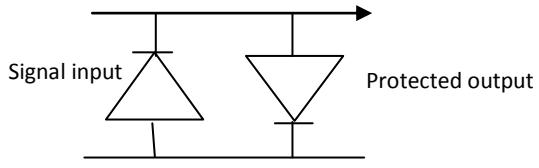

Figure 2.15 Diode clipper circuit

As described by Spencer [69], diodes must have a low capacitance (2nF) and an extremely small leakage current with the rise time of 15ns were discussed.

2.12 Process in Pre-breakdown and Breakdown of Gases

In the influence of an applied electric field, electrons drift in the direction opposite to the electric field. The electrons could be released from a cathode, or from a gas molecule, or atoms or ions, by photo or detachment These processes are as result of gained energy from the field and lose energy by collisions with the gas molecules or atoms in the inter electrode gap. The processes are accomplished by one or combinations of the following mechanisms: by collision ionization (i.e., by direct ionization and dissociative); gas phase photo ionization (i.e. with high [photon], energy collision with a gas molecule or atom will result to the gas molecule or atom to ionize; recombination (i.e., positive ion and an electron or negative ion form neutral atoms or molecules in the gas at the electrode) (image charges); excitation (i.e., electronic excitation, dissociative excitation and photo excitation); attachment (i.e., direct attachment, dissociative attachment and three-body attachment [stabilization and charge transfer]), detachment (i.e., auto-detachment, photo detachment, collision detachment processes); charge exchange (conversion) (i.e., defined as the mean number of negative ion conversion occurring per second per unstable negative ion); secondary electron emissions from surfaces, this includes secondary photoelectron emissions from surfaces, secondary photoelectron emissions by positive ion impacts from surfaces and secondary photoelectron emission by meta-stable from surfaces; and diffusion (i.e., the statistical random motion of specific types of particle will cause a net velocity from region of high concentration to region with a lower concentration resulting to anisotropic in the present of electric field) [58, 59].

2.13 Summary

Sourcing for means and improved methods of low current measurements has led to the search and study of different techniques of electric current measurements such as optical current (OC) method, current transformer method, shunt resistor current method, Hall Effect method, and Rogowski coil methods as described above. Thus, depending on the desired electrical parameters needed, advantages, and disadvantages from each or combination of these methods could be used to achieve efficient and effective low-current measurement. From the study, shunt resistor current method (low-side current sensing, sense resistor between load and ground) was chosen for this research due its characteristics and advantages as elaborated above. The technique shows that it is possible in reproducing replication of its type in its ratio. The chapter also explain the characteristic of dielectric probe and its module at zero input response. Electrical insulation mediums, ionization processes in gas, types of arcs, electrical discharge measurement methods were discussed. Finally peak current measurement, current zero pre-breakdown and breakdown processes were discussed. These enable the researcher to obtain and understand the fundaments research.

Chapter 3 Description of Equipment

3.1 Introduction

The equipment used in this research is briefly described as in figure 3.1a: power supply; dielectric probing circuit as the sensor; arcing current circuit use to created short circuit (fault) current; voltage probes used to inter-face the high voltage source with the oscilloscope; test circuit breaker and experimental earth.

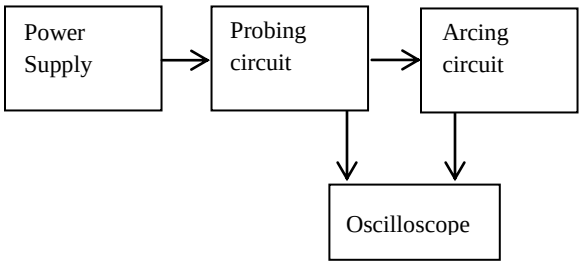

Figure 3.1a shows block diagram research apparatus equipment

3.2 Dielectric Probing Circuit

The dielectric probe is used to test the local dielectric strength of gas within a circuit breaker. This is done through the monitoring of small current flows in the probe circuit. As shown in figure 3.1b, it consists of isolated power supply transformer, a Brandenburg high-voltage power supply unit, coupling resistor R_1, capacitor C, and limiting resistor R_2 connected in series with dielectric probe and experimental earth (Ground). Figure 3.2 present the pictorial view of the schematic diagram of the probing circuit. The circuit components were measured to determine their values. These include the coupling resistors R_1 (1.585MΩ), the capacitor C; high voltage electrolytic capacitor (140μF, 133kV/50Hz), limiting resistor R_2 (58.4kΩ), as in figures 3.1 and 3.2

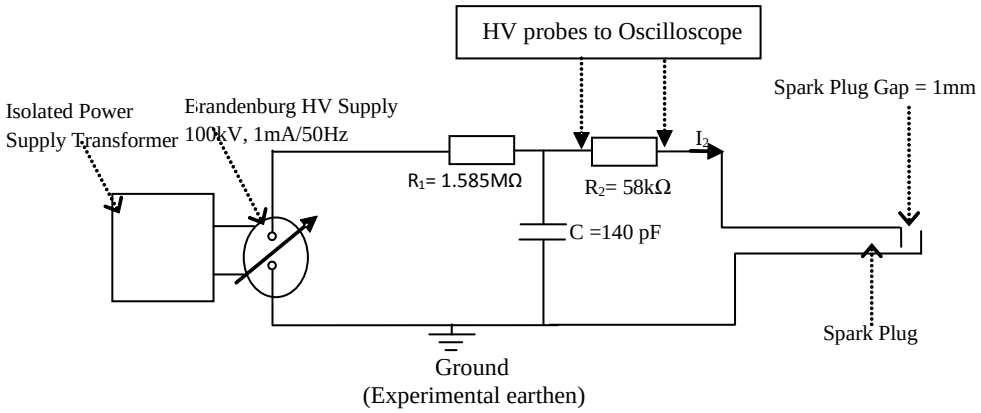

Figure 3.1b shows coupled dielectric probing circuit diagram

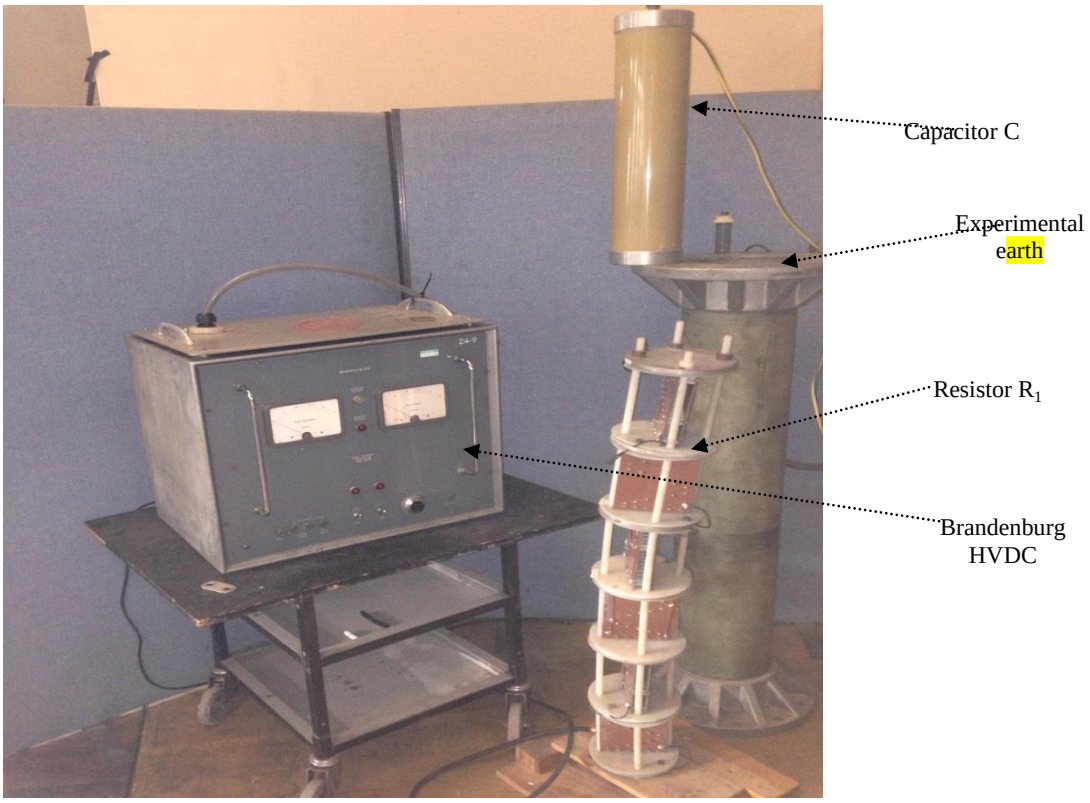

Figure3.2 shows photograph of dielectric probing circuit diagram

The isolating transformer supplies the Brandenburg high-voltage power supply unit. It serves to isolate the Brandenburg high-voltage power supply unit from the mains and potential earth faults.

The Brandenburg high-voltage DC (HV DC) power supply unit provides a negative output and is connected to the dielectric probing circuit. A series resistor (R_1) is connected between the HV supply and the probe to limit the current protecting the HV DC source over current. Resistor R_1 (figure 3.3a) is connected to capacitor C, and R_2 serves as a second limiting resistor to stop excessive current flow in the probe's gap. The time constant for this part of the circuit is (R_2C).

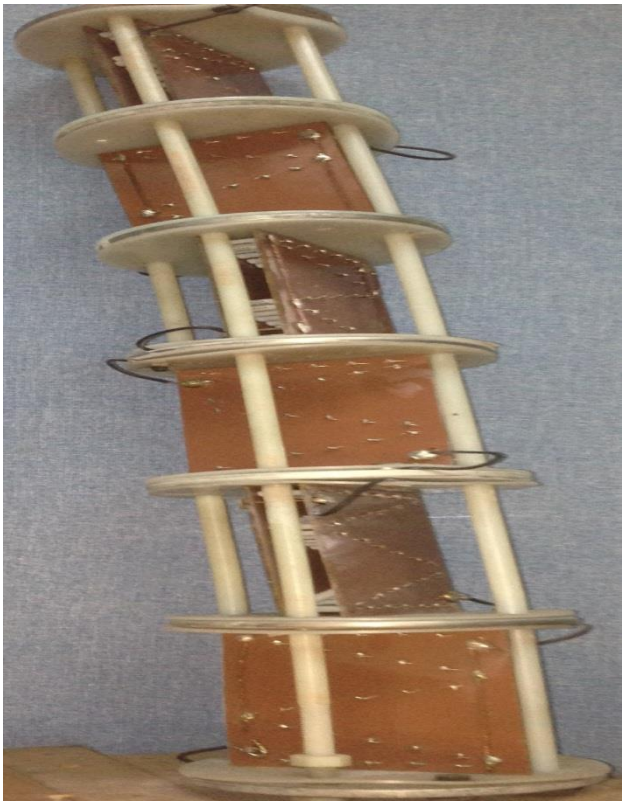

Figure3.3a shows resistors stack

Resistor R_1 is made up of groups of high voltage axial-lead colour coded resistor types, soldered on bread board and cascaded to obtain 1.585MΩ as shown in figures 3.2 and 3.3a.

Resistors R_2, as shown in figure 3.3b, are a series of ceramic resistor discs connected in series with copper foils to obtain 58.4kΩ. Each of the ceramic resistors was $1\frac{1}{4}$inches (31.75mm) in diameter and 0.984inches (25mm) in length. Lead foils (b) or copper foils (c) as shown in figure 3.4 were inserted between the ceramic resistors when connected in series. These foils enable better bonding between the resistors. Ceramic resistors have excellent stability at high temperatures within a specified voltage range, and are resistant to both humidity and mechanical shocks. They have instant overload capability with a low noise figure, and are non-flammable, low-inductance and precision resistance tolerance [70].

Figure 3.3b shows ceramic resistors in series with copper foil sheets in between two resistors.

Ceramic resistors are susceptible to failure under high voltage conditions. In circuits where there are possibilities of transient potentials, considerably high voltage may be applied to the resistor for a short period of time. Applied power within the specifications generally will not cause any significant degradation to the resistor but the resistance value may vary significantly due to repeated pulsing over a long period[43, 71]. The Brandenburg high voltage direct voltage source used was confirmed to have a rating of 50kV and 1mA.

A Tektronix oscilloscope and two high voltage probes, and a laptop with software, not shown, were used in data collation and processing. Figure 3.1 shows the schematic of the RC circuit with the dielectric probe connected. The gap length in this probe is adjusted for different operating conditions. The current into the probe and voltage drop across the limiting resistor (R_2) were measured during testing.

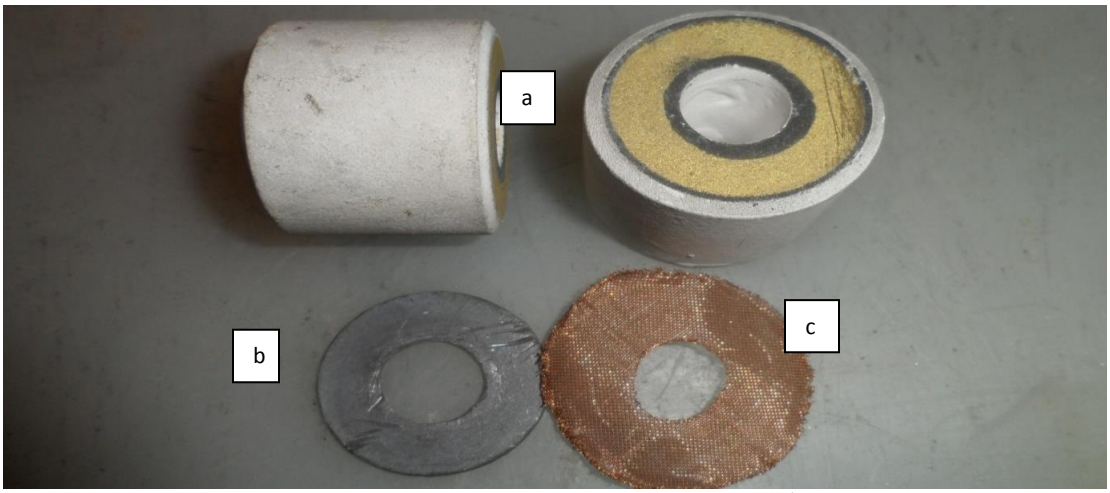

Figure 3.4 shows ceramic resistor (a), structured cylindrically of $1\frac{1}{4}$inches (31.75mm) in diameter and 0.984inches (25mm) in length resistor. Lead foil (b) and copper foil (c**)**

The oscilloscope type used is Tektronix, DPO2000 series, with 6 recording channels [72, 73]. The vertical and the horizontal sensitivities were set on 1kV/div and 10ms/div respectively. The Brandenburg HVDC source, oscilloscope and the laptop were powered from isolation transformers, not shown. Figure 3.13 shows circuit configuration of dielectric probe (a) connected to test circuit breaker (b) with limiting resistor (c) in series and high voltage probes (d) used in detecting voltage drop across the limiting resistor.

3.3 Voltage Probes

A number of voltages were taken in the probe and arcing circuits during testing. Two were used to record the differential voltage across the limiting resistor R_2 and therefore to deduce the current into the probe. Another voltage measured the arc voltage. The voltage probes are ISO900 compliant with the Tektronix 96015A passive high voltage probe [73]. The probe has corresponding capacitance compensation range of 7pF to 49pF and has 1000x attenuation factor such that the voltage displayed on the oscilloscope is understated by factor of 1000. Table 3.1 illustrates some specifications of P6015A, 1000x high voltage probe[72]. The current through the arc was measured using a shunt resistor (figure 3.12). Figure 3.12 shows the circuit connection for the dielectric probe (a) coupled to test circuit breaker and connected in series with the limiting resistor R_2 (c) and two HV probes.

Max input voltage	Bandwidth (MHz)/ft-cable	Rise time (ns)	Input impedance/ capacitance	DC attenuation
20kV(rms) 40kV -100ms	75/10ft-cable	4.6	100MΩ/3pF	1000x

Table 3.1 High voltage probe specification

3.4 Spark Plug Sensor (Dielectric Probe)

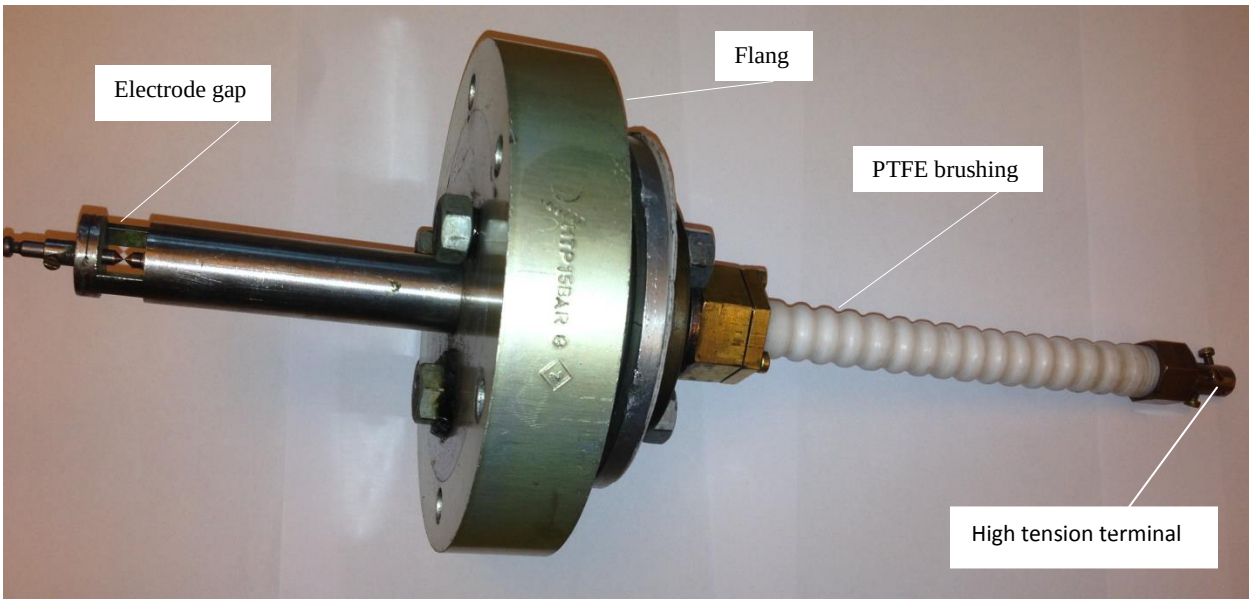

Figure 3.5 shows dielectric probe

Figure 3.5 shows the dielectric probe. The probe comprises two electrode tips made of 20% copper and 80% tungsten alloy that will withstand repetitive discharge activity with minimum wear. The gap length will be adjusted to fit the research purpose in various insulation gases.

3.5 Arcing Current Circuit

A block diagram of arcing current test circuit is shown in figure 3.6a. This is used to generate pseudo current (DC trigger) and half sinusoidal arc currents (AC trigger) that vary from zero to several kilo-Amperes peaks current. Figure 3.6b shows the schematic circuit diagram of the arcing current test circuit. Ignitron1 (DC trigger) with 4.5Ω resistor is used to generate a quasi-current, ignitron 2 (AC trigger) and ignitron 3 (AC trigger) generate a positive half-fault current and negative half cycle AC (fault) current through the reactor respectively. To achieve one

positive half AC current, the 33mF capacitor bank is charged up to 565V; on triggering ignitron 2, the capacitor will be discharged through the inductor (L) into the test circuit breaker and the current shunt resistor to the experimental earth is used to determine the arc current in the oscilloscope [69]. The ignitron 4 and ignitron 5 are used to dump residual energy during DC arcing while the mechanical pneumatic dumps are used to discharge the capacitor banks to earth after each experiment. These units are hooked up to the control panel that is sequentially set for trigger.

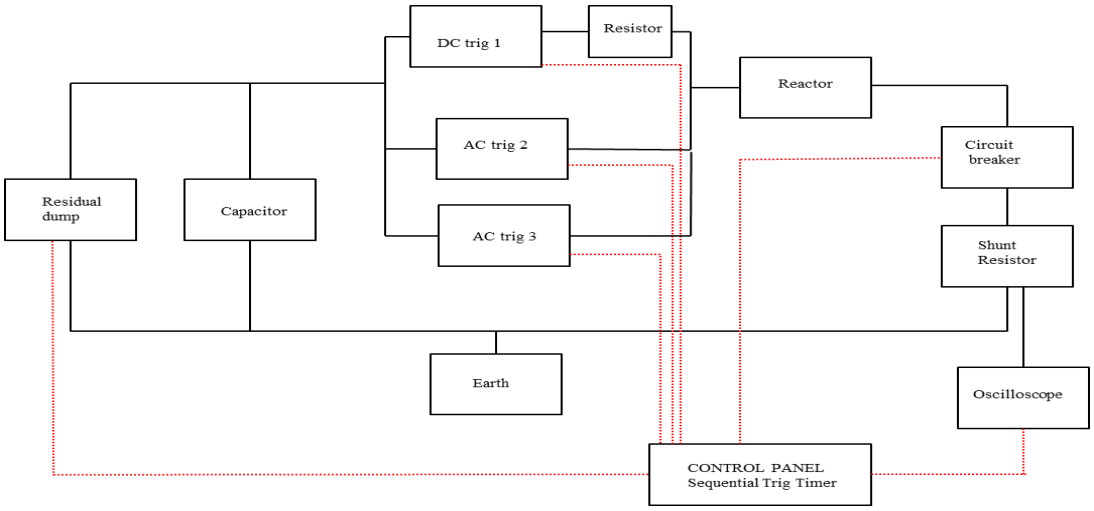

Figure 3.6a shows block diagram of arcing current test circuit

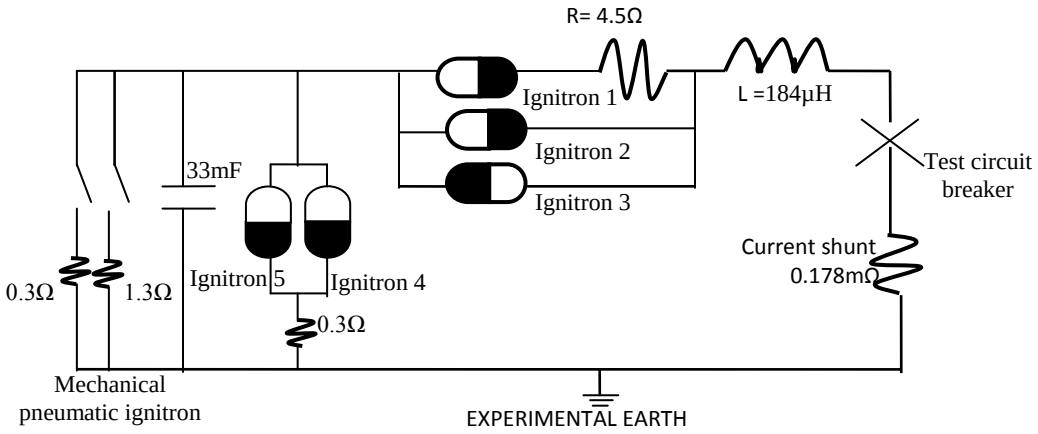

Figure 3.6b shows arcing current test circuit

Figure 3.7 is a photograph of the arcing current producing experimental test circuit. The photograph shows the capacitor bank (A), ignitrons and control signal interface (B), resistor stack (C), discharge mechanism and output cabling (D). These facilitate the formation of positive half currents that were triggered into the test chamber.

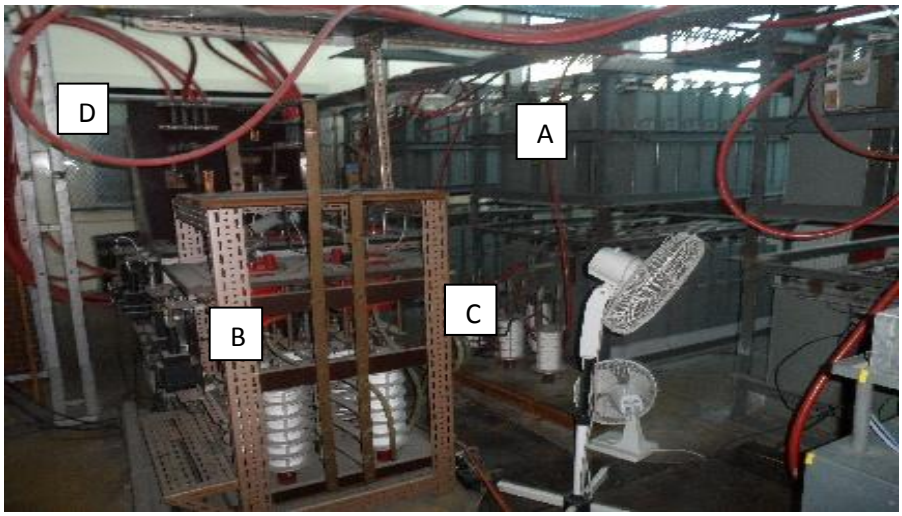

Figure 3.7 shows photograph of arcing current test circuit.

3.6 Arcing Current Circuit Operation

Figures 3.6a and 3.6b show the block and schematic circuit diagrams of the arcing current test circuit configuration. After the control panel is set as previously explained, the circuit is triggered from the control panel (sequential trigger timer); sequentially, the poker begins to move from the fixed contact, taking 10 milliseconds (ms) to begin opening, and opened fully within 40ms. Meanwhile, the ignitron 1 through the limiting resistor (4.5Ω) is triggered into the reactor (184μH) to generate pseudo (quasi) DC current from the capacitor bank voltage of about 575V during the breaker opening. This will result in a weak discharge between the contacts opening. At this point, the ignitron 2 is triggered through the reactor, bypassing the 4.5Ω resistor into the breaker and generating the fault current that will further increase the energy of the discharges

(arc current) into heat, lighten and electromagnetic reaction in the breaker chamber. After about 20ms of the ignitron 2 triggered, ignitrons 4, 5 and pneumatic ignitron are set on to discharge the residual energy of the capacitor bank and the system into the experimental earth. Shunt resistor of 0.178Ω connected in series monitors the fault current flow in the circuit breaker.

3.7 Test Circuit Breaker

The test circuit breaker unit is shown in figure 3.8: it has a tube steel with a wall thickness of about 3cm, a diameter of 27.5cm and a height of 148.5cm. Inside this steel enclosure are the inner electrodes, nozzle etc., providing a gas tight seal to the breaker. A viewing window in the steel enclosure allows optical access to the inner components. Attached to the external body of the circuit breaker (figure 3.8) are inlet and outlet points for mounting other accessories including a gas inlet, a pressure gauge, a pressure relief valve etc.; the enclosed volume can be filled with different gases. The electrical connection to the fixed electrode is made via cast resin brushing mounted to the fixed contact sub-assembly (figure 3.12) at the top of the steel pressure vessel flange. The fixed contact is made of cylindrical slits of copper fins 2cm in diameter and 20.1cm length (figure 3.11). The fins allow easy movement and proper contact with the poker. At the top of the steel pressure vessel, the flange is also fitted with a pressure relief valve to prevent over-pressurisation in the circuit breaker. Figure 3.12 shows the connections to the fixed contact cast resin brushing on test circuit breaker (A) of a high voltage probe (C), used in measuring arc voltage and current shunt resistor (B) used for fault current measurement. The current shunt measures the fault current i.e., a known resistance of shunt is placed in a series so that the entire fault current flows through it. The voltage drop across the shunt resistor is measured and the current flowing through the shunt resistor can be determined. The shunt resistance has a low value of R_{shunt} power dissipation in the shunt. If the shunt resistor value is

too large compared to the resistance of the circuit under test, the voltage burden causes large errors, resulting in excessive heating and reduced current flow, according to Matthaei [44]. In order not to disrupt the characteristics of the electrical circuit, the resistance of the shunt is normally chosen in order to be small, within the ranges of 0.1 to 0.178 milli-ohms, here used for the fault current measurement. Shunts are rated by maximum current [43]. The moving contact sub-assembly with the moving contact of 2cm in diameter and about 20.1cm in length with aluminium base is shown in figure 3.10. It is mounted on high-voltage Kevlar insulator with the moving contact assembly operated by an ETNA hydraulic mechanism unit. The hydraulic mechanism allows adjustment of the circuit breaker trip speed characteristic by modifying the hydraulic choke and the operating pressure via hydraulic switches. The mechanism is initiated using 125V, 52Ω DC trip and close coils activated from a signal timing unit. From the viewing window, the activities in the internal of the circuit breaker including the chamber, the arcing, fixed and moving contacts are observed. Figure 3.13 shows the dielectric probe (a) connected to test circuit breaker (b) with limiting resistor (c) and high voltage probe (d).

Figure 3.8 shows test circuit breaker outfit

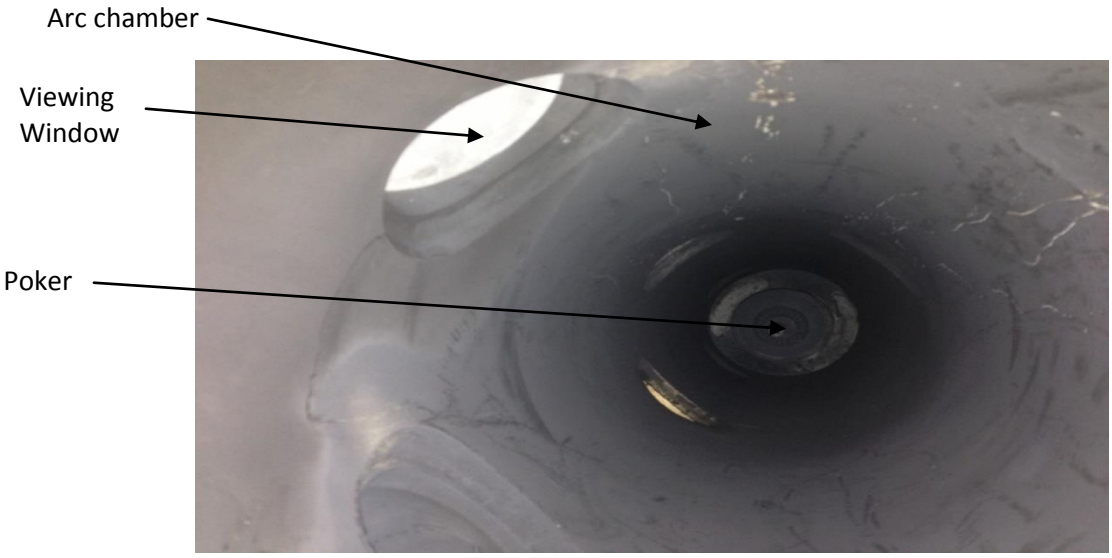

Figure 3.9 shows internal view of test circuit breaker chamber, viewing windows and the spindle (poker)

Figure 3.10 shows the moving contact sub-assembly

Figure 3.11 shows fixed contact sub-assembly.

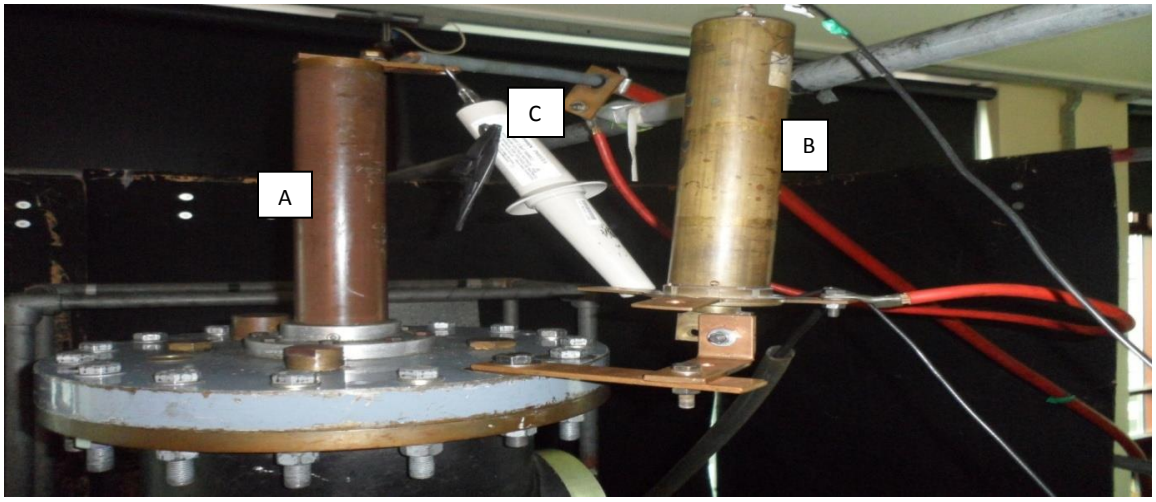

Figure 3.12 shows the fixed contact of test circuit breaker (A), current shunt resistor (B) and high voltage probe connection(C).

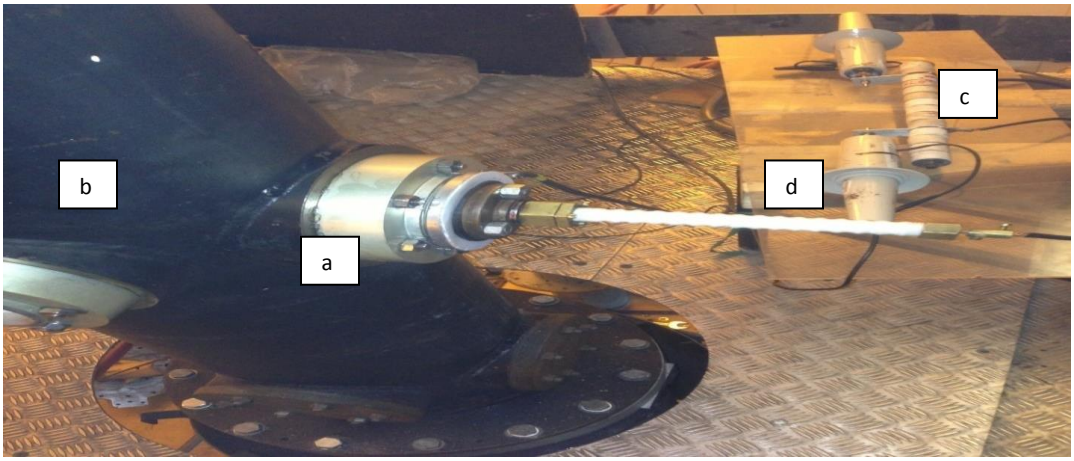

Figure 3.13 shows dielectric probe (a) connected to test circuit breaker (b) with limiting resistor (c) and high voltage probe (d)

3.8 Equipment Configuration

Figure 3.14 shows the complete set-up of the schematic experimental circuit diagram used in probing the gases. The dielectric probing circuit is coupled to the synthetic circuit through the circuit breaker, sealed and air-tight, placed about 55mm apart from the current-carrying electrode.

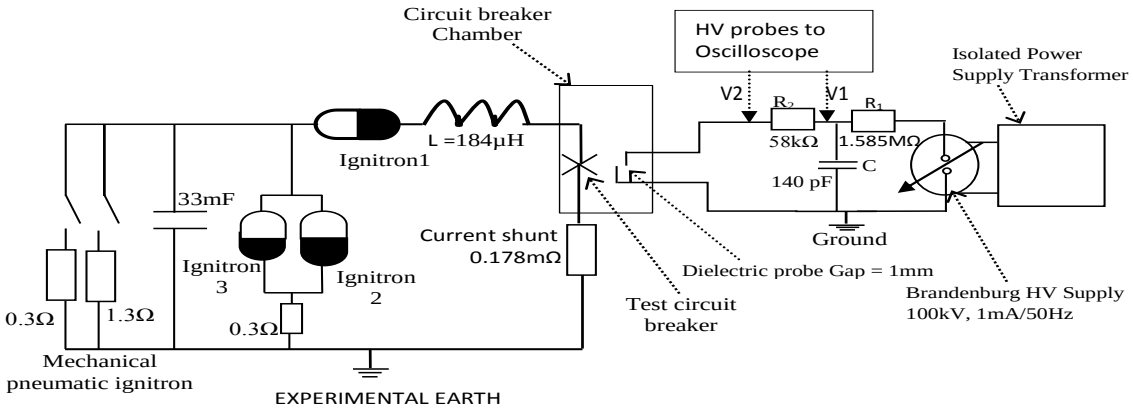

Figure 3.14 Coupled schematic diagrams of arcing current test (synthetic test) circuit and dielectric probing circuits

3.9 Gas Handling

Figure 3.15 shows the schematic diagram of test circuit breaker and the pneumatic manifold fitting. The circuit breaker is drained to a vacuum with Hanning Electroweak vacuum pump (E8LD4BI-162). The valves are ball valve with a pressure gauge connection for gas inlet and monitor into the circuit breaker. Valves V_1 and V_4 are close to the atmosphere and test gas while V_2, V_3 and V_5 are open to the circuit breaker and the vacuum pump evacuates the circuit breaker to vacuum.

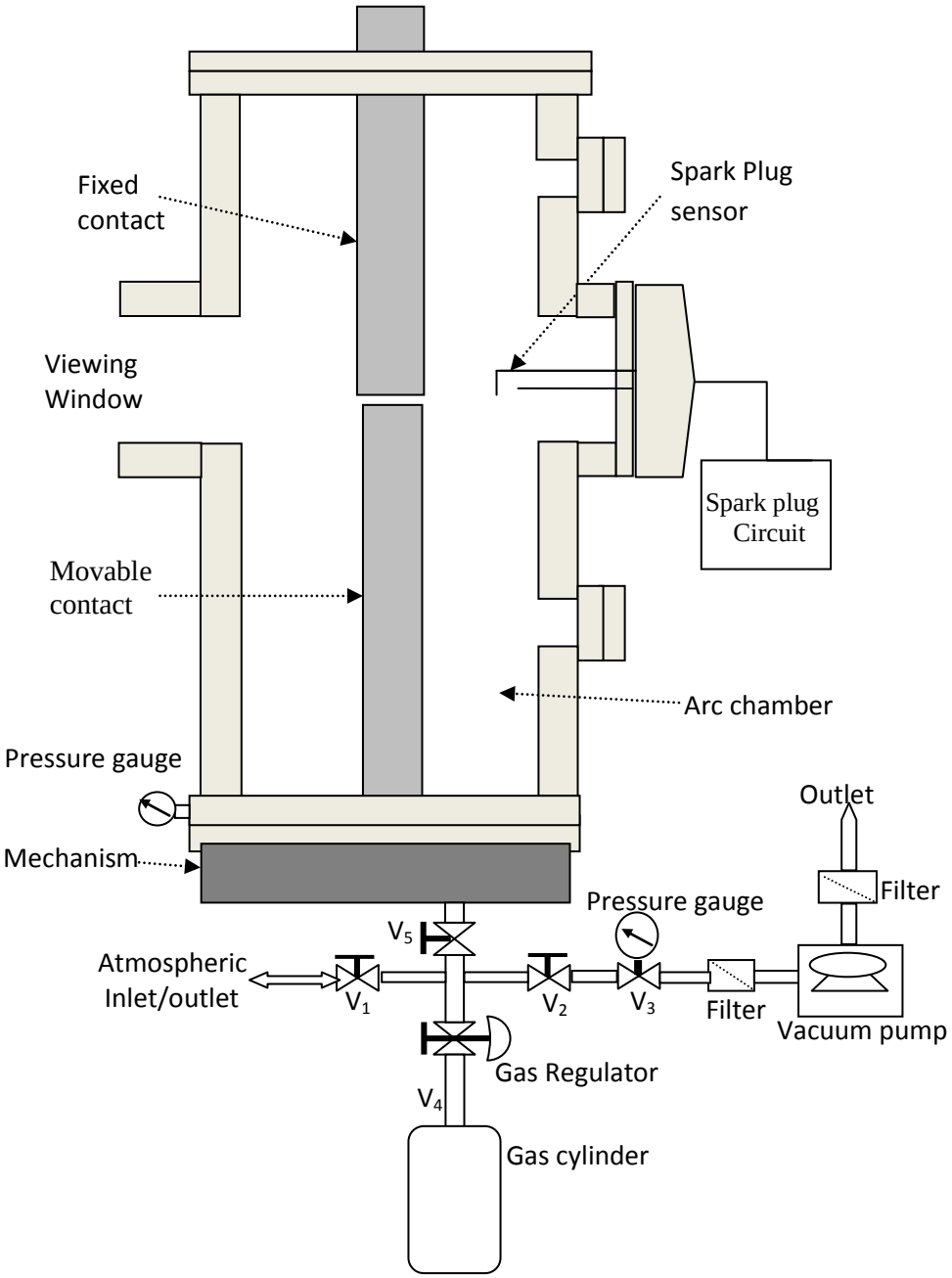

Figure 3.15 shows configuration of test circuit breaker and accessories

To refill the circuit breaker with gas, V_1, V_2, V_3 and V_5 are close. V_4 and the gas regulator on the gas cylinder is open and set to the desired pressure before opening V_5 to fill the circuit breaker.

A combined pressure and vacuum gauge is used to monitor and measure the gas pressure on the inside circuit breaker.

3.10 Experimental Earth

The experimental earth used consists of copper rods bonded and buried in the ground whose terminal outputs have zero potential. For measurement purposes, the experimental earth serves as a constant potential reference against which other potentials can be measured, as noted by Donald [49] [87].

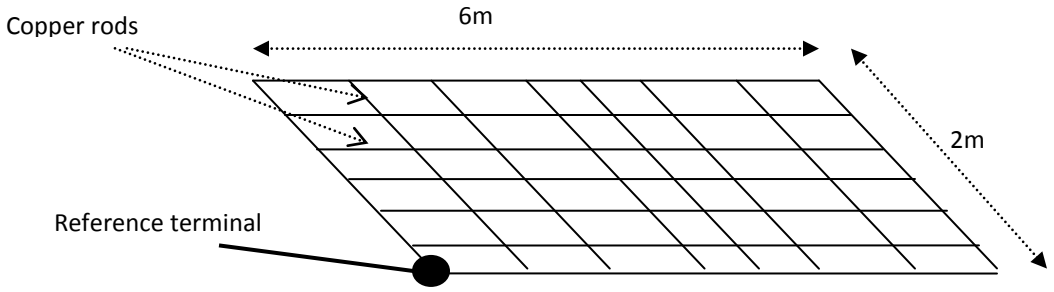

Figure3.16 shows copper rods structured into mat of $12m^2$ buried 4cm depth into the ground

In the laboratory setup, the experimental earth is buried near the experiment system, connected with shorter and lower impedance copper cables capable of carrying several kilo-amperes. Figure 3.16 shows a typical experimental earth. Copper rods were bonded and structured to form 6m x 2m mat and were buried at a depth of 4cm with a terminal output near the laboratory setup. Isolation transformers were used to eliminate any mains earth or mains looping problems that might be caused by powering equipment from either the same or different phases of the mains supply [69, 74].

3.11 Summary

The circuit configurations and components need to be familiar with as to ensure better response of the circuit components. This chapter explained the experimental apparatus and the setup. It commenced with simplified block diagram of the experimental structure as in figure 3.1a. This is followed by the diagrams of the dielectric probing circuit, arcing current circuit and the explanation of the circuits components. Figure 3.6a and 3.6b shows the block and circuit diagram of the arcing current test circuit connections. Figure 3.14 shows the complete schematic setup of the apparatus used for the research. The operations and functions of the circuit components are explained in this chapter and chapter 4.

Chapter 4 Experimental Setup and Preliminary Test

4.1 Experimental Procedures – Introduction

This chapter presents the experimental procedure used in probing the dielectric strength of different gases with a dielectric probe and explains how the dielectric circuit works. The chapter also presents the methods used to determine pre-breakdown of dielectric strength, weakened dielectric strength and dielectric strength breakdown of different insulation gases using a negatively biased high-voltage dielectric probe when fault current is passed in the gases. Preliminary checks and testing of the apparatus were performed before undertaking experimental tests in the presence of an arc.

4.1.1 Pressure Gauge Calibration

A pressure gauge of combined pressure and vacuum type was used to monitor the insulation gas pressures in the test circuit breaker. The pressure side ranges from 0 to 150 pounds per square inch (lb. /in^2) while the vacuum side ranged from 0 to -30 inches of mercury (inHg). This was checked and converted into absolute pressure in bars and then into kilo Pascal as shown in figure 4.1 and in table 4.1.

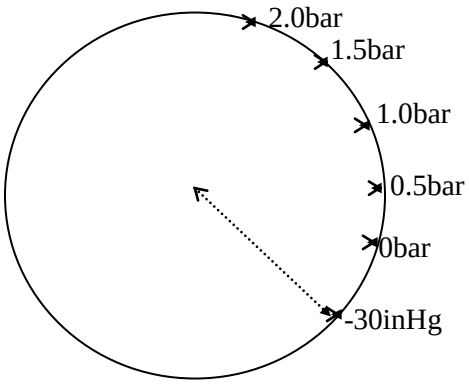

Figure 4.1 shows schematic pressure gauge scale

The checking and conversion is necessary to gauge the amount of pressure being fed into the circuit breaker during the research on a standard pressure scale.

Known that: 30inHg = 1.016bar =101.591kPa;

1 Atmosphere = 1.01325bar = 101.325kPa

Figure 4.1 shows the schematic figure of gauge scale measurement. Table 4.1 presents pressure in bars and then scaled into absolute pressure in kilo Pascal (kPa) scale in table 4.1. Also the soft vacuum pressure was scales as -30inHg = -101.591kPa.

Absolute pressure p_{ab} for -30inHg = -101.591kPa + 101.325kPa = -0.266kPa

Taking absolute pressure, the below table 4.1 of pressure conversion is obtained:

Gauge pressure scale	Absolute pressure		kPa
0bar	0 +1.01325	1.01325bar	101.325kPa
0.5bar	0.5+1.01325	1.51325bar	151.325kPa
1.0bar	1.0+1.01325	2.01325bar	201.325kPa
1.5bar	1.5+1.01325	2.51325bar	251.325kPa
2.0bar	2.0+1.01325	3.01325bar	301.325kPa

Table 4.1 presents gauge scale at absolute pressure

4.1.2 Preliminary Check of the Oscilloscope

Tektronix DPO2024 Digital Phosphor oscilloscope is used in this research, with the following specifications: 200 MHz bandwidth; 4 analogue channels; sample rates up to 1GS/s and 1 Mega sample record length on all channels; 5,000 waveforms per second (wfm/s), maximum waveform capture rate and a suite of advanced triggers, serial bus trigger and decode, at the same time using 1X/10X probe per channel. The test of the oscilloscope is necessary to confirm that the

oscilloscope specifications are within the calibration range of ±0.03V from the manufacturer's specification. A channels check of the oscilloscope without input from Brandenburg HVDC source was carried out. The voltage drop differences of both channels 1 and 2 were measured to be ±0.02V. This value is within acceptable limit of the Tektronix oscilloscope threshold accuracy of ±0.03V[72].

4.1.3 Probe Consistency Check

A probe consistency check is important in this research since the probes are to be used to determine potential differences across limiting resistors. This is to make sure that both probes have the same output characteristics. The calibrator generator on the Tektronix instrument generates a square wave of 5 volts which was applied to the two P6015A 1000X high voltage (HV) probes at the same point. The outputs were read from the oscilloscope (figure 4.2a) into an Excel file. A sample of such an Excel file is shown in figure 4.2b. As shown from both figures, the probe tends to have a signal-to-noise ratio of 244:1.

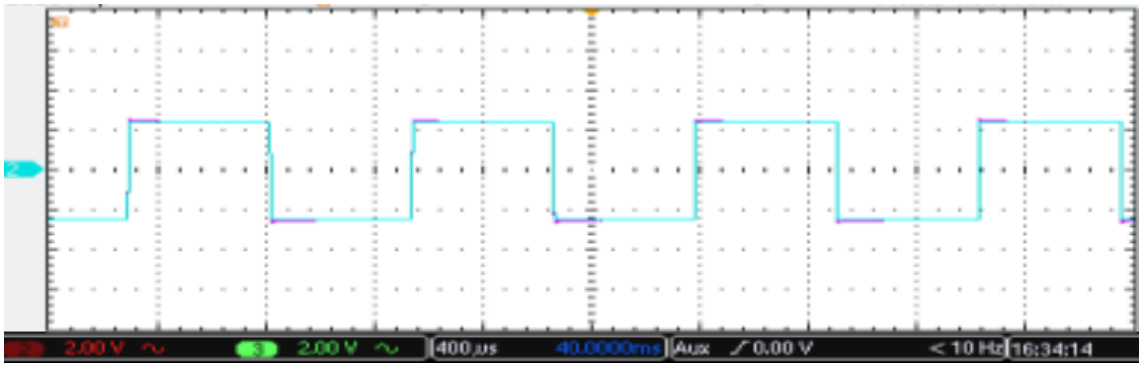

Figure 4.2a shows oscilloscope wave form output from the two P6015A 1000X HV probes

Although there was noise associated with the output signals from the probes, the probes reveal the same output signal within the range of 5V. The noise level from the oscilloscope input channels could be reduced from the variable low pass filter (noise filter) knob on the

oscilloscope. It is also noted that the digitization of the analogue signals adds additional noise which may be due to the bit range of the ADC (8 bits). The bit noise is reduced by using the full dynamic range of the screen setting.

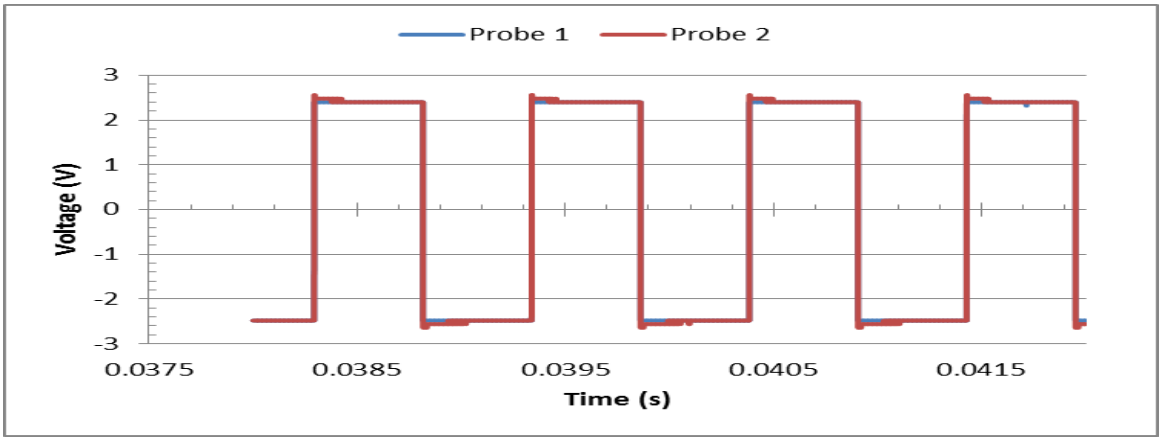

Figure 4.2b shows the Excel waveform output from the two P6015A 1000X HV probes with a 5 volt input signal from the Tektronix instrument

The DC calibration and comparison were also carried out on P6015A probes with no adjustments on the compensation box. The oscilloscope was set at 5V/div, 40ns/div and 10 MHz, with the calibrator generator signal at maximum output of 10V not shown, and the oscilloscope waveform output of the two probes shows a 19ns phase shift. This is skewed to 19ns to align both waveforms into the same phase. The result also shows the same output waveform from the high voltage probes.

4.1.4 Voltage Probe Calibration

Two P6015A 1000X HV probes were calibrated in order to ensure that the probes have the same reference. Both probes were connected to the output terminals of a Brandenburg high voltage source, through 10 metre length of coaxial cables and their respective compensation boxes and then to the Tektronix oscilloscope. The oscilloscope is set at 2kV/div on the vertical axis, 10ms/div on the horizontal axis and at 10Hz of frequency. The Brandenburg high voltage source

is switched on and allowed to stabilize; the high tension is then switched on and the voltage is increased in steps of 1kV until to 12kV. At every 1kV, the output from the Tektronix probes were read and recorded as shown in table A1 (see appendix A). With the same voltage applied to the probes, there was a difference of 650V at 12kV between probe 1 and probe 2 (i.e., probe 1 reads 12000V while probe 2 reads 11350V: see figure 4.3). With this, it becomes necessary to determine the correction factor k, used to normalise the voltage difference between both probes voltage measured at the same point. Figure 4.3 shows the input voltage in kV, the recorded voltage from both probes and the voltage difference from both probes (Probe 1 – Probe 2).

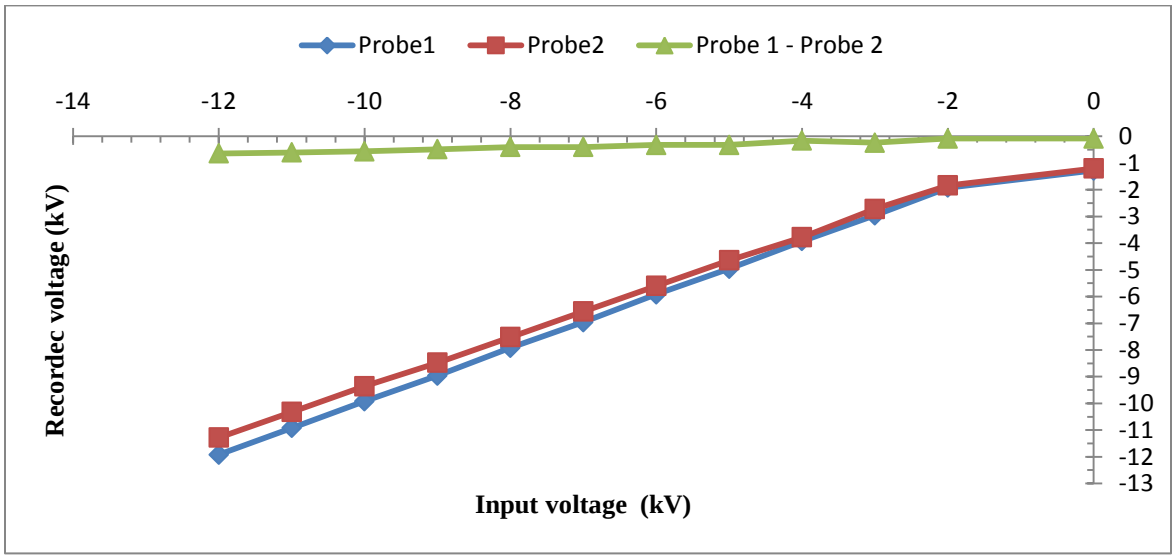

Figure 4.3 compares the voltage difference (V) between Probe 1and Probe 2 and the voltage drop from both probes plotted against input voltage (kV)

Figure 4.4 shows the graph used to obtain the correction factor k (i.e., the graph of voltage differences between Probe 1 and 2) at the same voltage point versus voltage recorded from Probe 1. Figure 4.4 shows the voltage difference between Probe 1 and Probe 2 at the same reference with the input voltage from Probe 1. The figure shows a linear trend line and the error bars. The

trend line was used to determine the correction factor k. The correction factor k was used in the research results implementation in chapter 5. Figure 4.5 shows the input voltage and the recorded voltage in kV from probe 1 and 2 after the application of the correction factor k (see table A1 in appendix A).

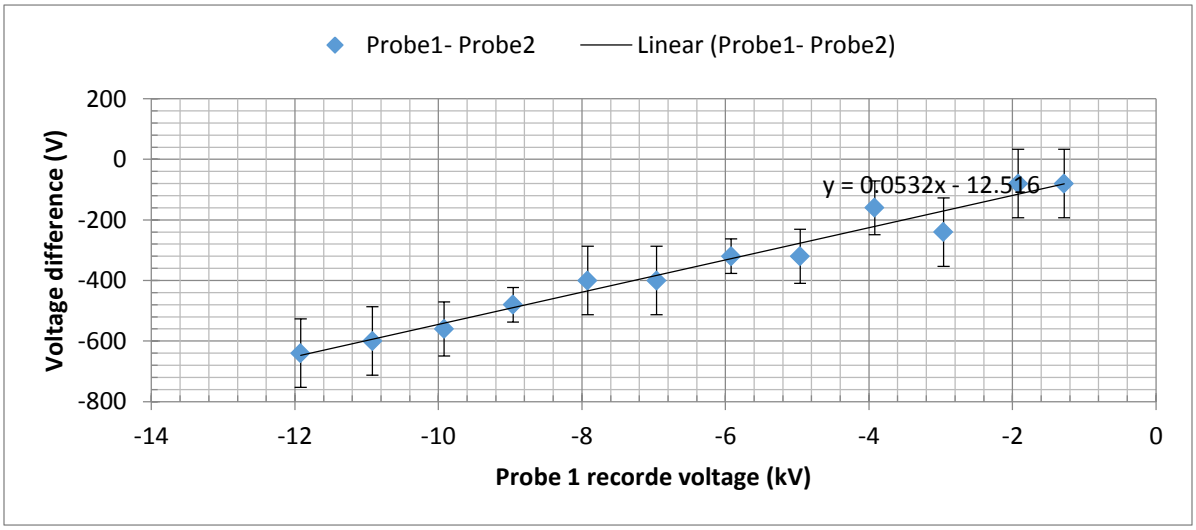

Figure 4.4 shows the graph of voltage difference between Probe 1 and Probe 2 at the same potential versus the recorded voltage from Probe 1.

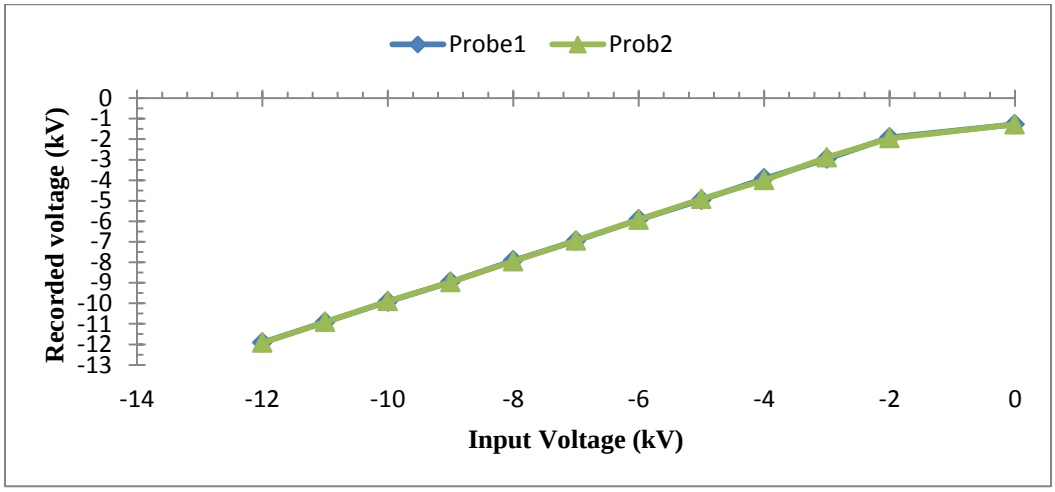

Figure 4.5 shows the input voltage in kV and the recorded voltage from Probe 1 and 2 after the application of the correction factor k.

The graph shows that for both probes (1and 2) voltage differences of 650V for 12kV output have been corrected.

4.2 Experimental Procedures

This section explains the measurement technique of leakage current in dry and probe current flow using the negatively biased dielectric probe when the fault current was passed in the vicinity of an interrupter. The section commenced with the operational procedure of the probing circuit (4.2.1) then followed the procedure in atmospheric air as to understand the experimental method of the probing circuit (4.2.2). The probing circuit is set up in dry air in a circuit breaker with varying voltage to ensure the leakage currents out are consistent (4.2.3). Next step is to the test the circuit breaker opening sequence with a 9VDC battery, which also shows a reliable opening (4.2.4); section 4.2.5 presents the technique to measure dielectrically weak gas probe current. The probe detects the dielectric strength of the gas locally and determines its current-carrying capacity.

4.2.1 Operation of Probing Circuit

Figure 3.1b shows the dielectric probing circuit configuration. When the Brandenburg high voltage source is switched on, the potential difference across the resistor R_1 is equal to this applied voltage. The voltage across resistor R_1 will start to reduce as the potential difference across the capacitor C increases as the capacitor charges up. At full charge, the potential difference across resistor R_1 will be close to zero, and, ideally, if no current flows through the test gap, it will be zero. However, when current flows through the test gap, it is supplied by the capacitor. The capacitor will begin to discharge and the voltage will decrease. The current is then supplied by the Brandenburg through the resistor to replace the lost charges. The R_2C (τ) is the

time constant of the circuit which determines the rate of charging and discharging of the dielectric probe circuit. This charging and discharging increases the temperature of the electrode tips and increases the energy levels of the electrode tip surfaces and gas, causing polarization and ionization of the gas atoms/molecules between arena of the dielectric probe. These processes occur due to highly induced energies in the gas atoms/molecules. This may result in the worst case of dielectric failure or dielectric breakdown of the gap. The voltage at this point is called breakdown voltage: the maximum voltage difference that could be applied across the gap before the gap insulation fails and conducts significantly. The high voltage source is regulated and maintained to the threshold voltage level of the dielectric probe before breakdown occurs. This could be termed as the pre-breakdown period when the gas atoms/molecules are ionized but still maintain some of dielectric properties. The electric field in between the gap will cause the charge carriers to move to their respective electrodes. If this happens then the charge flow would be detected as a current flow in the circuit. This charge flow will reduce the resistance between gap of the dielectric probe resulting in continuous flow of current which will depend on the amount of discharge from the capacitor C, the electric field and the nature of the gas of the electrodes. At the point of dielectric failure, as the current flow increases, the resistance of the gap will be reduced, resulting in the reduction of the voltage to the point where the current flow will stop followed by a recovery voltage period. This phenomenon has been explained by the Townsend avalanche or Streamer process [58, 60, 75].

4.2.2 Procedure in Atmospheric Air

The function of the dielectric probe was tested with atmospheric air as the host gas. This is to ensure correct operation of the probe and to understand the leakage current before deploying the spark plug in other gases. The dielectric probe is placed in air at atmospheric pressure and

connected as shown in figure 3.1b. The dielectric probe electrode gap is set at 1mm apart and connected to a limiting resistor R_2 through the R_1C (resistant-capacitor) circuit to a Brandenburg negative high voltage (HV) DC power supply. R_2C also serves as the timing components of the dielectric probing circuit. The Brandenburg unit is supplied by an isolation power transformer (1:1) from the mains. The purpose of the resistor R_1 is to limit the current from the Brandenburg unit, which also acts as a limiting resistor to limit the current to the dielectric gap electrodes. The isolation power transformer (1:1) is used to eliminate any mains earth or earth loop problems that may be caused by the interconnection of multiple earth from different sources. An electrical experimental earth is connected to the circuit, which has an appropriate current-carrying capacity in order to serve as an adequate zero-voltage reference part. The electrical experimental earth also serves as a zero voltage reference point against which other potentials can be measured. The Brandenburg power supply unit is switched on and allowed to warm up; the high tension is then switch on and gradually increased from 0 to about 6kV to observe and obtain the pre-breakdown and breakdown voltage of the dielectric probe gap. The input and output voltages across the limiting resistor are measured with two high-voltage single-end probes on a Tektronix oscilloscope (DPO2000 series) for processing. The voltage drop across this limiting resistor is divided by its resistance value to determine the current flowing in the gap. To achieve the leakage in milliamperes, the experiment started with limiting resistor of 0.25Ω and gradually increased to about 58.4 kΩ before the leakage within the range of milliampere was obtained.

4.2.3 Setup for Leakage Current Detection

Figure 3.14 shows the schematic circuit of dielectric probe circuit configuration and arcing current test circuit diagrams connected together. The previous circuit provides the arc current for

the test and the dielectric probe monitors the dielectric strength of the gas and its ability to carry low current.

Where:

R_1: is a current limiting resistor to protect the Brandenburg (approximately 1.585MΩ)

R_2: is a current limiting resistor (approximately 58.4kΩ)

R: is shunt resistor (0.178mΩ)

C: is high voltage capacitor (1400pF)

The test circuit breaker is evacuated to a vacuum (-30inHg) and later refilled with the test gas (e.g., dry air) at different pressure levels. The pressure is increased from 0 bars (atmospheric pressure of dry air), in steps of 0.5 bars, to 2 bars. At each pressure, the high voltage source from the Brandenburg unit is increased to a value just below the breakdown voltage of the dielectric probe in dry air and a set of readings were taken. The data were collected through high-voltage single-end probes to a Tektronix (DPO 2024 Phosphor) oscilloscope, and then input into the laptop for processing. The breakdown voltage is monitored by V_1 if it occurs and the leakage current through the gas is obtained by dividing the voltage difference ($V_1 - V_2$) across R_2. The dielectric probe circuit is coupled to the synthetic experimental test circuit shown in figure 3.14. As previously explained, the Brandenburg negative HV supply (equipment specification 50kV, 1mA) was used with an isolation transformer, coupled through a limiting resistor R_1 and a timing component (R_2C) to the dielectric probe. The voltage difference across the limiting resistor is measured, and the leakage current is also determined. The results are presented in chapter 5.

4.2.4 Circuit Breaker Timing Test

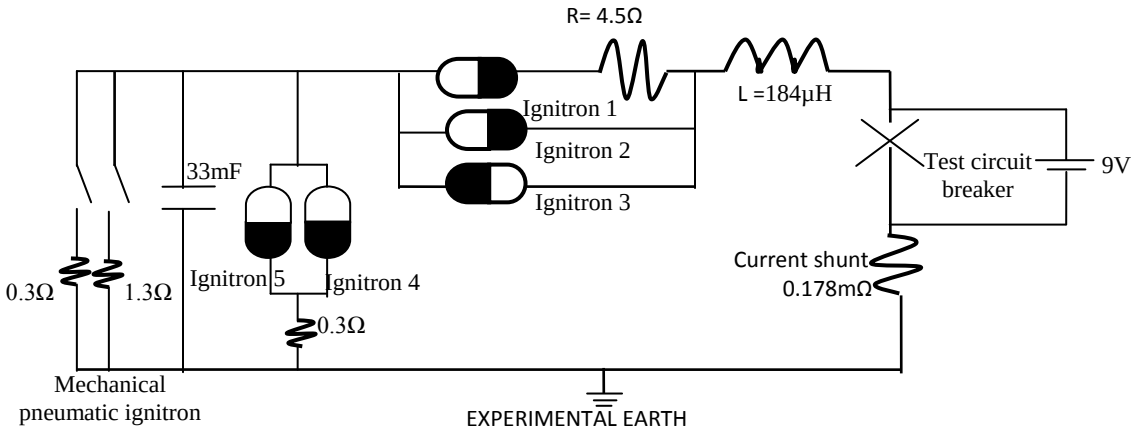

Figure 4.6 shows the Circuit Breaker Timing Test Circuit

The circuit breaker (CB) opening timing test is an important conditions in post-current zero measurement. If not properly set, it will result in a mismatch between the circuit breaker opening time and the triggering of the synthetic circuit. The test is used to set and check the duration of the CB opening with which the timing of the DC trigger unit and the half cycle AC unit will be determined and set on the control panel. To set the timing correctly, a 9-volt battery is placed across the terminals of the circuit breaker. The voltage is monitored across these terminals. When the breaker is operated, the contacts separate and the voltage is recorded across the terminals. This can be used to synchronize the opening of the circuit breaker with the various triggering events in the synthetic current circuit. Figure 4.6 shows the experimental set up of timing test circuit and the operations of the circuit component are presented in section 3.5.

In this trial, the test circuit breaker is kept in the closed position and the 9V battery is connected between the two terminals of the closed breaker and then triggered open without the operation of the arcing test and the dielectric probe circuits. Figure 4.8 shows an Excel waveform of circuit breaker contacts opening sequence. From zero (0) to twenty (20) milliseconds the poker moves

off from a fixed contact. Thereafter, the actual opening time duration lasted for the next ten (10) milliseconds as shown in the figure. This procedure was repeated for three consecutive times, each time obtaining the same result.

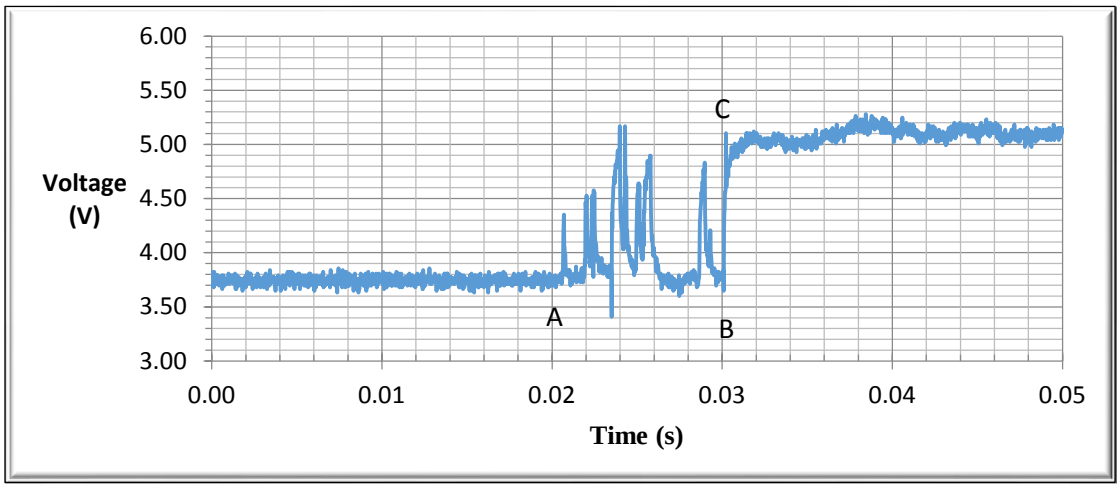

Figure 4.8 shows the opening sequence of the CB contacts

Figure 4.8 shows the opening of the contact in the circuit breaker. The spike type of signal between A and B indicates the "contact bounce type of effect". The breaker's contacts have separated at C. It takes 10ms from triggering to opening.

Information obtained from the opening time for the CB were used in setting the DC trigger unit at 20ms and the half-cycle AC unit at 10ms. The capacitor bank unit was set between 45 (on the capacitor bank setting) and above to generate about 575V, so as to obtain the pre-set fault current value and a dump trigger unit for the dumping of residual energy as set at 20ms.

Figure 4.8 shows the result of the Excel file waveform of the 9-volt test conducted on the circuit breaker. The figure shows the parting period (A and B) of the contacts in the circuit breaker. The spiked type of signal between A and B indicates "contact bounce type of effect". The breaker's contacts have separated at C. The circuit breaker takes 10ms from trigger to fully open. From zero (0) to twenty (20) milliseconds the poker (moving contact) begins to separate from the

fixed contact, this lasts for the next ten (10) milliseconds as shown in figure 4.8 (A-B). During the contact separation, a DC current is passing between the contacts (fixed and moving). As the contacts separate, a low-current AC arc discharge is produced. At a pre-determined time of 10ms, the AC current passes through the separated contacts. The triggering of the DC and AC currents is controlled, and each lasts for 20ms and 10ms respectively. Another trigger used to dump residual charges (energy) from the capacitor 20ms after the AC and the DC currents have ceased to flow. Repeating the procedures for three consecutive times obtains the same result. This shows that the breaker opening time is consistent and is synchronised with the synthetic circuit operation.

4.2.5 Setup for Dielectrically Weak Gas Detection

As shown in figure 3.14, the synthetic experimental test circuit and dielectric probe circuit are used together. To record arc voltage in the circuit breaker during the test, a high-voltage probe was connected to the fixed contact while the other in the circuit breaker is at experimental earth. A positive half-cycle of fault current, triggered from the capacitor bank, flows through the test circuit breaker and is measured from a shunt resistor (0.178mΩ), which is connected in series to the synthetic circuit. A coaxial cable takes the signal to the oscilloscope, as shown in figure 3.12.

The test circuit breaker is evacuated to approximately -30 inches of mercury with a vacuum pump and refilled with test gas (e.g., nitrogen gas). The dielectric probing circuit is switched on and allowed to stabilize, and the voltage is then set below the breakdown voltage. This is recorded while contacts were in closed position in the test circuit breaker. The synthetic experimental test circuit is switched on and allowed to warm up. The charging voltage on the capacitor bank is then set to approximately 575V. The sequence of triggers to operate the circuit

breaker starts the current flow and subsequent data capture is controlled from a control unit from the chamber. The arc will heat the surrounding gas to various temperatures (i.e., mono-homogeneity). Heating of the test gas (the interrupter) will cause ionisation and dissociation which can lead to current conduction if this gas flows through the dielectric probe. The conducted current can vary depending upon the condition of the gas. In the worst case, the gap of the dielectric probe may completely breakdown which will be indicative of severe dielectric failing of the gas. Figure 4.9 shows an oscilloscope waveform of pulse current and arc voltage triggered into the circuit breaker, inverted input and output voltage from the limiting resistor at dielectric pre-breakdown before impulse current, breakdown of dielectric strength of dielectric probe during the impulse current and dielectric strength recovery during and after current zero periods in insulation gas.

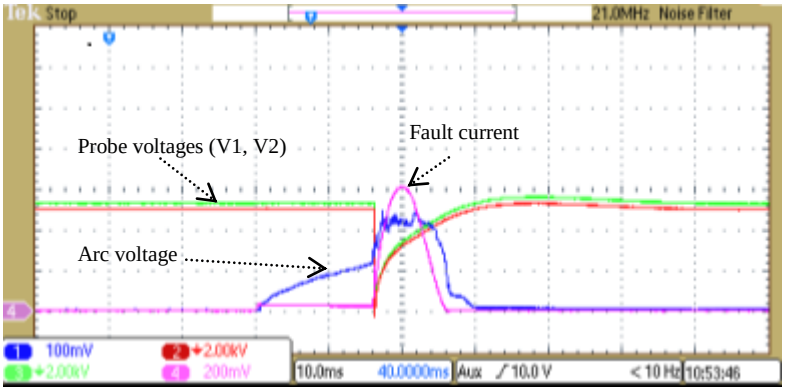

Figure 4.9 shows typical oscilloscope waveform of dielectric breakdown.

This test is repeated, but the high voltage applied to the dielectric probe is lowered to such a level as to negate voltage breakdown as shown in figure 4.10. A voltage drop should occur without dielectric strength breakdown. A small current flow will happen due to an increase in the conductivity in gas through the gap of the probe. The state of the gas is determined by its temperature, ignoring any electrode impurity. The probe current detected during the test will

depend on the type of insulation gas (type of interrupter), the gas pressure, the electric field, the orientation (0 or 90 degree) of the dielectric probe and the magnitude fault current. The information from the probe will allow assessment of the nature of the gas during arcing and the recovery period after current zero. In general, the following events occur during the test process. At trigger period and post current zero period, heat generated from the arc due to the pulse current will fuse into the interrupter gas, weakening the dielectric capability of the gas; heat might be generated during the current interruption due to electromagnetic reaction at the point of contacts separation which are passed into the test gas (e.g., nitrogen); and during the dielectric strength recovery at and after current zero periods might result in reigniting low current.

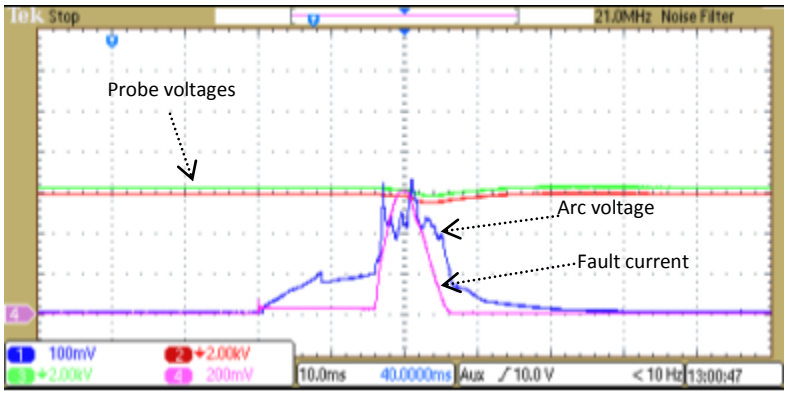

Figure 4.10 shows oscilloscope waveform of inverted input and output voltage drop due to dielectrically weakened gas detected.

Within these processes in the arc chamber, low current flow may be detected by the dielectric probe. Detailed explanation of ionisations processes were discussed in Meek [58] and Blower[76]. The voltage drop due to dielectric weakened strength in the gas as a result of induced heat from the arc voltage was detected with the spark plug sensor (see figures 4.10 and 4.11) The recorded figure 4.10 shows the oscilloscope waveform of fault current and arc voltage. Also shown are the voltages V1 and V_2 across R_2. The change shows dielectrically weak gas

detected by the probe. Figure 4.11 shows the pulse current and arc voltage and the two probe voltages across the limiting resistor and the associated flowing of probe (discharge) current. The results and the analysis are presented in chapter 5 and chapter 6 respectively.

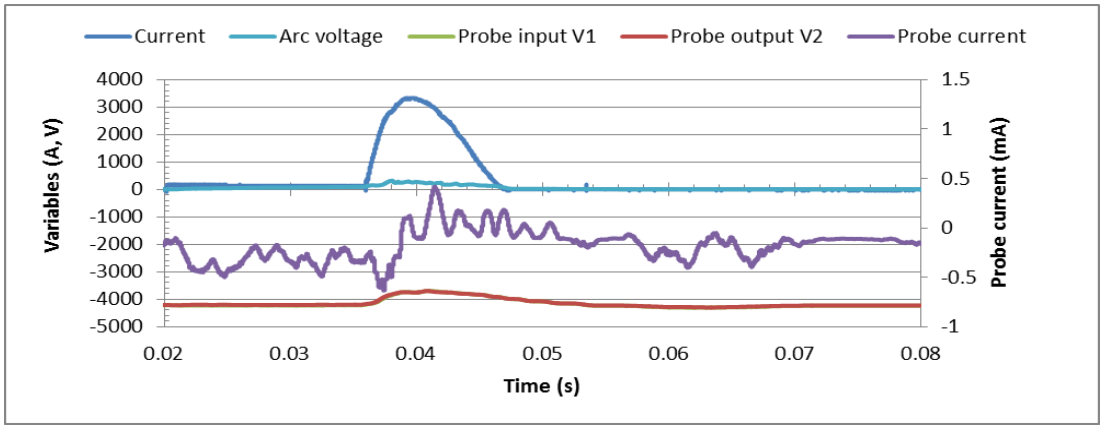

Figure 4.11 shows the arc current and voltage triggered into the circuit breaker, input and output voltage drop from the limiting resistor and discharged current due to dielectrically weak gas detected during the impulse arc current.

4.2.6 Observations

The ceramic limiting resistors tend to increase their value when subjected to repeated high value of DC voltages, ranging from 6kV and above. This may be that the ceramic resistors have positive temperature coefficient. At this value, the spark plug sensor will be hissing without breakdown and Brandenburg milli-ammeter will overage. This will damage the power supply, if not protected by R_1. The limiting resistors are polarised, having diode characteristics (i.e., forward and reverse biasing). The characteristics of the ceramic resistor were discussed in section 3.2 and shown in figure 3.4, [71, 77][82], [83]. The spark plug sensor tips do carbonise, reducing the set gap of 1mm.

4.2.7 Precautions

After every experimental test, a short time of about three minutes was set aside before carrying out another experimental test since ceramic resistors are susceptible to failure under high-voltage conditions. Applied power within the specifications generally will not cause any significant degradation to the resistor, but the resistance value may vary significantly due to repeated pulsing over a long period [43, 71]. The limiting resistors are stacked in a forward direction when being stacked as to avoid reversed value. The tips of the spark plug sensor were regularly inspected and the surface de-carbonised to ensure proper contact to the insulation gases on test at the commencement of the experiment. The tips are re-adjusted to 1mm gap apart to maintain the same gap distance.

4.2.8 Summary

In the chapter the experimental procedure and setup for the research carried out were discusses. It start with an introduction which is followed by pressure gauge verification, preliminary checks on the oscilloscope, probe uniformity check as in subsections 4.1.4 and 4.1.2. These are followed by the experimental procedure and setup which includes probing circuit operation, probing circuit operation in atmospheric air, leakage current detection, circuit breaker timing test and dielectrically weak gas detection. The chapter concludes with observations and precaution taken during the research.

Chapter 5 Experimental Results

5.1 Introduction

This chapter reports experimental results taken during this research. The results are taken from a probe used to determine the dielectric condition of a gas when it has been subjected to an arc discharge. The probe dielectrically stresses the gas by applying a relatively high negative voltage across a small gap between two electrodes. The chapter begins with the calibration of the voltage probes and the functionality of the negative high voltage power source. This is followed by results taken to determine current loss due to corona discharge etc. This leakage current was determined in compressed dry air and used in section 5.2. The experimental results of probe currents detection are presented in three sub-sections of section 5.3 for nitrogen gas (sub-section 5.3.1), dry air (sub-section 5.3.2) and sulphur hexafluoride SF_6 gas (sub-section 5.3.3) when a fault current is passed through these gases. The dielectric capacity of each gas is determined by applying a negative high voltage DC to the dielectric probe during the half-cycle AC fault current and immediately afterwards. Chapter 6 presents the results analysis and discussions.

5.2 Leakage Current in Dry Air

Results of leakage current tests in dry air with the dielectric probe electrode tips set at separation distance of 4.85mm and with an applied negative voltage are presented below. The circuit breaker chamber is pumped down to a vacuum (-30mmHg) and then filled with dry air to three different pressures (0, 0.5 to 2bar). At every pressure increment, the output of the HV source is increased gradually to a point where the dielectric probe begins to breakdown. The applied voltage is then reduced to just below breakdown voltage point of the dielectric probe. The time-varying voltages during the test are recorded (see tables in appendix 2B). The data obtained for

probe voltage V2 corrected by adding the calculated voltage differences between probes V1 and V2. Appendix B explains and shows the typical data and calculations. Figures 5.4a and 5.4b show the results. Fig 5.4a shows a typical result of probe voltage (input V1 and output V2) increasing across the limiting resistor as the pressure of dry air is increased. Figure 5.4b shows the graphical result of probe current variation in dry air at different pressures when a negative voltage DC is applied to the probe before the breakdown of the dielectric of the probe. The graph shows a negative current (approximately -0.5mA) at 0.5bar of the dry air and positive current at the remaining three pressures (1, 1.5, and 2 bar) as shown in figure 5.4b. The graph shows three separate experimental results carried out to ascertain the probe response at different pressures of dry air. The results show experimental "shot to shot" variations as expected, but they also show a consistent behaviour at the various pressures.

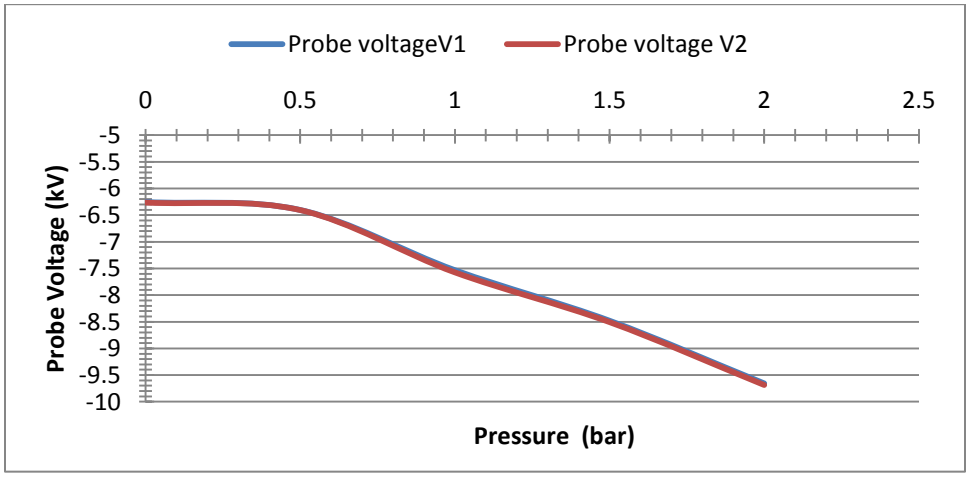

Fig 5.4a shows typical result of probe voltage (input V1 and output V2) across the limiting resistor in dry air.

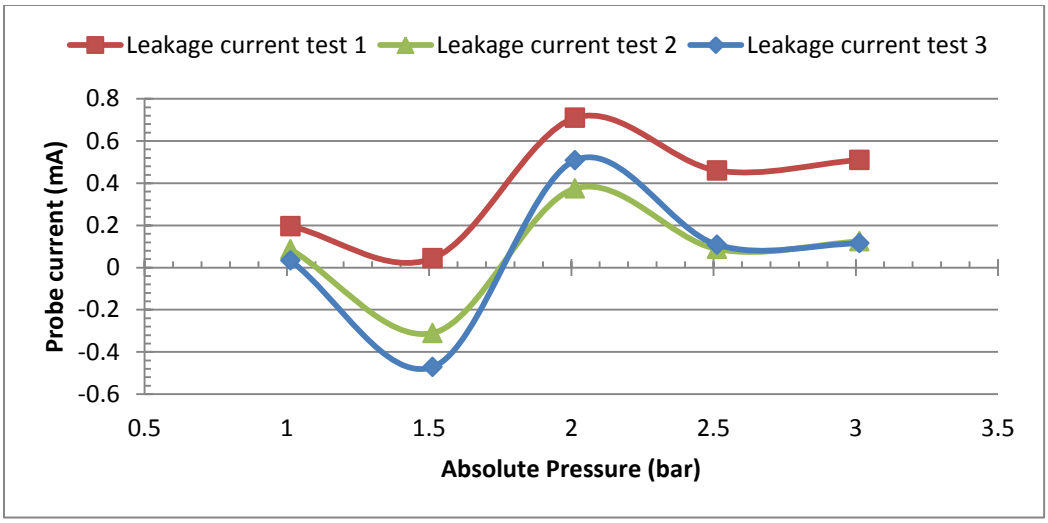

Fig 5.4b shows variation in leakage current in dry air at atmospheric pressure (table 4.1).

5.3 Probe Current in Gases

This section presents the experimental results of probe currents detected in nitrogen gas, dry air and in sulphur hexafluoride gas when the fault current passes in the arena of the gases respectively**.** These results will clearly show the behaviour of each gas when the negative high voltage DC is applied to the dielectric probe during the passage of the fault current near the gases.

5.3.1 Probe Current in Nitrogen Gas

5.3.1.1 Detection of weakened Dielectric Strength in Nitrogen Gas

This sub-section reports the results for a probe current flowing through the dielectric probe in nitrogen gas during arcing fault current. The dielectric probe gap is set to 1mm and then coupled into the test circuit breaker. The dielectric probe is placed 55mm from the contact electrodes where the AC arc discharges are produced in the test circuit breaker. The circuit breaker is pumped down to a vacuum (-30inHg) and then refilled with nitrogen gas at various pressures from 0 to 2bar in 0.5bar steps (see table 4.1). Negative high voltages were applied to the

dielectric probe ranging from -3.5kV to -12kV for the pressure used. The high voltage DC is set just below the dielectric breakdown voltage of the gas inside the circuit breaker filled with the nitrogen gas. The fault current of about 3.8kA peak with frequency of 50Hz passes through the circuit breaker producing an arc with a voltage of about 575V. The current is supplied from a 33mF capacitor bank through an 184µH reactor. The arc heats the test gas causing it to dissociate. This may also diffuse, producing ionized products if sufficient energy is transferred into the test gas. During the dissociation, ions are formed and electrons are free to move, resulting in low current flow.

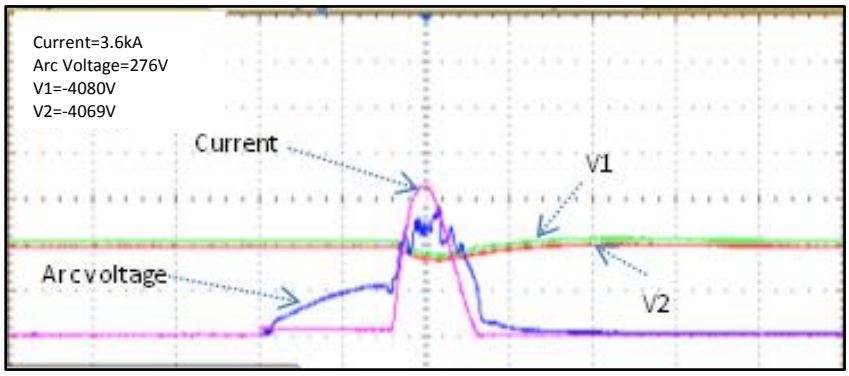

Figure 5.5a shows oscilloscope waveform.

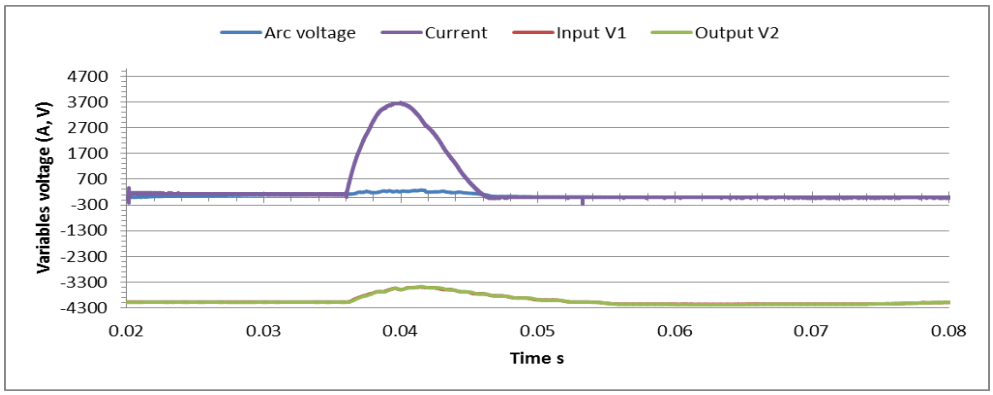

Figure 5.5b shows an Excel download of oscilloscope waveform data.

As the gas moves away from the arc, it cools, and recombination takes place. Gas further away from the arc is heated by conduction, convection and radiation, increasing the energy level of the

atoms/molecules of nitrogen gas. Figure 5.5a shows the recorded oscilloscope waveforms of the positive half-cycle AC current of about 3.6kA at 50Hz with the associated arc voltage. The figure also shows inverted voltages V1 and V2 across the limiting resistor connected to the dielectric probe. The pressure is 0bar and the orientation is at 90^0. Figure 5.5b shows the result of Excel file waveform of negative voltage DC (Probe input voltage V_1 and Probe output voltage V_2) from the limiting resistor applied to the dielectric probe for nitrogen gas at atmospheric pressure when the fault current passes in the circuit breaker with time. It shows reduced negative voltage between 0.034s and 0.056s during the dielectric strength weakened period and gradual dielectric strength recovery after the arcing current is extinguished. The high voltage DC applied to the dielectric probe enhances the drift of any ions towards the anode and cathode of the probe. Depending upon the type of ion charges in the leakage current, this indicates the current-carrying capacity of the gas. The more ionized the test gas, the higher the probe current. A high probe current flow will indicate a weakened dielectric state of the gas. The reduced dielectric strength of the probe gap shows as voltage drops across the limiting resistor as shown in figure 5.5b.

Results

For clarity in figure 5.6, the following terms are briefly explained:

Variables (A, V) denote current in Amperes and arc voltage in Volt

Current denotes fault current in Amperes.

Probe input V1 and probe output V2 in Volts indicate voltages from the limiting resistor before and during the arcing periods with time in seconds

Probe current denotes low current flow in milliampere detected in nitrogen gas at atmospheric pressure.

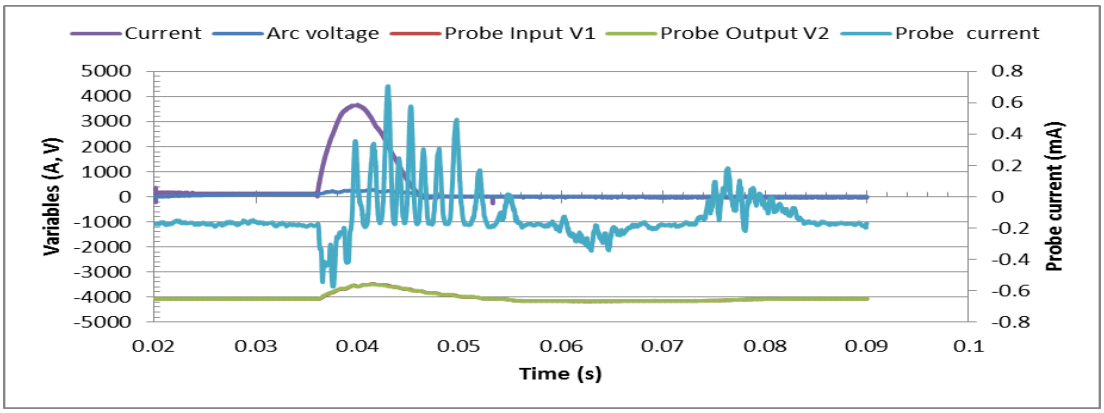

Figure 5.6 shows the complete arcing period at atmospheric pressure of nitrogen gas.

Figure 5.6 shows the results for a typical case in nitrogen gas at atmospheric pressure, an example to illustrate the behaviour of nitrogen gas at the passage of fault current in it. The figure shows low current flow through the dielectric probe in milliampere (probe current), probe voltage (input V1) and probe voltage (output V2) in volts with time in seconds across the limiting resistor for nitrogen gas at atmospheric pressure during and immediately after arcing of the positive half AC current period. The derived current passing through the dielectric probe has an initial negative value at the beginning of the arcing period. This is followed by a period of positive values that is highly oscillatory. At about 0.06 seconds, there is a negative value for the current followed by a positive value starting at .07 seconds. The result shows a complex picture emerging from the test condition, and chapter 6.3.1.1 presents the analysis and discussion.

5.3.1.2 Current Directions during Arcing Periods in Nitrogen Gas

This section presents the results of the dielectric probe response to low current flow in the gas before, during and after the arc current in the circuit breaker filled with nitrogen gas ranging from 0bar to 2bars. Tests performed in 0.5 bar steps and with negative high voltage DC applied to the dielectric probe. The experimental data determined the value and the direction of the

probe current flow, and the direction of electron (e^-) flow in the circuit are analysed and discussed in sub-section 6.3.1.2.

5.3.1.2.1 0 bars of Nitrogen Gas

Figure 5.7a shows arc current and arc voltage produced in the circuit breaker, the probe voltages V_1 and V_2 from the limiting resistor connected to the dielectric probe at atmospheric pressure. The leakage current through the dielectric probe is negative before an arc discharge is initiated. This may be related to a higher applied voltage. However, there is a small increase in the negative value at arc initiation. The current will become positive for the majority of the arcing period and beyond before returning to a slightly negative value at 0.052 seconds. The trend is similar to those observed in figure 5.6. Figure 5.7b shows V1, V2 and the corresponding value of the probe current. It shows a reduction in the applied negative voltage drop during the dielectric strength-weakened period. After the extinction of the fault current between 0.05 seconds and 0.07 seconds, the figure shows an increase in the applied negative voltage and in the probe current flowing, followed by the return of these variables to the previous level.

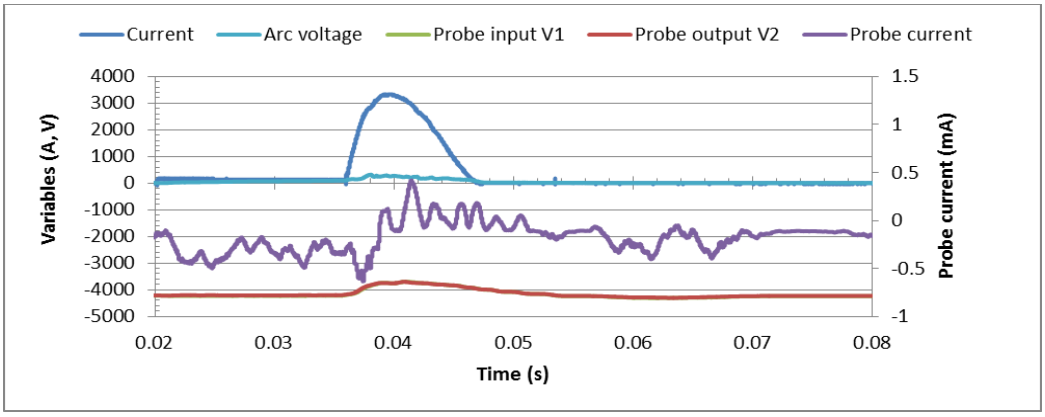

Figure 5.7a shows the graph of the arcing periods for atmospheric pressure of nitrogen gas.

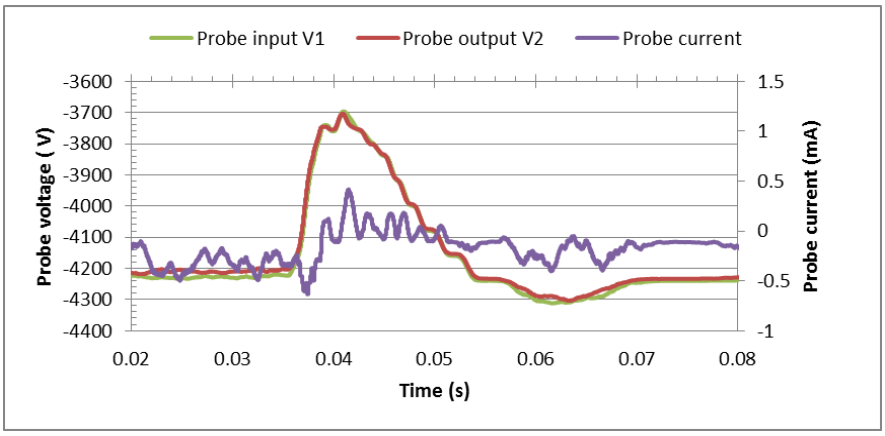

Figure 5.7b shows increase in the applied negative after fault current zero.

It was shown in sub-section 4.2.3 (leakage current detection) that experiments were carried out to detect leakage current in dry air when no impressed arc current and in section 5.2 (experimental result), the results show leakage currents detected and measured. And, section 6.2 (current variation in dry air) discussed the current flow before dielectric breakdown at no fault current. These explain the typical characteristic of the gases' behaviours in an electric field. When the arc current was discharged, it results in an increase in the leakage (probe) current flow (i.e., weakened dielectric strength and breakdown of dielectric strength) and then followed by dielectric recovery. These were repeated in dry air, nitrogen and sulphur hexafluoride to justify that the leakage current obtained were not noise measurements.

The heat generated due to the arc in the interrupter is in-homogeneous; this might lead to positive and negative rise in the probe current flow.

5.3.1.2.2 0.5 bars of Nitrogen Gas

Figure 5.8a shows the arc current, voltages V1, V2 and the derived dielectric current for 0.5 bars of nitrogen gas. The probe current flow through the gas is positive at about 0.58mA within the period of 0 to 0.036s before arcing commenced, but increased in negative value when the arc was initiated to about -1.13mA at 0.036s. It lasts for a while before commencing a decrease in the value of about 0.35mA at 0.41s after the peak arcing fault current period. An oscillatory

waveform of probe current lasted for 5ms before the fault current zero periods. It may signify a non-uniform hot gas from the arc is mixing with the nitrogen gas, resulting in the variation in the probe current flow. This period shows the weakened dielectric strength of the probe in the gas, which is similar in trend to that in nitrogen gas at atmospheric pressure. At post-current zero periods, there is a small decrease in the probe current from 0.87mA at 0.046s to approximately 0.58mA at 0.047s. In addition, there was another increase in negative value of -1.14mA at 0.052s, followed by a decrease in its value to 0.58mA at 0.056s. Between 0.059s and 0.074s, there was a small increase and a decrease in the probe current flow before it returned to its initial value. The large increase in negative value in probe current at 0.052s might be due to spikes from the ignitron during the dump of residual energy from the capacitor bank to the experimental earth. Within the periods 0.059s to 0.074s, the probe current flow may be due to the remnants of the hot gas remaining in the nitrogen gas since the arcing current is zeroed.

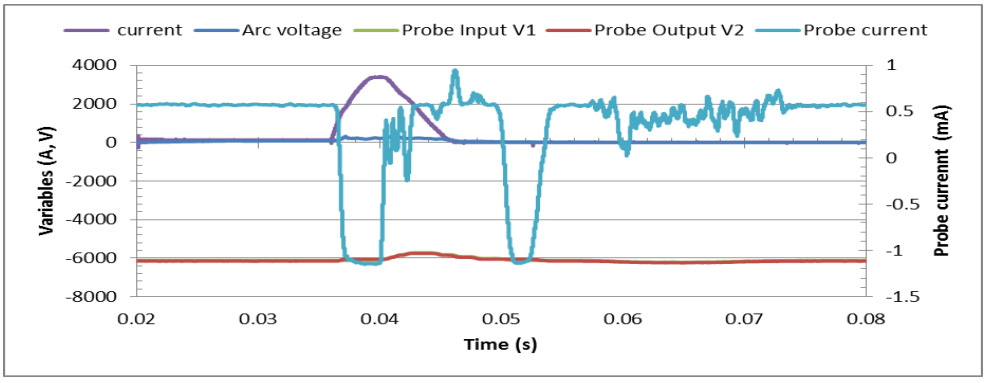

Figure 5.8a shows the graph of the arcing periods in 0.5bars of nitrogen gas.

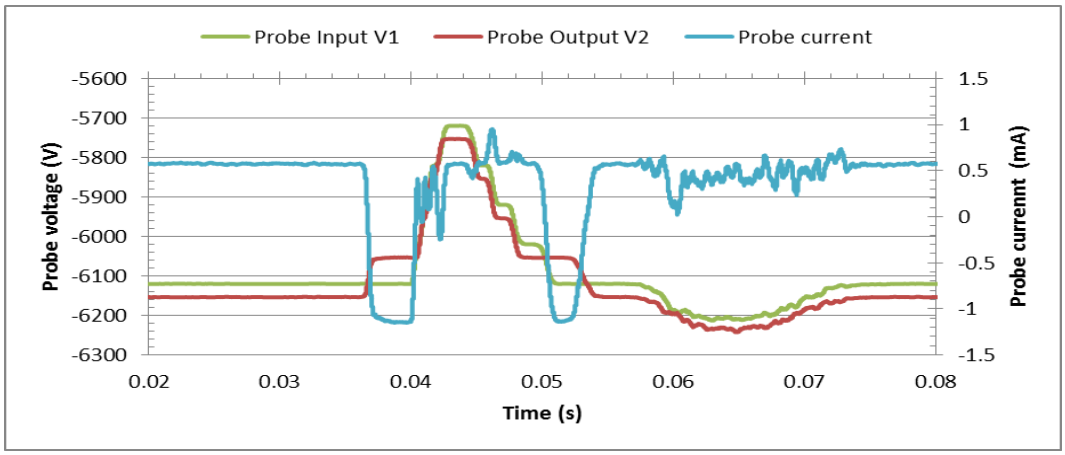

Figure 5.8b shows the graph voltages (V1, V2) and the probe current for 0.5 bars of nitrogen gas.

Figure 5.8b is a detailed illustration of figure 5.8a as discussed previously. The figure shows the reduced negative voltage drop during the weakened dielectric strength for 0.5bar of nitrogen (between 0.0366s and 0.0466s), an increase in the negative voltage at post current zero (from 0.0466s to 0.08s) and the probe current flow during these periods.

5.3.1.2.3 1.0 bar of Nitrogen Gas

Figure 5.9a shows the arc current, probe voltages (V1, V2) and the probe current for 1.0 bar of nitrogen gas. The probe current flow through the gas is negative before the arc commenced, but, on initiating the arc, the current flow increased in positive value. The current flow has a complex trend of positive current flow during the arcing of the fault current period (within 0.038s and 0.048s) and, in the post-current zero periods (from 0.048s to 0.08s), followed by the return to its previous value. Within the arcing of the fault current and post current zero periods, there are continuous increases and decreases in probe current flow. This may indicate the period the heat from the arc is diffusing in the nitrogen gas. In addition, the rise in the probe current flow signifies that the dielectric strength of the probe weakens in the gas.

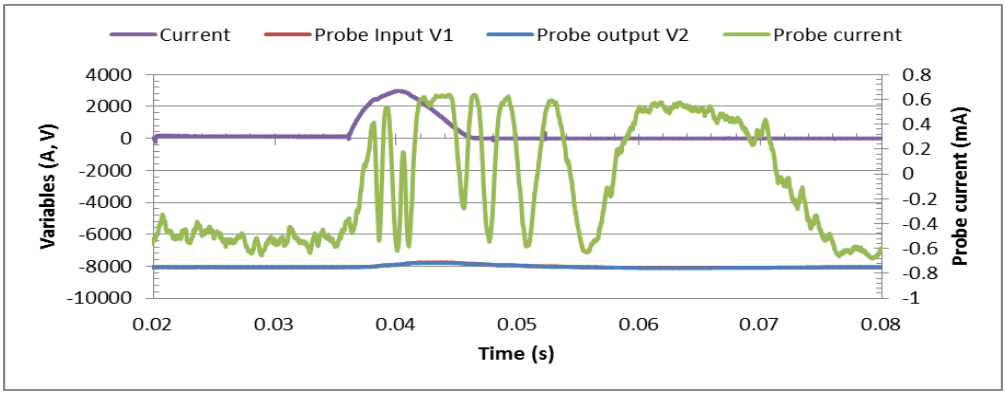

Figure 5.9a shows the graph of the arcing periods for 1.0 bar of nitrogen gas.

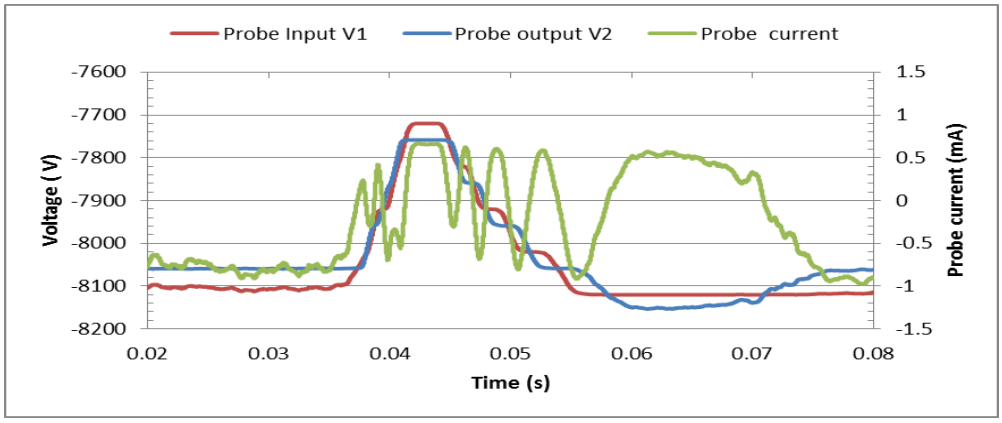

Figure 5.9b presents the graph probe voltages (V1 and V2) and the probe current for 1.0 bar of nitrogen gas.

Figure 5.9b illustrates figure 5.9a in more detail, showing probe voltages V_1 and V_2 and probe current before, during and after the fault current arcing periods. Specifically at 0.044s, the maximum of the weakened dielectric strength occurs and the maximum of the probe current flow of about 0.65mA flows in the dielectric medium. As in the previous figure, this an increase in the applied negative voltage and the derived current in the post current zero periods is seen between 0.057 seconds and 0.077 seconds in the figure 5.9b.

5.3.1.2.4 1.5 bars of Nitrogen Gas

Figure 5.10a shows the arc current, voltages (V1 andV2) and the derived dielectric current for 1.5 bars of nitrogen gas. The probe current flowing through the gas also shows a negative value

of about -0.38mA before the arc commenced but increased in negative value to about -0.99mA at 0.037s seconds during the arc initiation. This continues by decreases and increases in the negative value within the arcing periods. This is an indication of weakened dielectric strength of the gas in the arc.

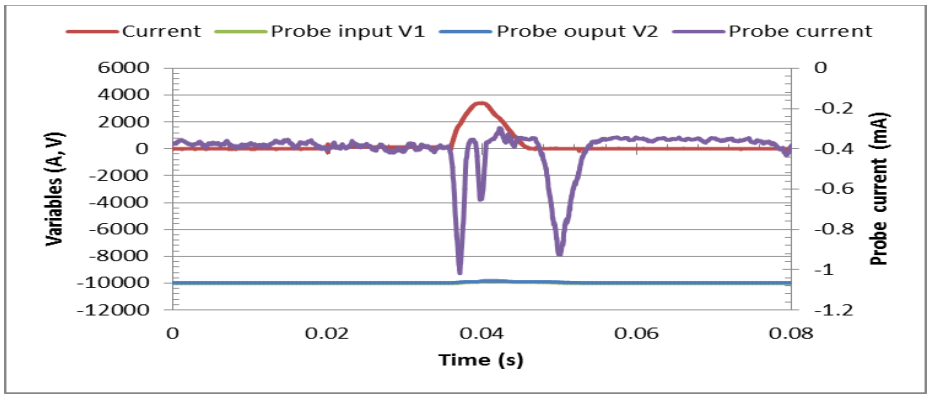

Figure 5.10a shows the whole of the arcing periods for 1.5 bars of nitrogen gas.

At extinction of the fault current, there is a rise in the negative probe current flow to -0.92mA at 0.05s, followed by a recovery to its previous state. The current flow at this point might be due to the spike from the ignitron dump of residual energy from the capacitor bank to earth.

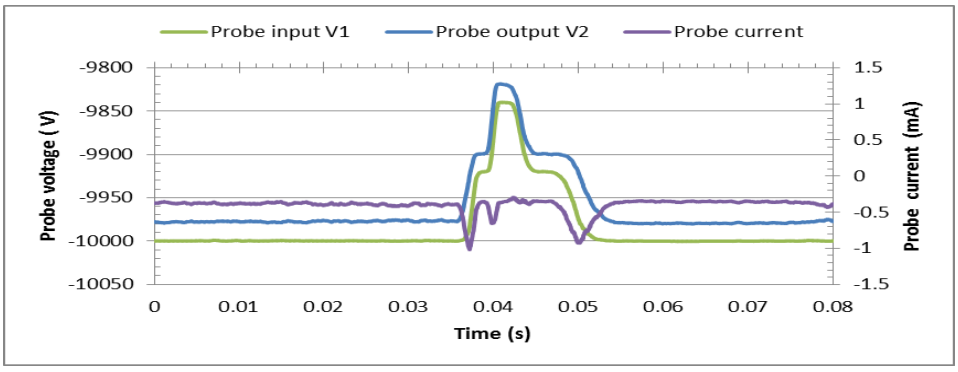

Figure 5.10b shows the graph voltages (input V1 and output V2) and corresponding probe current for 1.5 bars of nitrogen gas.

Figure 5.10b shows figure 5.10a in more detail, showing the applied voltages V_1 and V2 across the limiting resistor and the corresponding probe current during the completely arcing periods. It shows reduced voltage drops and an increase in the negative probe current during the weakened dielectric period of the gas at 0.037s, the point of initiation of the fault current as explained above. As in figures 5.8b and 5.9b, where there was an increment in the applied negative voltage after the fault current was extinct. Figure 5.10b shows an increment in the applied negative voltage with the corresponding probe current flow during the post-current zero periods, though smaller in value.

5.3.1.2.5 2.0 bars of Nitrogen Gas

Figure 5.11a shows the arc current, voltages (V1, V2) and the derived dielectric current for 2.0 bars of nitrogen gas. In this case, the probe current flowing through the gas is positive (0.33mA at0.037s) before the commencement of the arc at 0.036s but increased in positive value to 0.65mA at 0.04s. The current flow recovered to about 0.33mA at 0.0428s and then continued to increase and decrease in negative values to -0.93mA at 0.045s and 0.33mA at 0.048s in the post-current zero periods. These signify the dielectric weakened periods in the gas. There is a rise in positive probe current to 0.91mA at 0.051s, which might be due to highly ionised particles, electromagnetic energy or/and to ignitron dump. This is followed by a small oscillatory probe current flow before final recovery period at 0.08s. The current flow at this point may be due to the retained hot gas from the arc in the nitrogen gas after current zero periods resulting ions dissociation and current flow in the dielectric medium.

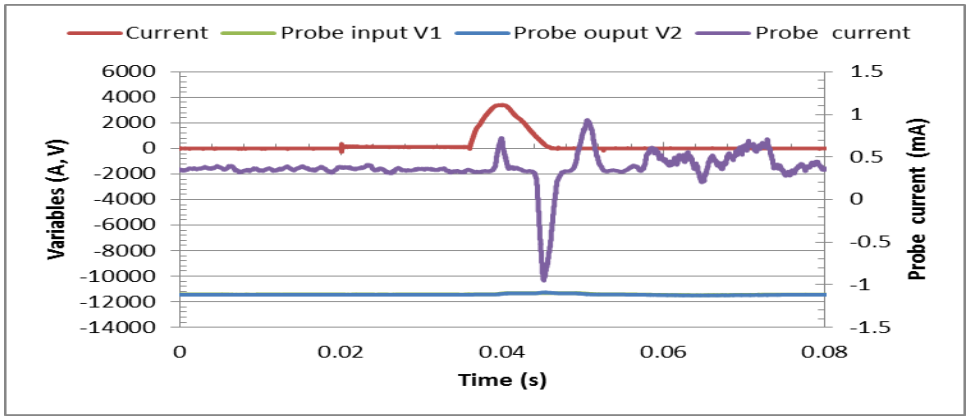

Figure 5.11a shows the whole of the arcing periods in 2.0 bars of nitrogen gas.

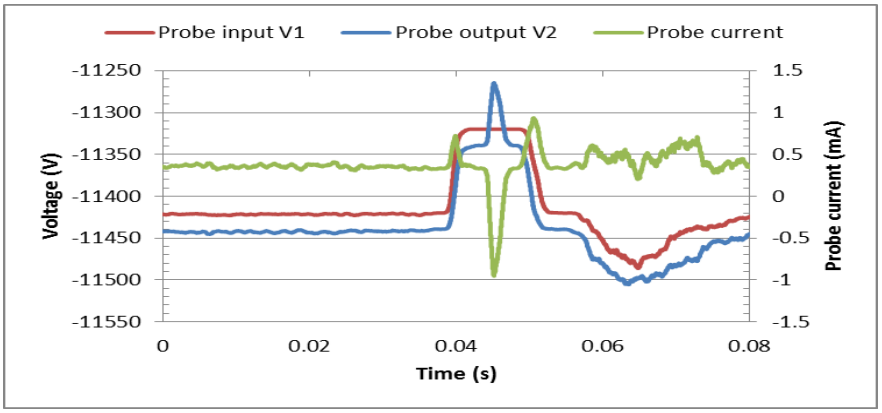

Figure 5.11b shows the graph probe voltages (V1 and V2) and corresponding probe current for 2.0 bars of nitrogen gas.

Figure 5.11b shows probe voltages (input V1 and output V2) across the limiting resistor and the corresponding probe current before, during and after arcing periods. It shows a more detailed analysis of figure 5.11a. The applied negative voltage shows an increase in its value just immediately at the end of the fault current arcing period as seen between 0.051seconds and 0.08 seconds, before returning to its initial state. It shows a similar trend as can be observed in the previous figure such as figures 5.7 and 5.8.

5.3.1.3 Dielectric Probe Orientation in Nitrogen Gas Results

Results from tests probing current-carrying capacity of dielectrically weakened gas when the dielectric probe is oriented to 0^0 (figure 5.12a) and 90^0 (figure 5.12b) are reported. The orientation of the probe is changed to understand the effect that this has on its response. The aim of this work is to detect and compare the probe (low) current flowing during the hot gas in nitrogen gas when the probe is oriented to 0^0 (figure 5.12a) and 90^0 (figure 5.12b) during the arcing current periods. Figures 5.12a and 5.12b show the directions of 0^0 and 90^0 orientations of the dielectric probe as coupled to the circuit breaker. The experiments are carried out in nitrogen at gas pressures between 0.0 bar to 2.0 bar, at 0.5 bar steps with a voltage set between -4kV to -9kV applied to the dielectric probe when a positive half cycle (fault) current of about 3kA peak is passed through. At current zero, recombination is taking place and local thermal equilibrium exists such that there are equivalent amounts of ions and electrons. The post-current zero is the period immediately after the fault current is extinct. Immediately after current zero, a voltage stresses the gap between the arcing electrodes, post-arc current can flow, and a low current is formed. The dielectric probe may detect the re-ignition of the arc through its response to dielectrically weakened gas. The low arc current will create ions from the test gas (nitrogen gas) which will result in probe current flow and weakened dielectric strength in the dielectric medium.

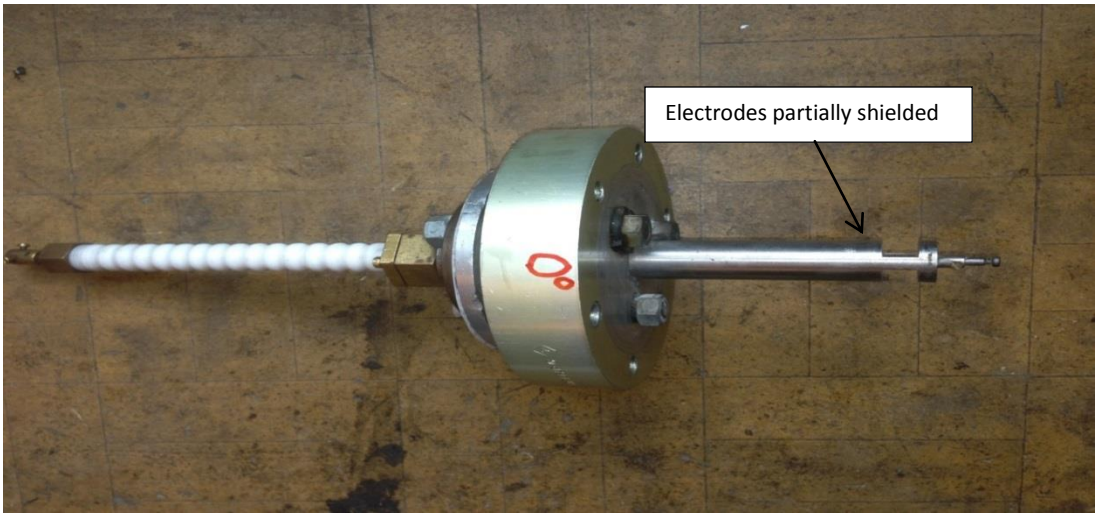

Figure 5.12a shows dielectric probe at 0-degree orientation position.

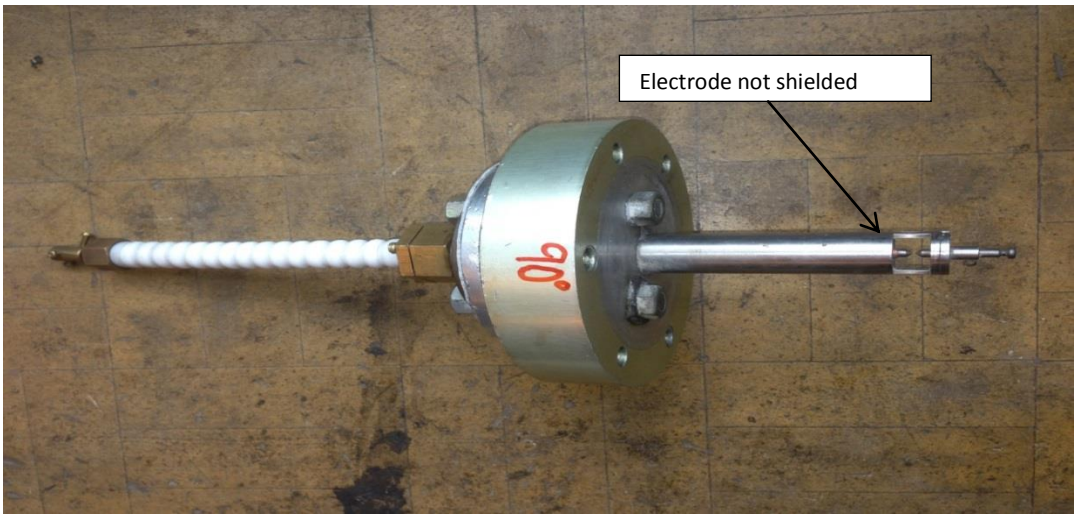

Figure 5.12b shows dielectric probe at 90-degree orientation position.

5.3.1.3.1 Result for 0 bars of Nitrogen Gas

Figures 5.13a and 5.13b show the result of applied half-cycle AC (fault) current of about 3kA at 50Hz producing an arc voltage in the circuit breaker in nitrogen gas at 0.0 bar with a negative high voltage DC applied to the dielectric probe which is oriented at either 0^0 or 90^0. Section 6.3.1.3 presents the discussion of these results and shows the results of the whole dielectric probe

response to low current flow in dielectrically weakened nitrogen gas at 0^0 and 90^0 orientation with an arc current of about 3kA peak.

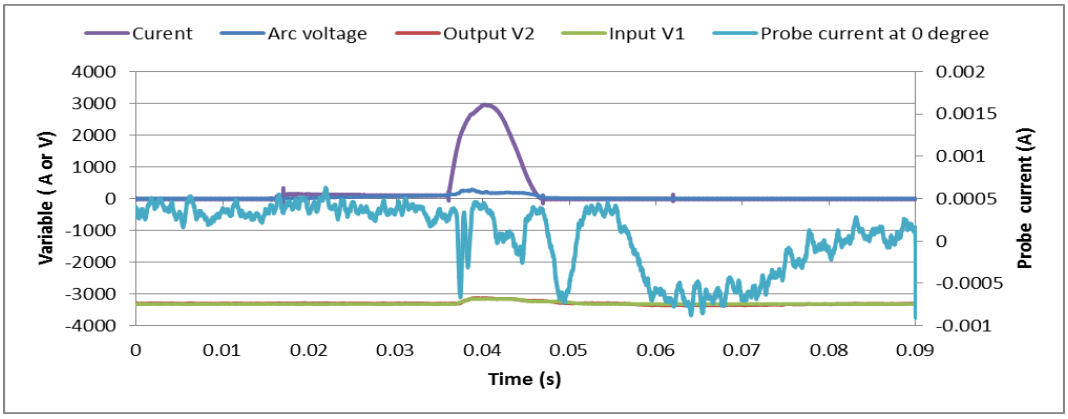

Figure 5.13a shows fault current, arc voltage, low current detected, probe voltages (V1 and V2) across the limiting resistor at 0^0orientation of the dielectric probe.

At 0^0 orientations, figure 5.13a shows the derived current passing through the dielectric probe before, during and after the trigger period of the arcing fault current. Between 0.0 seconds and 0.037 seconds, there is an average leakage current of about 0.19mA. This is followed by a trigger period that shows negative increase and decrease in the derived current that passes through the dielectric probe. It shows the complex and variable response of the dielectric probe during the discharge, followed by the post-current zero periods that starts at 0.047s. The probe current flow indicates the commencement of dielectric strength-weakened periods of the probe for 0.0bar of nitrogen gas. Within the period 0.047s to 0.06s, the probe current increases and decreases to the value of 0.37mA and -0.61mA, this is followed by a recovery toward its initial value. The current flow might be due to the retained hot gas in the nitrogen gas after fault zero.

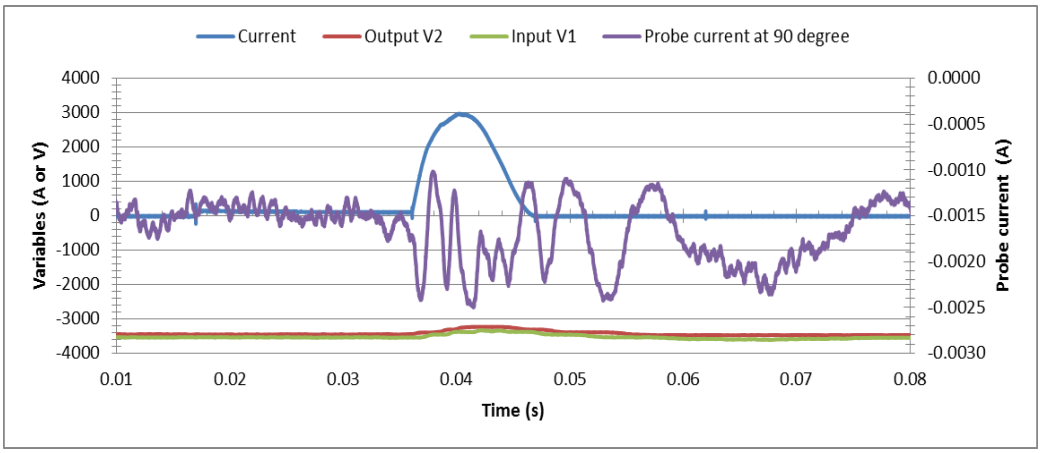

Figure 5.13b shows fault (current), probe current flow, probe voltages (V1, V2) across the limiting resistor for 90° orientation of the dielectric probe.

For 90^0 orientations, figure 5.13b shows the derived current passing through the dielectric probe. The current flow is at the average current of -1.5mA within the time of 0.0 seconds to 0.0356 seconds and then followed by periods between 0.0356 seconds and 0.047 seconds commencing with an oscillatory probe current. This period shows the complex and variable response of the dielectric probe, followed by the post-current zero periods between 0.047 and 0.08 seconds that shows an increase and decrease in the probe current flow in this period. In addition, the directions of current flows are in anti-clockwise directions, which may be because the V1 is less negative than V2 and may depend on the condition of the circuit. The result of orientations are discussed in sub-section 6.3.1.3.1

5.3.1.3.2 Result in 0.5 bars of Nitrogen Gas

Figures 5.14a and 5.14b show the results for 0^0 and 90^0 orientations for a fill pressure of 0.5 bars of nitrogen gas under similar conditions as in the previous test.

The probe current flowing through the dielectric probe at both orientations before the arc shows initial time-varying current flow at these periods.

However, during the trigger for 0^0 orientations shows increase and decrease in the probe current flow in the positive value between 0.036 seconds and 0.048 seconds. This arcing fault current period resulted in weakened dielectric strength of the probe in the gas. This is followed by an increase in negative current flow of -0.18mA from 0.048 seconds towards 0.054 second, and then continued to decrease to 0.99mA at 0.065s and finally returned to its previous value at 0.08s. These periods are termed post-current zero with arcing current extinguished.

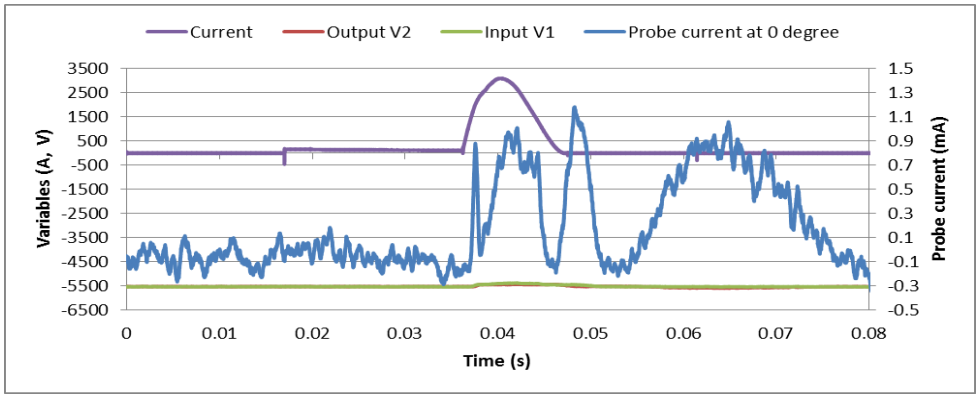

Figure 5.14a shows fault current, probe current detected, probe voltages (V1 and V2) across the limiting resistor at 0^0 orientation of the dielectric probe.

The probe current flow at these periods may be due to either ignitron dumps of residual energy and/or due to the remnant hot gas from the arc in nitrogen gas after current zero. The direction of probe current flow is clockwise and may be due to the influence of the voltages polarities and the state of the circuit. In the case of 90^0 orientations within the 0.0 second to 0.036 seconds, shows a probe current of about -0.11mA. During the arcing period, the probe current flow increased to 0.28mA at 0.038s, decreased to -0.55mA at 0.039s and then increased to 0.14mA at 0.048s at fault current zero periods.

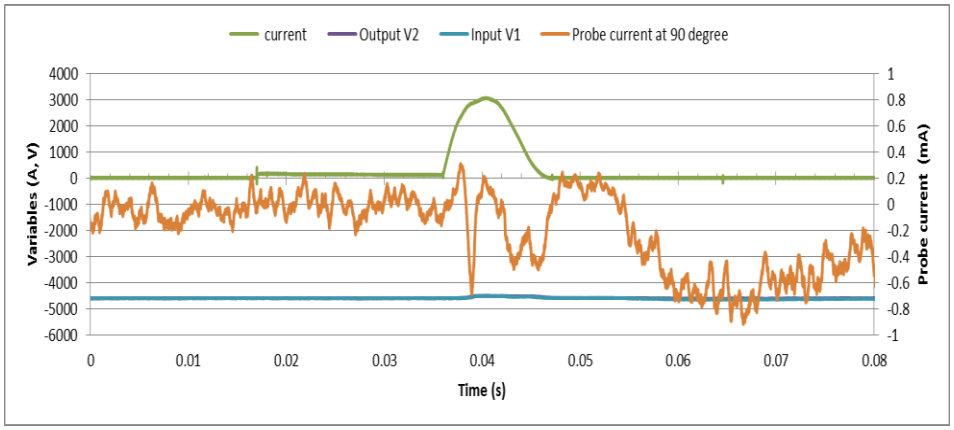

Figure 5.14b shows fault current, low residual current detected, probe voltage (input V1 and output V2) from the limiting resistor at 90° orientation of the dielectric probe.

This probe current continues into the post-current period with a gradual reduction to -0.89mA at 0.067s before turning to the previous value at 0.08s. The large probe current flow at the arcing period signifies weakens dielectric of the nitrogen gas. During the post-current zero, an increase in negative probe current flow is shown. These might be due to the same reasons stated during the 0^0 orientation. The direction of probe current flow is counter-clockwise and may be due to V1 being more negative than V2. The discussion of the combined graphs of both orientations is in sub-section 6.3.1.3.2

5.3.1.3.3 Result in 1.0 bar of Nitrogen Gas

Figures 5.15a and 5.15b show the results for 1.0 bar fill of nitrogen gas at the same conditions for 0^0 and 90^0 orientations obtained respectively.

Both probe currents passing through the dielectric probe have initial small varying positive and negative values before the arcing current at about 0.032 seconds. At this point for 0^0 orientation, the probe current starts increasing negatively to about -0.65mA at 0.036s and then decreases in value to about 0.31mA at 0.039s. Between 0.039s and 0.048s, there is an oscillatory probe

current flow in the fault current arcing periods; this continued up to 0.052s in the post-current zero periods before regaining its initial values towards 0.08s. The increase in the negative probe current between 0.032s and 0.036s may be due to the arcing quasi-current before the arcing fault periods where the probe current increases positively. These caused the dielectric weakness of the nitrogen gas. In the post-current zero periods, the rise in probe current may be due to the ignitron dump and the retained hot gas from the arc in the nitrogen gas after the fault current has stopped arcing. In addition, V1 is more negative in value as compared to V2 and the state of the circuit which determines the probe current flow in a counter-clockwise direction at this period.

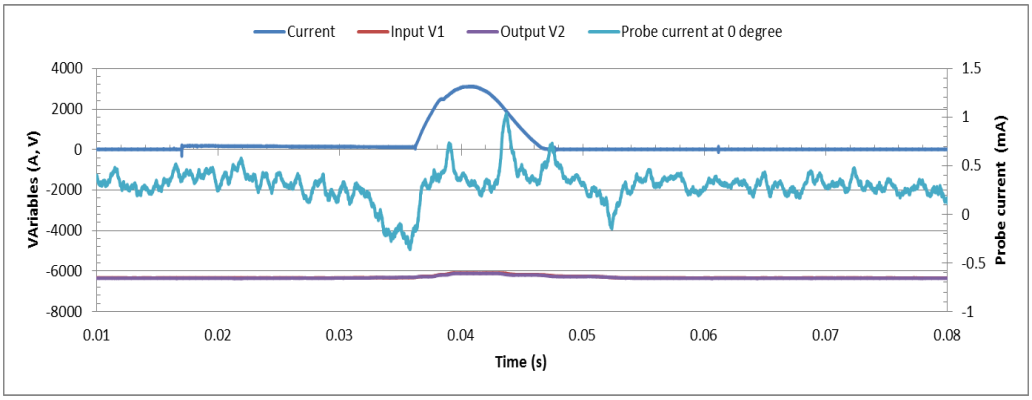

Figure 5.15a shows fault current, probe current, and probe voltages (V1and V2) across the limiting resistor for 0^0 orientation of the dielectric probe.

For 90^0 orientations, the probe current starts increasing positively from 0.21mA at 0.037s to 0.68mA at 0.039s and back to 0.25mA at 0.042s. The probe current flow shows a small increment of about 0.33mA at 0.045ms and a decrease to 0.25mA at 0.048s before rising to 0.91mA at 0.052s in the post-current period, followed by regains of the current flow to its initial value at 0.08s. As previously, the dielectric weakness of the nitrogen gas commences within the period of 0.037s to 0.048s and caused by the arc discharges. Then, in the post-current zero periods (0.048s to 0.08s), there is an increase and decrease in the probe current flow that might

be due to the ignitron dump and the hot gas retained in the nitrogen gas just immediately after fault current zero. The direction of probe current flow is clockwise which signifies that V1 is less negative than V2 and may depend on the circuit. The combined figures 5.15a and 5.15b are discussed in sub-section 6.3.1.3.3.

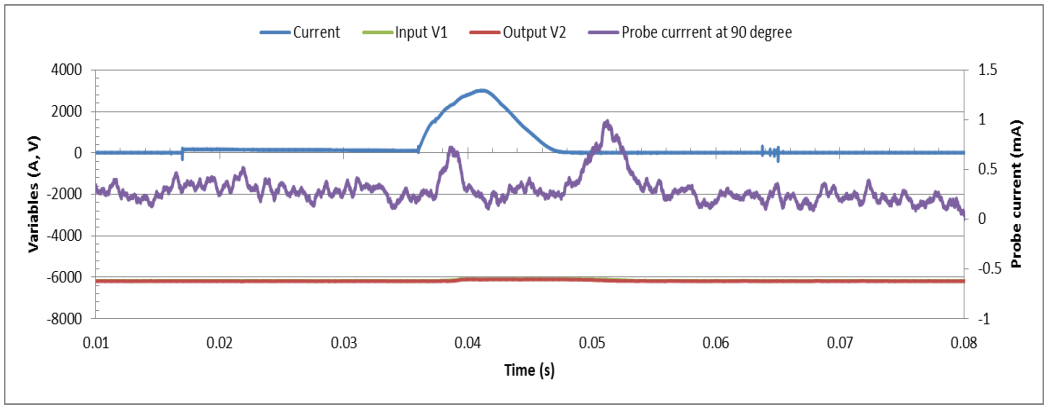

Figure 5.15b shows fault current, probe current flow, probe voltages (V1and V2) across the limiting resistor at 90^0 orientation of the dielectric probe.

5.3.1.3.4 Results in 1.5 bars of Nitrogen Gas

Figures 5.16a and 5.16b show the results for 0^0 and 90^0 orientation tests conducted for 1.5 bars of nitrogen gas within the same the experimental conditions as previously discussed respectively. Both results have approximately the same initial values of probe current flowing through the dielectric probe except at about 0.031 seconds, just before the trigger period where the probe currents flowing start showing differences in current flow magnitudes.

For 0^0 orientations, figure 5.16a shows probe current increase from -0.27mA at 0.031s to 0.26mA at 0.036 seconds followed by -0.52mA at 0.037s. This is followed by a small increment of -0.35mA at 0.038 seconds before increasing from -0.49mA at 0.04 seconds to about 0.57mA at 0.043 seconds and then decreasing to -0.56mA at 0.0476 seconds during the arcing period. In the post-current zero periods, immediately after current zero, there is an increase and decrease in

the probe current flow to 0.4mA at 0.052 seconds and -0.67mA at 0.059 seconds before a return toward the original value. As discussed previously, the arcing period causes the dielectric weakness of the nitrogen gas. The increase and decrease of the current flow during the post-current zero might also be due to the ignitron dump and/or the retention of the hot gas from the arc in the nitrogen gas after fault current zero. At this point, V1 is more negative than V2; hence, the current flow is in a counter-clockwise direction.

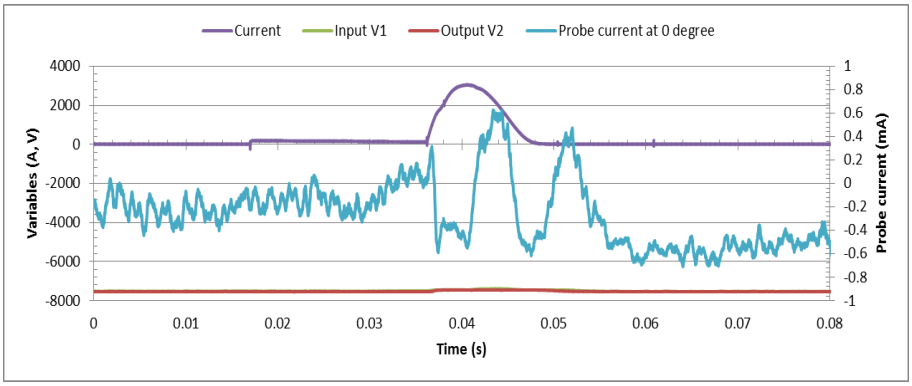

Figure 5.16a shows fault current, probe current flow and probe voltages (V1, V2) across the limiting resistor for 0^0 orientation of the dielectric probe.

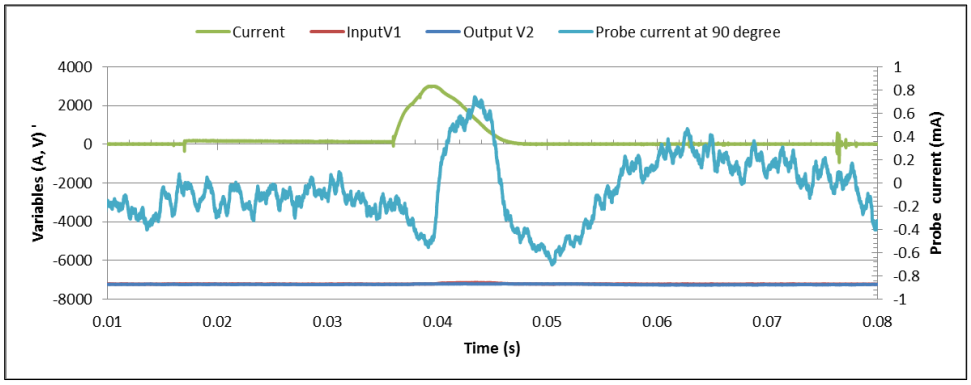

Figure 5.16b shows fault current, probe current detected, probe voltages (V1, V2) across the limiting resistor for 90^0 orientation of the dielectric probe.

For 90^0 orientations as shown in figure 5.1.6b, probe current also decreases from 0.16mA at 0.037 seconds to –0.49mA at 0.04 seconds and then increases to about 0.67mA at 0.044 seconds.

At this point, the current flow starts increasing and decreasing. It starts from -0.61mA at 0.05 seconds to 0.44mA at 0.062 seconds, before returning to its earlier value at 0.08s. The upsurge and reduction in the probe current flowing through the dielectric probe during the arcing period is an indication of dielectric weakness of the nitrogen gas. In addition, after fault current zero, there is current flow. As previous, this might due to spikes from the ignitron dump and/or residual heat retained in the nitrogen gas during the arcing period. Moreover, the current flow direction is clockwise at this period. This implies that V1 is less negative than V2 in polarity. Sub-section 6.3.1.3.4 presents the discussions of the combined orientations.

5.3.1.3.5 Results in 2.0 bars of Nitrogen Gas

Figures 5.17a and 5.17b show the results for the 2.0 bars of nitrogen gas test with dielectric probe orientations for 0^0 and 90^0 under the same experimental conditions. Both figures show a similar trend in varying probe current with time, between 0.0 to 0.026 seconds before the arcing current. Immediately after this period, both currents have different details.

For 0^0 orientations, the probe current increased negatively from -0.18mA at 0.036 seconds to 0.75mA at 0.037 seconds and then continued to increase and decrease up to -0.82mA at 0.05 seconds during the arcing fault current periods. This was followed by an increase to 0.25mA at 0.053 seconds and decrease to -0.92mA at 0.064 seconds, before return towards its initial value at 0.08 seconds in the post-current zero periods. As before, the rise in the probe current flow signifies the weakened dielectric strength of the dielectric probe in gas.

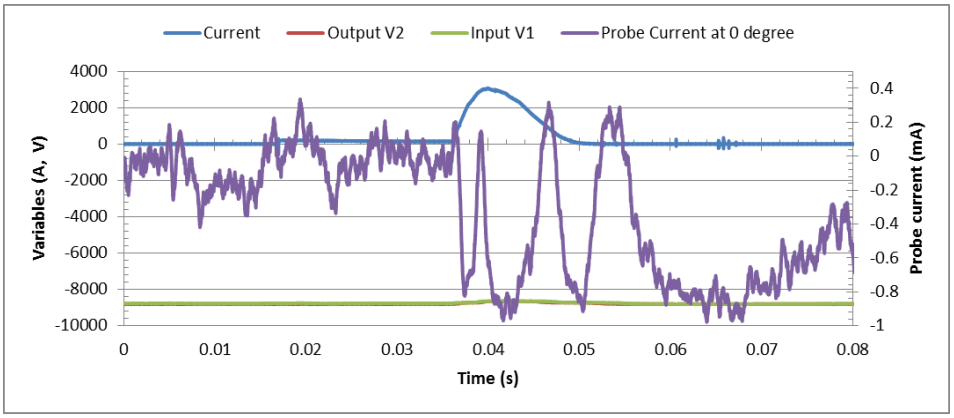

Figure 5.17a shows fault current, probe current and probe voltages (V1, V2) across the limiting resistor for 0^0 orientation of the dielectric probe.

In the post-current zero periods, the rise in the probe current might be due to the residual energy from the ignitron dump and/or hot gas retained in the nitrogen gas after fault current zero. At this period, the V1 is more negative than V2 in polarity causing the probe current flowing in a counter-clockwise direction.

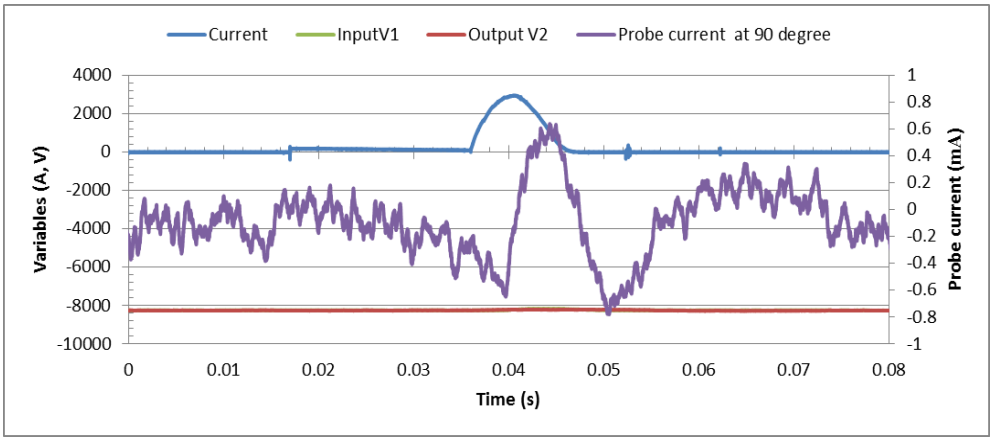

Figure 5.17b shows fault current, probe current, and probe voltages (V1, V2) across the limiting resistor for 90^0 orientation of the dielectric probe.

During the arcing period, the probe current had a negative value of -0.62mA at 0.04 seconds as in figure 5.17b for 90^0 orientations. This is followed by an increase to 0.55mA at 0.045 seconds before fault current zero periods. At arc current zero, there is another increase and decrease in

negative probe current flow to -0.68mA at 0.051 seconds and 0.3mA at 0.065 seconds before a return to its previous value. The current flow during the arcing period is an indicator of weakened dielectric strength of the probe during the arc discharge in the gas. The current flow during the post-current zero periods might be due to the residual energy from the ignitron dump to the earth and the probe current is flowing in a clockwise direction, meaning V1 is less negative than V2 at this point in time. Sub-section 6.3.1.3.5 presents discussion of both orientations.

5.3.2 Probe Current in Dry Air

This section reports the result of low current flowing through the dielectric probe during the arcing period in dry air. The research is to study and find the dielectric probe response to probe current flow during dielectrically weakened dry air. The test conducted in dry air of zero bar of pressure with a negative DC voltage set between -4.5kV to -5kV applied to the dielectric probe when a positive half-cycle AC current of about 3kA peak passed in the dry air locality. The dielectric probe gap is set at 1.5mm and then coupled into the test circuit breaker at the same experimental conditions as discussed in the previous sections (i.e., in nitrogen gas test). The reduced dielectric strength of the gap is present in terms of voltage drops across the limiting resistor and probe current flowing through the dielectric probe during the dielectric weakened period in the dry air as shown in figure 5.18a. Repeating the tests at 0.5 bar increments within the same test conditions did not achieve the weakened dielectric strength in subsequent readings. Sub-section 5.4.2.1 presents the typical results of the test.

5.3.2.1 Results in 0 bars of Dry Air

Figure 5.18a presents the results for 0.0 bars of dry air showing the AC fault current, arc voltage, probe voltages (V1, V2) into the dielectric probe, and the probe current flow during the test. The probe current flow response of the dielectric probe is positive in value before the fault current begins and then goes to negative and positive values during the arcing period of the fault current.

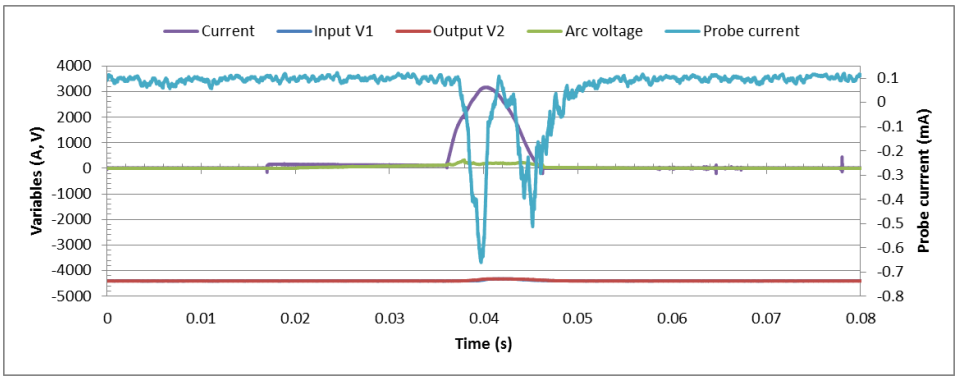

Figure 5.18a shows half AC fault current, input and output voltages, arc voltage and low current flow in dielectric of dry air at atmospheric pressure.

This is immediately followed by the recovery of the probe current to its previous state after the fault current has been extinguished at about 0.046 seconds. The figure also shows reduced applied negative voltages at this period. Figure 5.18b illustrates the input and output voltages across the limiting resistor applied to the dielectric probe before, during and after the arcing fault current periods. It shows the reduced voltage drop during the peak period of the arcing fault current at about 0.041 seconds.

Figure 5.18c shows the result of the complete arcing periods of dielectric probe response to low current flow; it is made of pre-trigger initiation period (A-B), trigger initiation period (B-C),

arcing period (C-D) and post-current zero periods (D-E). The section of 6.3.2 presents the detailed discussion of this figure.

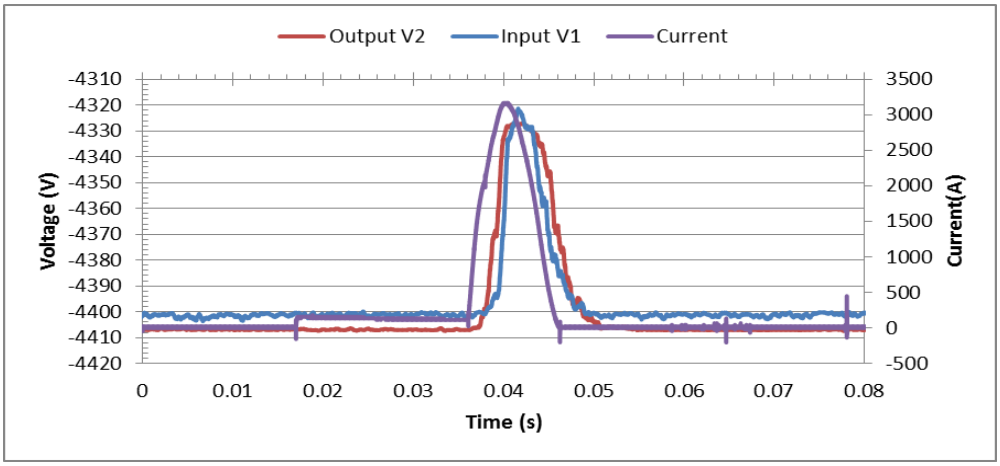

Figure 5.18b show the completely arcing fault current period with the corresponding voltage drop for dry air of atmospheric pressure.

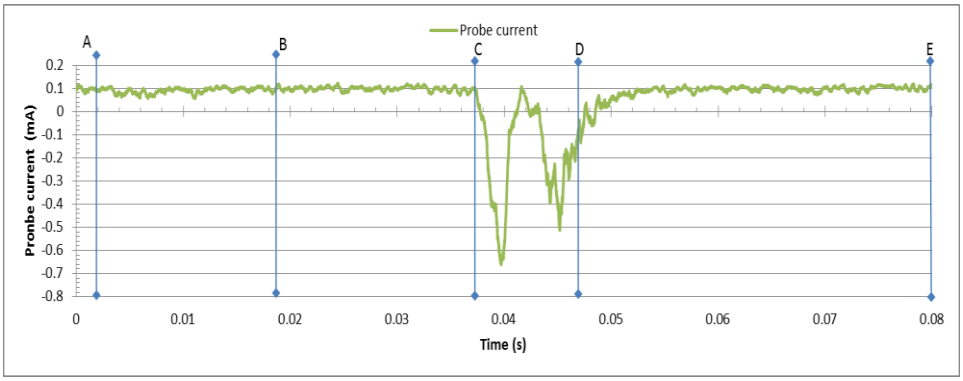

Figure 5.18c shows the probe (low) current flow through the dielectric probe for dry air at atmospheric pressure.

5.3.2.2 Results in 0.5 to 2.0 bars of Dry Air

Repeating the experiment for 0.5 to 2.0 bars in dry air did not show the reduced dielectric strength as seen in the previous tests. As shown in figures 5.19a, typical results were obtained at the increment of dry air pressure to 0.5sbars. Figure 5.19a shows that, at 0.044 seconds, there is a change in the probe current flow in the dielectric probe from its previous positive and negative

varying values to a positive one of 0.53mA. This is then reduced to -0.29mA at 0.056s and then returns to its prior value of 2.7µA at 0.08s. However, there is an indication between 0.05 and 0.06 seconds of an increase in the negative probe current.

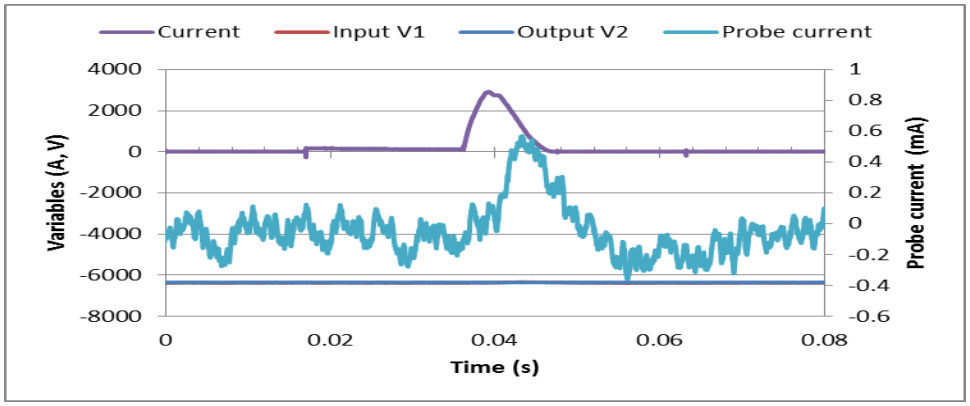

Figure 5.19a shows fault (current), probe current flow and probe voltages (V1, V2) across the limiting resistor with time.

5.3.3 Probe Current in Sulphur Hexafluoride (SF_6) Gas

The results for SF_6 dielectric strength probing using the dielectric probe with gap set at 0.5mm connected to a negative DC voltage with fault currents of about 3kA and 18.5kA passing through the gas are presented respectively. The results show dielectric breakdown (figures 5.20 and 5.22) and no breakdown (figures 5.21 and 5.23) of the gas during the arcing periods. The weakened dielectric strength has been difficult to achieve with this configuration of dielectric probe in sulphur hexafluoride gas.

5.3.3.1 Fault Current of 3.2kA in SF_6 Gas

Figure 5.20a shows the results of oscilloscope waveforms of an inverted negative DC voltage (input V1 and output V2) in volts from the limiting resistor with time applied to the dielectric probe when a fault current of about 3.2kA passed in the circuit breaker producing an arc voltage of 260V. The dielectric probe gap is set at 0.5mm with applied voltage of about -4.5kV. Figure

5.20b shows the results of Excel file waveforms of the negative DC voltage (input V1 and output V2) from the limiting resistor applied to the dielectric probe when the fault current passed in the circuit breaker produces an arc. A low residual current flow through the dielectric probe after it has broken down.

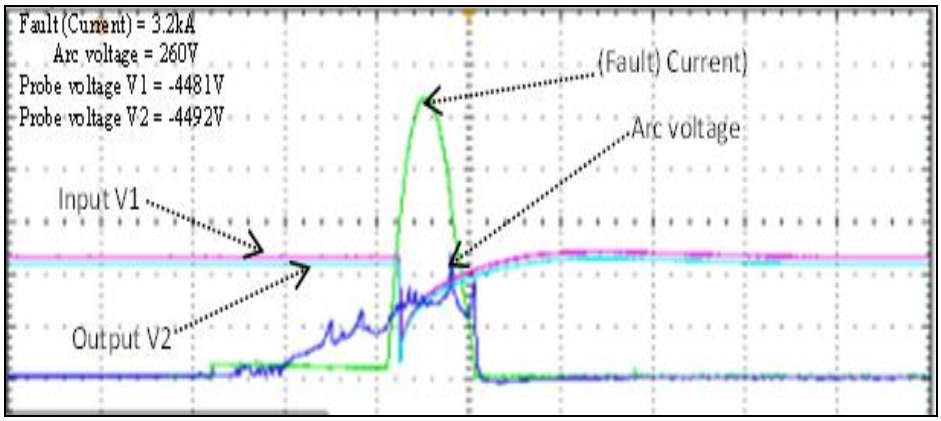

Figure 5.20a shows oscilloscope waveform results of fault current, arc voltage and an inverted negative DC voltage (V1, V2), in Volts across the limiting resistor with time.

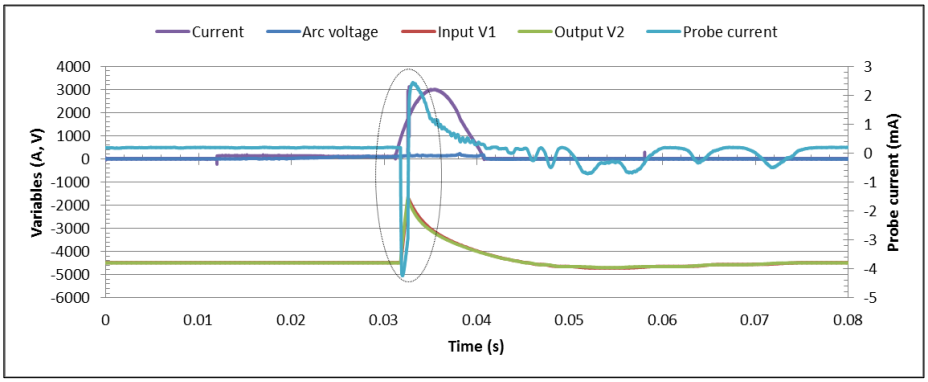

Figure 5.20b shows the results of Excel file waveforms of the fault current, arc voltage, negative DC voltage (input V1 and output V2) and low current flow though the SF_6 gas.

Figure 5.20c is a magnified Excel file of waveforms of the fault current, dielectric probe current, arc voltage and V1, V2 from the limiting resistor with time during the arcing period. As in figure 5.20c, the low probe current is detected at about 0.195mA before of 0.0316s. Then dielectric breakdown commenced with an increase in negative current of about -4mA at 0.0319s and then dielectric recovery period with maximum current detected as 2.3mA at 0.0332s. The figure also

shows a decrease in applied negative probe voltage as the dielectric probe current increases during the breakdown period and is then followed by recovery voltage as the gap of the dielectric probe recovers.

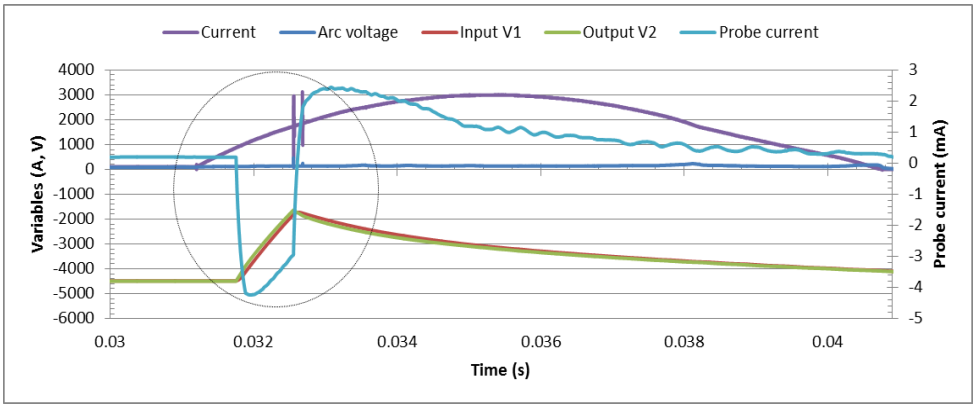

Figure 5.20c shows magnified Excel file waveforms of figure 5.20b.

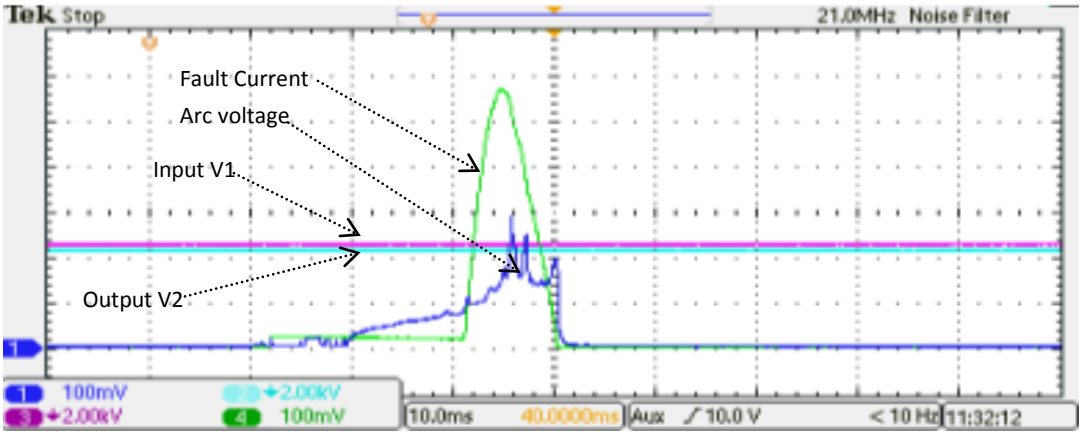

Figure 5.21a shows the results of oscilloscope waveforms of the fault current, arc voltage and V1, V2 in Volts across the limiting resistor with time at no SF_6 dielectric breakdown

Figure 5.21a shows the results of oscilloscope wave forms of V1, V2 in volts from the limiting resistor with time when a fault current of 3.2kA passed through the circuit breaker. This produces an arc with an arc voltage of about 300V. There is no dielectric breakdown of the dielectric probe in SF_6 gas as previously recorded. The dielectric probe gap is set at 0.5mm with applied voltage of about -4.5kV. Figure 5.21b shows the results of Excel file waveforms of

figure 5.21a with dielectric probe current flow through the gas. It also shows leakage in steady current of -0.447mA and there is no dielectric breakdown period detected.

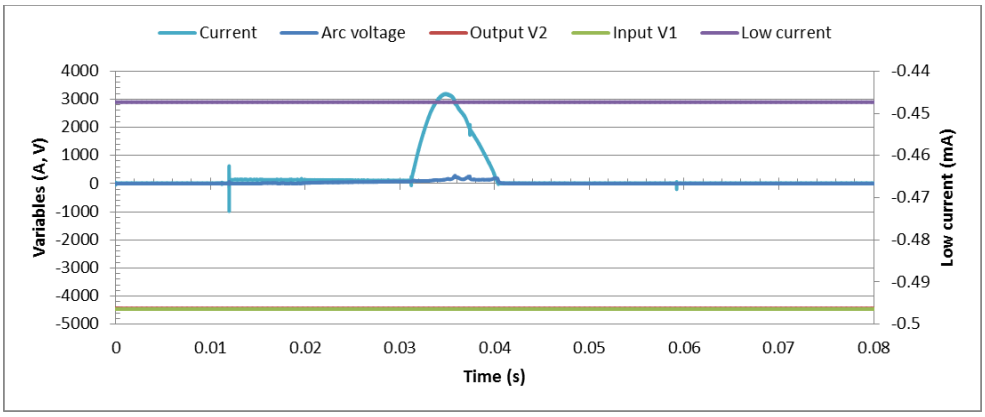

Figure 5.21b shows the results of Excel file waveforms of figure 5.21a with derived dielectric probe current flowing through the circuit breaker.

5.3.3.2 Fault Current of 18.5kA in SF_6 Gas

The experiment in section 5.3.1.5.1 was repeated with a higher positive half-cycle fault current of about 18.5kA with the results as in figure 5.22a. The results shows oscilloscope waveforms V1and V2 from the limiting resistor with time applied to the dielectric probe when a fault current of 18.5kA passed through the circuit breaker filled with sulphur hexafluoride gas at atmospheric pressure. The dielectric probe gap is set at 0.5mm with applied voltage of about -5kV. Figure 5.22b shows the results of the Excel file waveforms of V1, V2, the arcing current and the detected probe current flowing through the dielectric probe in SF_6 gas at atmospheric pressure. Figure 5.22c is a magnified result of Excel file waveforms of figure 5.22b. It also shows a probe current flow detected of about 0.73mA at 0.0396 seconds before dielectric breakdown, and then the dielectric breakdown period is followed with an increase in negative current of about -3.77mA at 0.0399 seconds. This continued with the dielectric recovery period. The figure also

shows a decrease in negative voltage as the probe current rises during the breakdown period and is then followed by the recovery voltage.

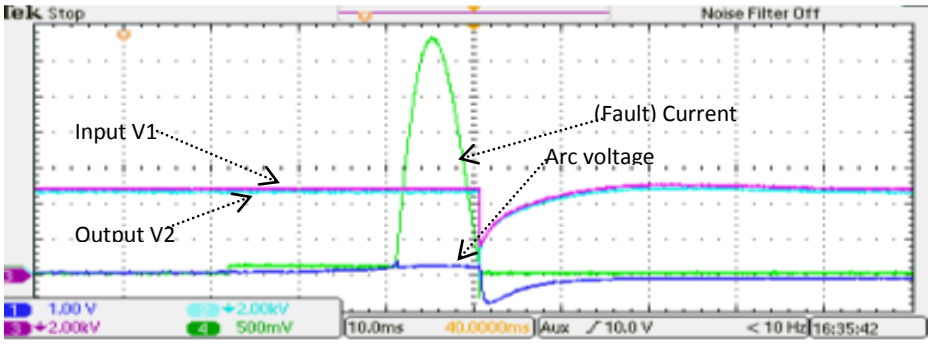

Figure 5.22a shows the results of the fault current, arc voltage and V1, V2 in Volts across the limiting resistor with time at SF_6 dielectric breakdown

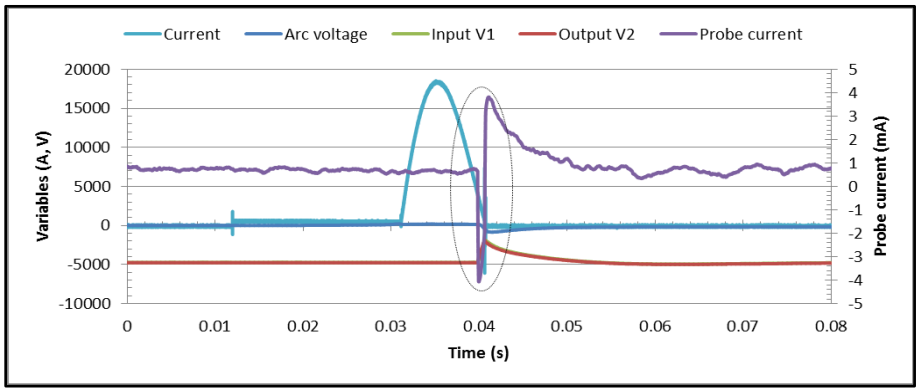

Figure 5.22b shows the results of Excel file waveforms of figure 5.22a with dielectric probe current flowing through the gas.

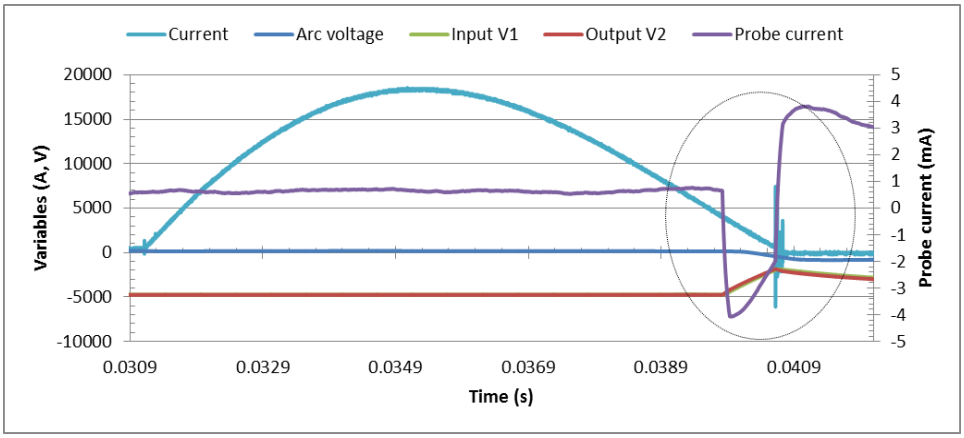

Figure 5.22c shows magnified waveforms of figure 5.22b.

Figure 5.23a shows the results of oscilloscope waveforms of an inverted V1 and V2 applied to the dielectric probe when a fault current of 18.5kA is passing through the circuit breaker.

There was no dielectric breakdown of the dielectric probe in sulphur hexafluoride gas as seen in figure 5.23a. The dielectric probe gap is set at 0.5mm with applied voltage of about -5kV. Figure 5.23b shows the results of Excel file waveforms of figure 5.23a with the leakage steady current of 0.72mA flowing through the gas and no dielectric breakdown record at this period.

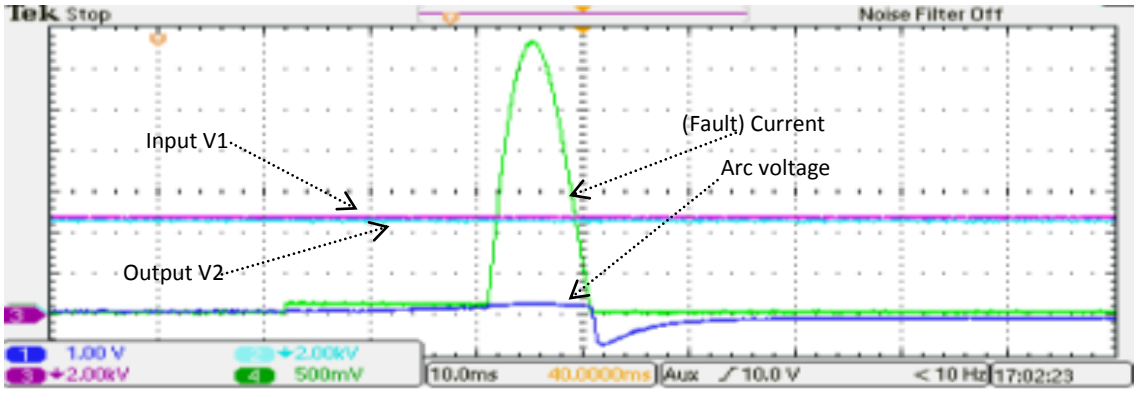

Figure 5.23a shows the results of the fault current, arc voltage and V1, V2 in Volts from the limiting resistor with time at no SF6 dielectric breakdown.

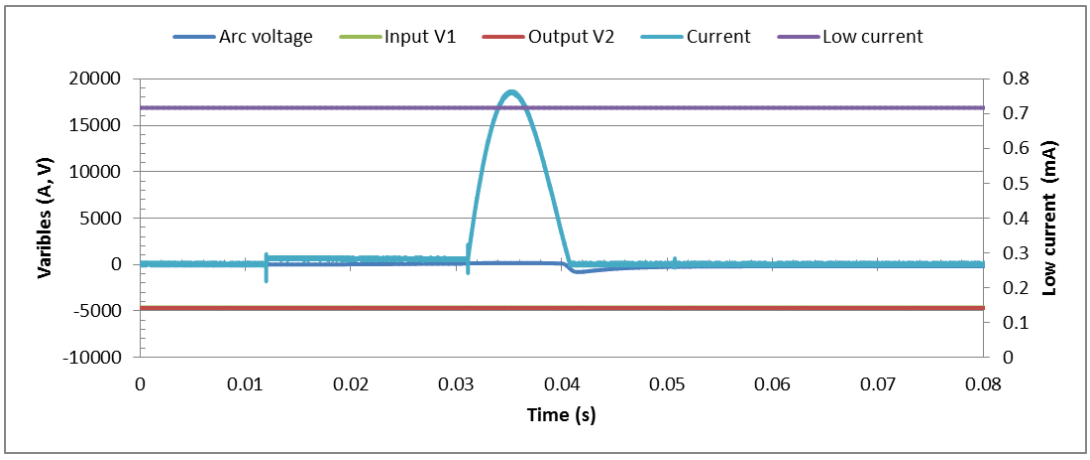

Figure 5.23b shows the Excel file waveforms of figure 5.23a with dielectric probe current flowing through the gas at no dielectric breakdown.

Figure5.24a

Figure 5.24b

Figure 5.24 compares the dielectric probe states before (figure 5.24a) and after (figure 5.24b) the usage in an arcing fault current period in SF_6-filled circuit breaker. Figure 5.24b shows decomposed particles of sulphur-fluoride gases and metal-fluoride, by-products of white powdery substances as seen during the test in SF_6 gas. These particles may be partially contributing factors to the SF_6 dielectric breakdown during the arcing period. Figure 5.25 shows the effect of the arcing current on the current-carrying electrode. The hot gas from the arc voltage may heat up the parting electrodes, resulting in the melting and wearing of the electrode as shown in figure 5.25b. Figure 5.25a shows the copper electrode before usage while figure 5.25b shows the electrode after use in the circuit breaker.

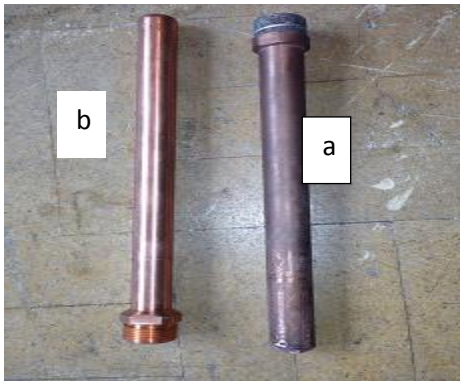

Figure 5.25

This chapter presents the test results of probing N_2 gas, dry air and SF_6 gas. A negative voltage-biased dielectric probe was used in an arcing fault current environment to investigate these gases. The chapter begins with the results of experimental components validation, which includes high-voltage power source, high-voltage probe, dielectric probe and the test circuit breaker. This was followed by the results of probe current flow for N_2 gas and probe current flow for 0^0 and 90^0 orientations of the dielectric probe at the same experimental settings. The result shows that when the fault current was passed and extinguished, the dielectric probe response to the probe current detected confirms the presence of thermal energy (hot gas) in the circuit breaker. The discussion of the direction of probe current flow is in the next chapter. The test result for dry air followed next. The weakened dielectric strength obtained only in atmospheric pressure when the probe tips were set to 1.5mm as compare to 1mm set for N_2. The result also shows a very quick recovery at the extinction of the arcing fault current. In SF_6, the results show either dielectric breakdown (figures 5.20 and 5.22) or no dielectric strength breakdown (figures 5.21 and 5.23). However, the recovery process shows a similar trend to that of nitrogen recovery when the arc was extinct. The discussion and analysis of results are in the next chapter.

Chapter 6 Results Analysis and Discussion

6.1 Introduction

This chapter presents the results, analysis and discussions of the experimental results obtained in chapter 5. It analyses and explains in detail the physical processes and behaviour of low current flow in the dielectric probe. The probe is connected to a negative high voltage DC source and is used to interrogate the insulation strength of various gases. The gas pressure is varied from 0 to 2 bars. Tests were done in the presence of an electrical discharge, aiming to determine the effect of the arc on the insulation integrity of the gases used.

6.2 Current Variation in Dry Air

Leakage current variation in the dielectric medium of dry air (section 5.1) is shown in figure 5.4b. This result was obtained with a negative voltage being applied to the dielectric probe. The graph shows a gradual increment in negative current from 0 bars to 0.5 bars which then reduces and becomes a positive current at about 1 bar. The trend then reverses and increases negatively towards the 1.5 bars as shown in figure 5.4b. The graph shows consecutive results exhibiting tests to test variation but with a consistent trend. The trends are broadly similar although their magnitudes vary. The trend behaviour is encouraging. The difference in the current magnitude may be due to changing environmental conditions (e.g., temperature, humidity and the circuit breaker chamber) all of which affect the dielectric condition of the gas. Others factors could include electrode field configuration, the nature of electrode surfaces in the probe and availability of initial species for ionisation processes[53, 55]. Researchers Frank [78] and Meek [58] have shown that leakage current (in term of sparkover voltage) increases as the pressure increases in an increasing electric field but above a certain pressure, the current starts decreasing

with increasing pressure until a critical pressure is reached due to increased space charge effect. Above the critical pressure there is a gradual rise in the discharge current with the pressure increments, confirming that the sparkover voltage above a certain maximum pressure was due to corona stabilization during field modification arising from the space charges. In addition to the critical pressure, the corona-onset and sparkover voltage coincides resulting in an increment in the sparkover voltage only slightly increasing in gap spacing. It was suggested that, within the maximum pressure, corona streamer propagation across the gap is enhanced by reduced positive-ion diffusion and secondary process is by photo-ionization at a higher gas density. These would cause the decrease in sparkover voltage and disproportionately low increase in sparkover voltage with gap spacing at high pressures [58, 78]. The tests tend to confirm the proper operation of the dielectric probe.

6.3 Probe Current in Gases

6.3.1 Nitrogen Gas

6.3.1.1 Probe Current in Nitrogen Gas

Section 5.3.1.1 describes the result of probe current flow detected in nitrogen gas from the dielectric probe biased with negative voltage during an arc event in the circuit breaker. The gas (nitrogen) in the chamber will be heated up by energy dissipated by the arc from the fault current. The arc heating will dissociate the surrounding gas, producing ions and electrons. The biased dielectric probe will attract positive ions, and because the probe is operating below the breakdown voltage then the assumption is that these positive ions are from the gas as a result of the arc. A small current flows in the probe when a positive ion is neutralised by the probe. Hence, the probe response is related to the ionised state of the gas (figures 5.5a and 5.5b). The figures are typical examples of the experiment repeated three times in nitrogen gas. The results

show the same trends but have different magnitudes. The voltage drop is recorded across the limiting resistors with the two high voltage probes connected to the Tektronix oscilloscope for processing and analysis.

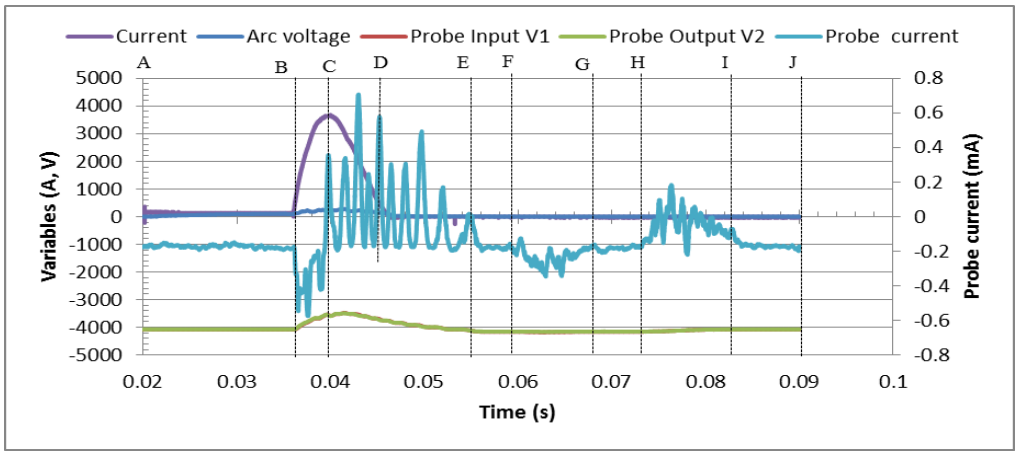

Figure 6.1 shows a labeled figure 5.6 in the previous sub-section 5.4.1.1. (A, BD, C, D reference the vertical lines)

Figure 6.1 shows the probe current in milliamps flowing through the limiting resistor and by implication through the nitrogen gas is at 0 bar (atmospheric pressure). This current was detected during the arcing event. The probe voltages (V1, V2) in volts with time in seconds are also shown.

Before the main arcing period between 0 and 0.0356s (figure 6.1A-B), the circuit breaker mechanism is opening and a low current dc arc is drawn between the electrodes in the circuit breaker. During this period, the probe current is approximately -0.18mA flow. This initiation period lasts for 0.016s with a quasi-DC arc of about 135A being drawn between the electrodes. This period is followed by the main arc period with a duration of about 0.0104s starting at 0.0356s and finishing at 0.046s (Figure 6.1BD). The main arcing period has the peak fault

current at 0.0396s (figure 6.1C) and the current zero period occurring at 0.046s (figure 6.1D). There is a recovery period after current zero that lasted for about 0.0412s (figure 6.1D-J).

Energy from the discharge will be dissipated to the gas from the beginning of arcing (figure 6.1B) to the end (figure 6.1D). From 0.0356s to 0.0396s (figure 6.1B-C), the probe current increases to about -0.53mA at 0.0375s and then decreases to about -0.31mA at 0.0397s. At this point in time, it is unlikely that this is the effect of hot dissociated gas may be due to optical radiation triggering the gap in the probe, since the transit time of the hot gas between the arcing electrodes and the sensor is about 12.3ms in an estimated temperature of 200^0C from the arc for nitrogen gas at atmospheric pressure, NIST [79]. Figure 6.1a shows the distance between the arcing electrode and the dielectric probe, and the transit time of the hot gas to the probe, with a 55mm distance between the arcing electrodes and the dielectric probe.

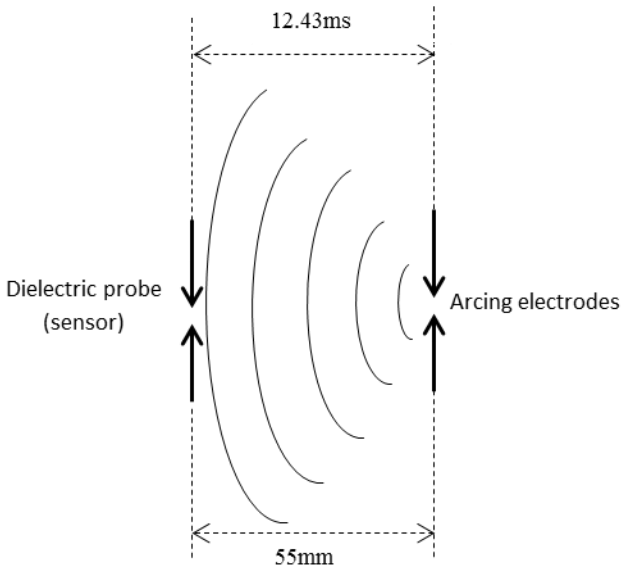

Figure 6.1a shows the travelled distance and time of the hot gas for nitrogen gas at atmosphere to the dielectric probe.

From 0.039s to 0 0532s (figure 6.1C-E), rapid positive oscillations are seen with an average frequency of about 640Hz. This period consists of peak fault current period, current zero period

and part of the post-current zero recovery periods. The dielectric probe response shows continuous change in the probe current, which reduces as the gas recovers from the arc discharge. After fault current zero period (0.0461s) as in figure 6.1D, the probe response still shows repetitive oscillations of the probe current up to the time of 0.0564s (figure 6.1E). These oscillations may signify the presence of the hot gas from the arc. At the period (figure 6.1D-E), the current flow in the probe may continue due to the residual heat in the gas. Then between 0.0604s and 0.0684s (figure 6.1F-G), the current flows in negative direction with a gradually increases. This may also indicate the highly ionized particles during the hot gas mixing phase with the nitrogen gas. This may cause this low current flow after current zero prior to full recovery of the dielectric strength of the gas. Al figure 6.1(H-I) shows a positive rise in the probe current during this recovery period and then complete recovery between 0.0684s to 0.086s (figure 6.1H-I). These changes in the polarity of the current might be due to hot gas and retained ionized products from the arc. These may further reduce the dielectric strength of the dielectric probe and is then followed by dielectric recovery back to the normal energy levels, with the results indicating a highly complex gas structure. Since at fault current zero, it is expected that recombination is taking place and that local thermal equilibrium exists such that there are equivalent amounts of ions (the positive ions and negative ions) and electrons, it is implied that the voltage drop across the current limiting resistor of the probe, probe current flow detected and weakened dielectric strength are due to heat transfer from the the arc to the nitrogen gas as from figure 6.1(B-J) during the arcing fault current.

6.3.1.2 Current Directions during Arcing

The results of direction of probe current flow were presented in chapter 5, sub-section 5.4.1.2. Figure 6.2a shows a labelled diagram of figure 5.7a. It is used as a typical example to illustrate

the direction of probe current and electron flowing in the probing circuit. Figure 6.2a show V_1, V_2 and probe current flowing through the dielectirc probe for 0.0bar of nitrogen gas before the arcing fault current. It also shows V_{1min} , V_{2min} and corresponding probe current flow at the same period, where V_{1min} and V_{2min} are voltages across the current limiting resistor at the point of weakened dielectric in nitrogen gas at atmospheric pressure.

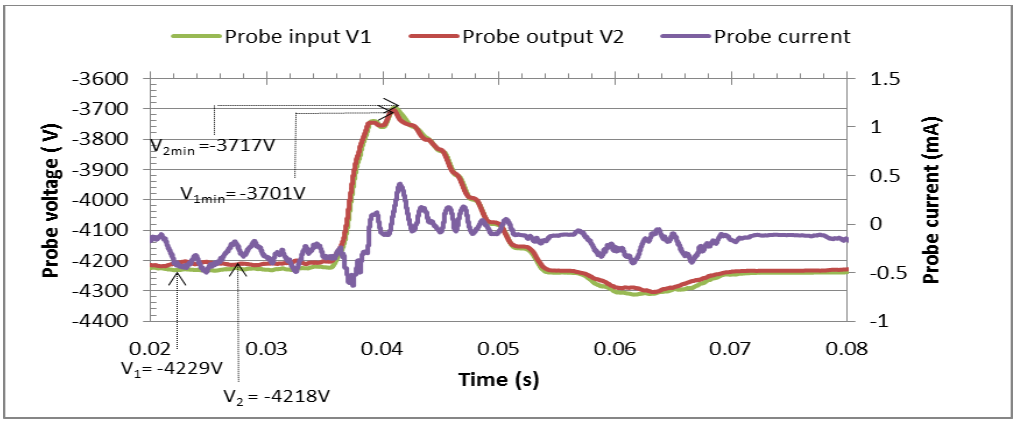

Figure 6.2a shows the graph of voltages (input V1 and output V2) and the probe current as illustrated in figure 5.7a.

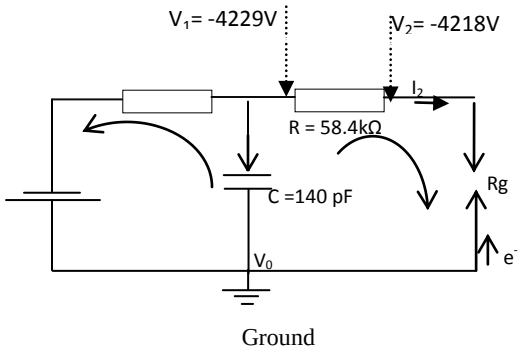

Figure 6.2b illustrates the probing circuit before the arc.

From figure 6.2b, the voltage difference from both probes is obtained as:

$$\Delta V = V_1 - V_2$$

$$\Delta V = (-4229)\ V - (-4218)\ V = -11V$$

And the probe current I_2 is calculated as:

$$I_2 = \frac{V_1 - V_2}{R} = \frac{\Delta V}{R} = \frac{-11\text{V}}{58.4\ x\ 10^3\Omega} = -0.19mA$$

while the gap resistance is R_g is obtained as:

$$R_g = \left|\frac{V_0 - V_2}{I_2}\right| = \left|\frac{0 - (-4218V)}{0.19x\ 10^{-3}A}\right| = 22.4M\Omega$$

The calculated probe current I_2 is a negative current, the direction of probe current I_2 in a counter-clockwise direction while the electrons flow in a clockwise direction before the arcing fault current discharges. Figure 6.2c shows the circuit status, the directions of the calculated probe current and the electron flow.

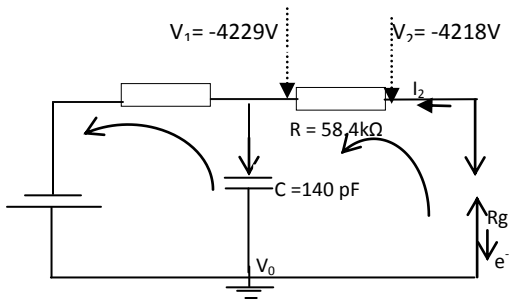

Figure 6.2c illustrates the directions of probe current and the electron flow before the arcing faut current.

Figure 6.2d shows the direction of probe current I_{2w} and electron flow during the period of the dielectrically weakened gas and is detemined as follows:

$$\Delta V_w = V_{1min} - V_{2min}$$

where ΔV_w is the voltage difference between V_{1min} and V_{2min}, during the arcing period, see figures 6.2a and 6.2d.

$$\Delta V_w = (-3701)\ V - (-3717)\ V = 16V$$

$$I_{2w} = \frac{\Delta V_w}{R} = \frac{16V}{58.4\ x\ 10^3\Omega} = 0.274mA$$

where $\Delta V\ and\ \Delta V_w$ voltage differences before and during arcing periods.

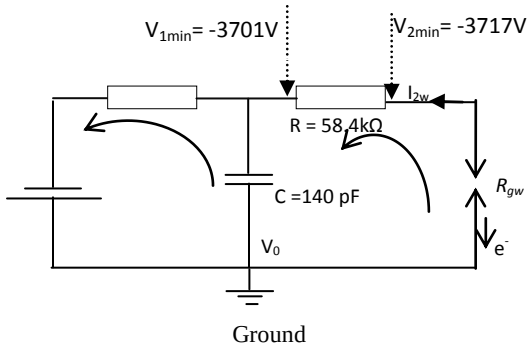

Figure 6.2d illustrates the circuit diagram during the peak of the arcing fault current.

Then the gap resistance R_{gw} is obtained as:

$$R_{gw} = \left|\frac{V_0 - V_{2min}}{I_{2w}}\right| = \left|\frac{0 - (-3717)V}{0.274mA}\right| = 13.57M\Omega$$

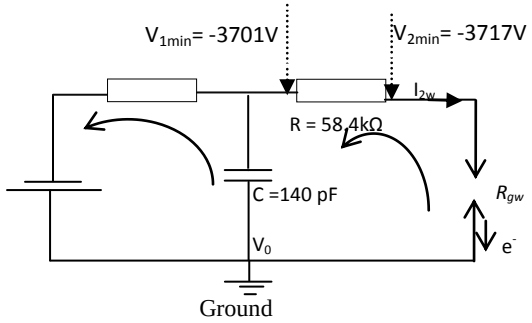

Figure 6.2e shows the direction of calculated probe current and electron flow during the peak arcing fault current.

The probe current I_{2w} may flow in a counter-clockwise direction while the electrons may flow in the clockwise direction since the calculated current I_{2w} is a positive value as shown in figure 6.2e. The experiments were repeated with various values of nitrogen gas pressure from 0 to 2 bars, incremented at 0.5 bar step. The summarized data are presented in table 6.1 and table 6.2 obtained before and during the arcing fault current period respectively. The probe voltages before (input V_1 and output V_2) and during (input V_{1w} and output V_{2w}), used for the pre-set pressures, are shown in figures 6.3 and 6.4. Figure 6.3 shows that the voltage increases (made more negative) as the pressure rises. V_{1w} and V_{2w} are shown during the arcing in figure 6.4. The

probe voltages before arcing shows a higher negative value than the probe voltage during the arcing period as compared from both tables. This is an indication that nitrogen gas has higher dielectric strength before the arc period as compared to the arcing (dielectric strength weaken) period. The dielectric strength of nitrogen is also described in terms of the gap resistance as seen from table 6.1 and table 6.2. It shows higher gap resistance before the fault current period as compared to the arcing period which has a low gap resistance. Figure 6.5 shows probe current variation in nitrogen gas pressure (I_2) before and (I_{2w}) during the arcing current. Moreover, figure 6.5 shows the increase in probe current flow (I_{2w}) to about +1mA at 0.5bar and then reduces to about +0.74mA at 1.0 bar then followed a gradual rise to -0.8mA for 2.0 bars of nitrogen gas during the arcing period. Before the arc, the probe current flow (I_2) shows the same trend as exhibited by I_{2w} during the fault current but has lower values of the current flow. The probe current flows during the arcing periods were obtained for the dielectric weakened periods in the nitrogen gas.

Pressure	Input V_1	Output V_2	ΔV	I_2	R_g
bar	V	V	V	mA	MΩ
0	-4229	-4218	-11	-0.19	22.4
0.5	-6120	-6154	34	0.583	10.57
1	-8108	-8060	-48	-0.822	9.81
1.5	-10000	-9977	23	0.394	25.33
2	-11422	-11442	-20	-0.342	33.41

Table 6.1shows the pre-set pressures, probe voltage (input V_1 and output V_2), calculated probe current I_2 and gap resistance R_g before the arc.

The direction of probe current flow depends on the polarity of the probe input voltage V_1 and the probe output voltage V_2, meaning if the input voltage V_1 is more negative than the output voltage V_2, the probe current may flow from V_2 toward V_1 (counter-clockwise direction in the circuit as

in figures 6.2c). The obtained calculated probe current I_2 is in negative polarity which implies that the leakage current will flow in a counter-clockwise direction while the electrons will flow in the opposite direction as in figure 6.2c before the arc.

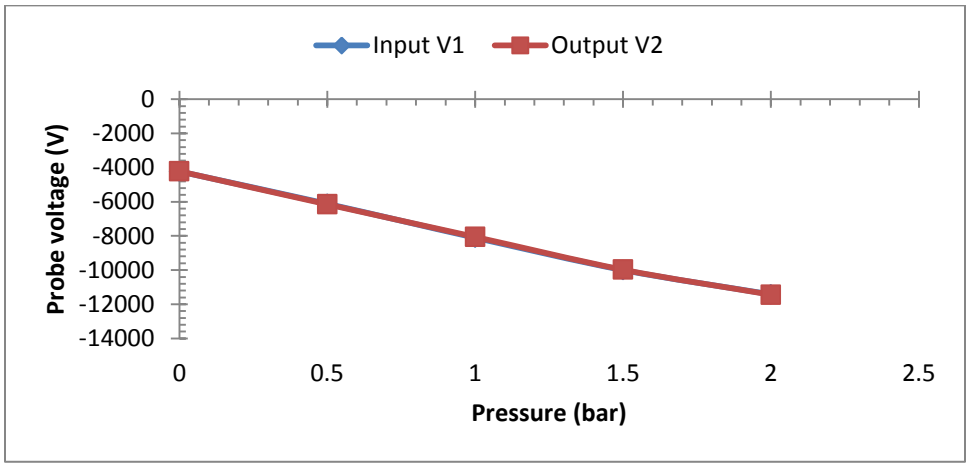

Figure 6.3 shows the graph of probe voltages (input V_1 and output V_2) from the limiting resistor R versus the pre-set pressure before the arc.

Pressure	Input V_{1w}	Output V_{2w}	ΔV	I_{2w}	R_{gw}
bar	V	V	V	mA	MΩ
0	-3701	-3717	16	0.274	13.57
0.5	-5720	-5778	58	0.993	5.8
1	-7727	-7770	43	0.736	10.55
1.5	-9841	-9882	41	0.702	14.08
2	-11320	-11273	-47	-0.805	14.01

Table 6.2 shows the pre-set pressure, probe voltage (input V_{1w} and output V_{2w}), calculated probe current I_{2w} and gap resistance R_{gw} during the arcing fault current (dielectric weakened) period.

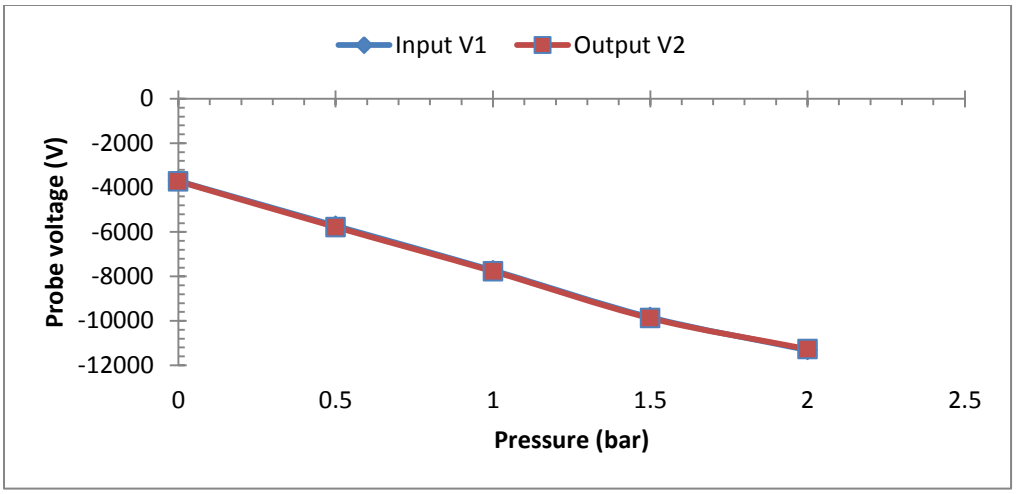

Figure 6.4 shows the graph of probe voltages (input V_{1w} and output V_{2w}) from the limiting resistor R versus pre-set pressure during the arc.

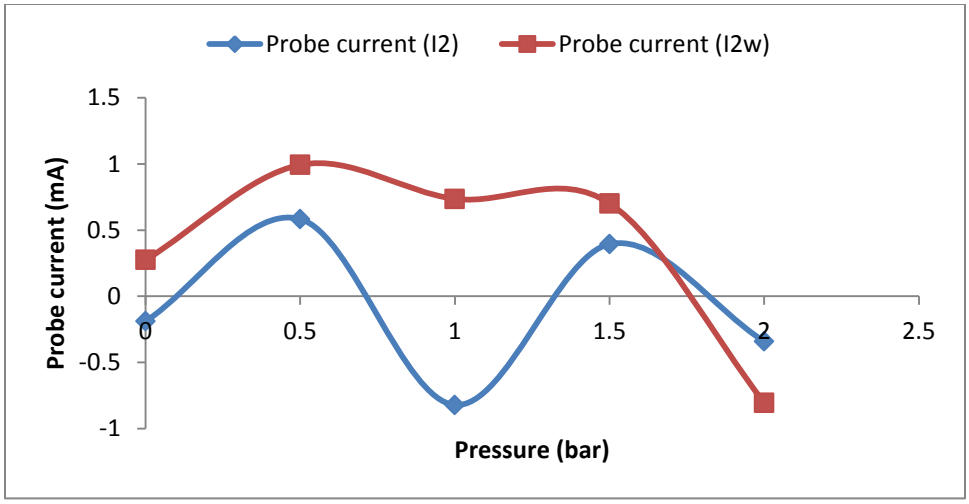

Figure 6.5 shows the graph of varying probe current I_2 before the arc (no dielectric weakened period) and probe current I_{2w} during the arc (dielectric weakened period) versus pressure.

In another scenario, as shown in figure 6.2e, V_{1min} is less negative than V_{2min} and the probe current flows from V_1 toward V_2 (counter-clockwise direction in the circuit). The calculated probe current I_{2w} is in positive polarity which implies that the current will flow in a counter-clockwise direction while the electrons will flow in the opposite direction during the arcing.

Added to these, during the arcing process, the heat transferred into the nitrogen gas spreads throughout the whole circuit breaker chamber. By implication, the direction of probe current flow may depend on the circuit operating condition since the dielectric probe operates below the breakdown voltage. And the probe current and the calculated gap resistance may depend on the chamber conditions as at the time of the experiment.

6.3.1.3 Probe Orientation in Nitrogen gas

6.3.1.3.1 Result in 0 bars of Nitrogen Gas

Dielectric probe orientation in nitrogen gas and the results being presented in section 5.4.1.3 are discussed in this section. The objective of the dielectric probe is to understand the effect that this may have on the probe response to low current flow during the arcing period of a positive half-cycle AC current in the circuit breaker filled with nitrogen gas at different pressures.

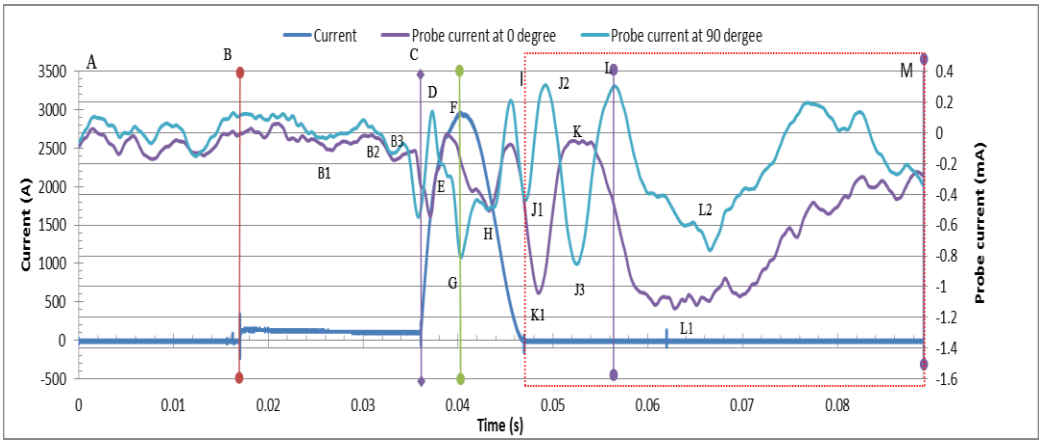

Figure 6.6 compares the probe current detected during post current zero periods for 0.0bar of nitrogen gas for 0^0 and 90^0 orientations.

Figure 6.6 shows the graph of the probe current flow during the whole of the arcing period for a positive half cycle of fault current in nitrogen gas with time, for 0 bar and for 0^0 and 90^0 orientations. In figure 6.6, between 0 and 0.017s (A-B) shows an approximate varying probe

current flow for the dielectric probe orientations, though the current flow for 90^0 shows more positive than that for 0^0 orientations. Then from 0.0172s to 0.0353s (B-C) the arc current rises to about 90A (quasi dc current), the probe current starts changing towards the negative value. At 0.0172 seconds both probe currents read -3.5 μA for 0^0 and 0.12mA for 90^0. There is little decrease and increase between B1, B2 and B3 in figure6.6 before the main trigger with -0.52mA at 0.037s for 0^0 and -0.51mA at 0.036s for 90^0. The probe current flow is low between 0 and 0.0172s (A-B) looks similar, but shows that shot-to-shot variation may produce the difference in both current magnitudes. This is followed by the period 0.0172s (B) that shows a gradual rise in probe currents to 0.027s (B1) followed by a decrease at 0.032s (B2) and at B3. This may indicate the transfer of heat to cooler gas from low quasi-steady DC arc before the main arc current is triggered at C. Between 0.033s (B3) and the trigger period 0.036s (C), the probe currents look similar, indicating that the orientation of the probe is not important during this period. At about 0.036s (C), there is an increase in probe current to about -0.51mA and then followed by an increase to 0.13mA at 0.037s (D) for 90^0 orientation. And the 0^0 orientation at the time of 0.037s had a probe current of about -0.52mA (D) and then reduces to about -8.1μA at 0.0388s (F). This variation may signify a non-homogeneous mixing of the hot and cooler gas. This increase in probe current is due to heat transfer from the arc voltage during the passage of the half fault current into the nitrogen gas. The dielectric probe response between 0.036s and 0.037s (C-D) shows fast responses for 90^0 and 0^0 orientations. At 0.037s, both probe currents read -0.51mA for 90^0 and -0.14mA for 0^0. Both probe currents exhibit a similar pattern although the detail is different in both magnitude and the occurrence of the arc peak and trough of the waveforms. This difference may indicate the effect of the shield on the probe response at 0^0 orientations.

Between 0.037s (D) and 0.04s (G) is the peak fault current period. The probe current increased to about -0.8mA at 0.0404s and then reduces at 0.044 (H), subsequently increasing to 0.16mA at 0.045s for 90^0 orientations (I). For a 0^0 orientation, from 0.039 to 0.044 (F to H) is a slow rise in probe current of about -0.48mA at 0.044s which is then followed by the period where the current is -0.1mA at 0.045s. At (G), the arc current is at maximum and, at this time, there is maximum heat transfer to the surrounding gas. The current zero periods at 0.047s (I) means that the rapid fluctuations start just after arcing continues through into post-current zero approximately (L). Both orientations of the probe display similar trends of behavior, but the 90^0 orientation of the probe shows a positive current flow. After (L), there is an increase in the negative value of the probe current flow, reading a maximum at L1/L2 followed by a slow decay to M. Although there are detailed differences in the response of the probe in the two orientations, the result from each are markedly very similar. The dielectric probe shows a period where there are rapid fluctuations in the probe current which may be an indication of the non-homogeneous nature of the hot gas spread. This is then followed by a relative steady period which may indicate that sufficient mixing of hot and cooler gas has taken place to produce a more homogenous gas structure.

6.3.1.3.2 Result in 0.5 bars of Nitrogen Gas

Figure 6.7 shows a graph of probe current flow during the arcing period of the fault current for 0.5 bar of nitrogen gas with time for 0^0 and 90^0 orientations. Between 0.0 (A) and 0.036s (C), both probe current flows show about -0.12mA at 0.0s to -0.077mA at 0.036s just before the arc. The figures also show initial time varying probe currents at these periods. During the arcing fault current between 0.036s and 0.047s (C-D), the probe current commences with increases and decreases in positive values for a 0^0 orientation. It rises from -0.167mA at 0.0364s to 0.79mA at

0.0375s and reduces to -0.025mA at 0.038s. This is followed by another increase to 0.95mA at 0.041s and decreases to -0.16mA at 0.046s and then increases to 1.1mA at 0.048s (D) in post-current zero period. For a 90^0 orientation, the probe current starts with a small increase followed by a decrease to a negative value. It decreases from 0.32mA at 0.038s to -0.52mA at 0.039s and is then followed by another decrease from 0.21mA at 0.04s to -0.36mA at 0.044s and finally an increase to 0.22mA at 0.048s. During this period, both orientations show almost similar trends, though with differences in the magnitudes of current flows. It also shows a point of coincident of -0.05mA at 0.047s for both probes at fault current zero.

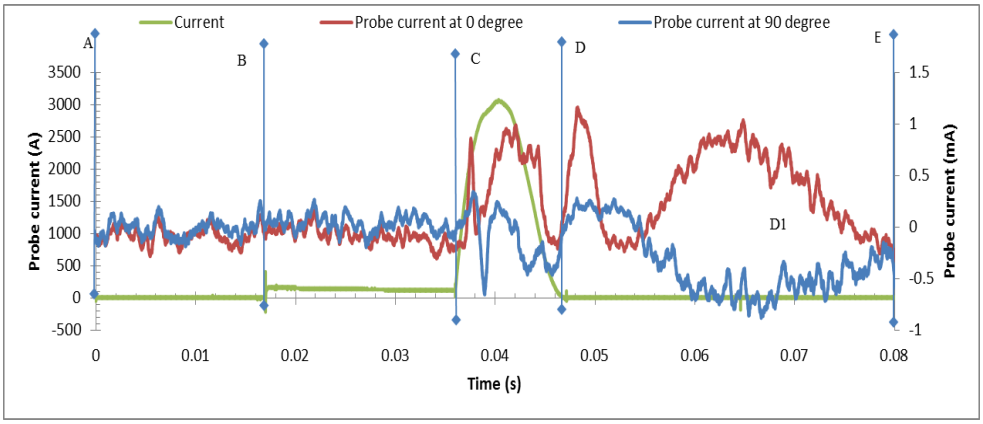

Figure 6.7 shows probe current detected during post current zero periods (D-E) in 0.5bar of nitrogen gas.

Just after current zero periods (D), the probe response shows a relatively steady period of change (0.0484s) from the rapid changes in probe output seen after current zero. This is similar to the previous test (figure 6.6) and the same reasons hold for the behavior. However, the 0^0 degree probe orientation has a positive current response whereas, previously (figure 6.6), this was only seen for 90^0 orientations. The implication at this stage is that this may be a random event and not due to the arc light affecting the operation of the probe.

6.3.1.3.3 Result in 1.0 bar of Nitrogen Gas

Figure 6.8 presents probe current flow for probe orientations for 0^0 and 90^0 in 1.0 bar of nitrogen gas with time; 0.048s (D) shows the end of fault current and commencement of post-current zero regimes from 0.048s to 0.089s (D-E). At the current zero, the probe's response has similar trends but different magnitudes. The rapid oscillations seen in the previous results during the arcing period are not as marked as before (i.e., in figures 6.6 and 6.7).

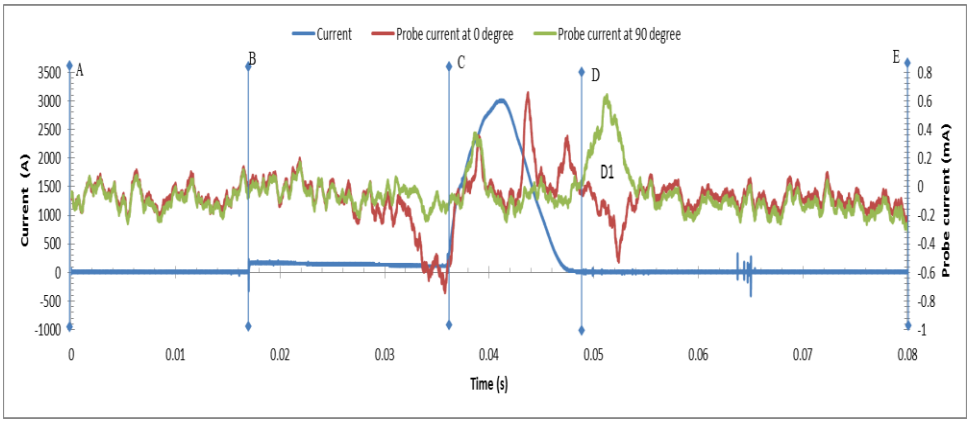

Figure 6.8 shows the probe current flow during post-current zero periods (D-E) for 1.0 bar of nitrogen gas.

The current zero period is also less pronounced with a quicker recovery of the gas being implied than the previous two tests. This implies that, whilst there is still the same non-homogeneity in the heating, it is less evident.

6.3.1.3.4 Result in 1.5 bars of Nitrogen Gas

Figure 6.9 shows probe current flow during the orientation of dielectric probe for 0^0 and 90^0 in 1.5 bars for nitrogen gas. Figure 6.9 (D) shows the end of the fault current and commencement of post-current zero regimes (D-E). During the arcing period, the probe detected a rapidly changing environment. This is followed in the period after current zero by a relatively slower changing

environment as the gas recovers from the effect of the arc. Both probes show a positive current response.

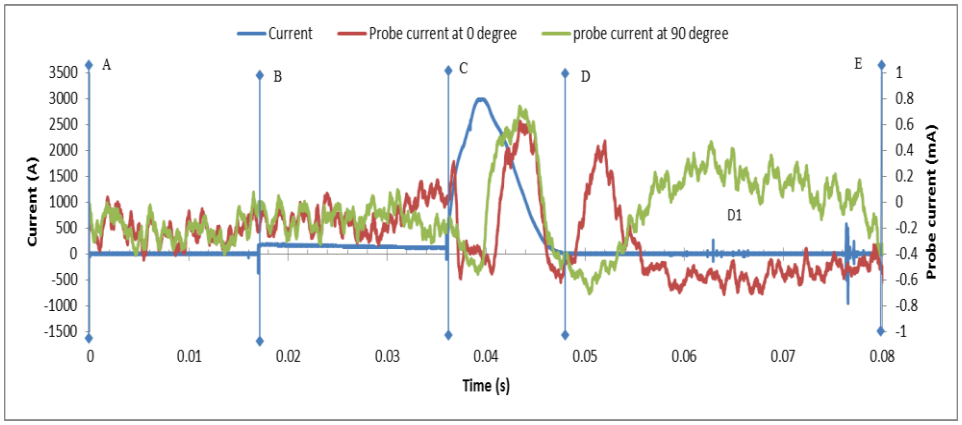

Figure 6.9 shows the arcing current, probe current detected during post-current zero periods (D-E) in 1.5 bars of nitrogen gas for 0^0 and 90^0 degree orientation.

6.3.1.3.5 Result in 2.0 bars of nitrogen gas

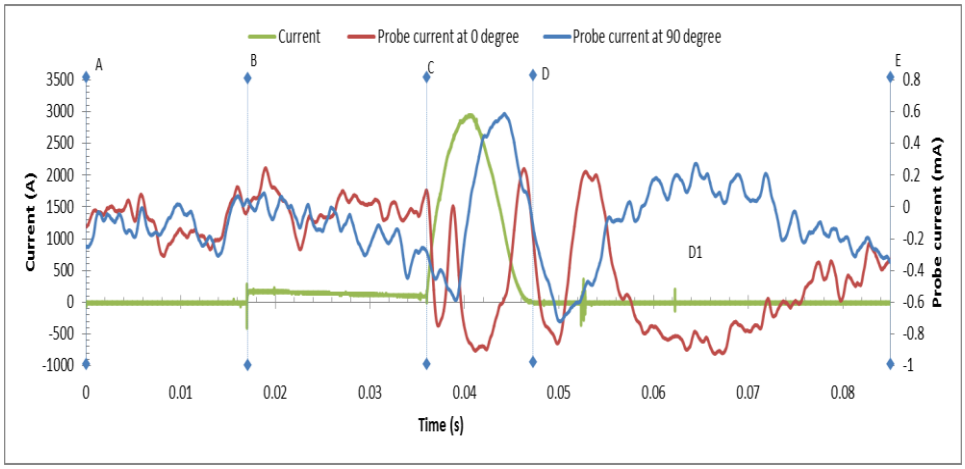

Figure 6.10 shows arcing current, probe current flow during post-current zero periods (D-E) for 2.0bar of nitrogen gas.

Figure 6.10 shows probe current flow for 0^0 and 90^0 orientation of dielectric probe for 2.0 bars of nitrogen gas. The figure 6.10 (D) shows the end of the fault current at 0.047s and the beginning of post-current zero periods between 0.047s to about 0.085s (D-E). At the arcing period, C-D is

an oscillatory waveform of the probes current; as in the previous tests, it is seeing a rapid change towards the current zero and the point of coincident of both current flows. The probe currents changing continued into the post-current zero, and at about 0.056s there is a gradual increase and decay towards the period at 0.085s.

6.3.2 Probe Current in Dry Air

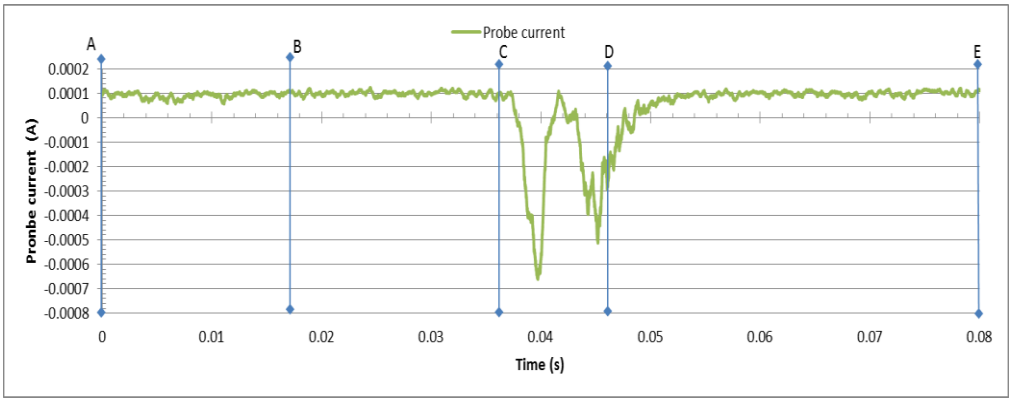

Figure 6.11 shows probe current flow for 0.0 bars of dry air in an arcing current.

Figure 6.11 shows the graph of dielectric probe response to probe current flow for dry air at atmospheric pressure. This result was obtained from the dielectric probe whose tips were set at 1.5mm and biased with negative voltage in an arcing fault current as described in sub-section 5.4.2.1. At the initial periods between 0.0s to 0.017s (A-B), before the arc shows approximate probe current flow of 0.076mA; this is followed by periods between 0.017s to 0.036s (B-C) with quasi-fault currents of about 134.8A. The probe current at this period is approximately measured to be 0.12mA at 0.024s. This is followed by the arcing fault current period at 0.036s (C). The current flow begins a negative value increase from about 0.1mA at 0.037s to -0.64mA at 0.039s and is then followed by a rise to about 0.1mA at 0.0415s, continuing for another negative value of -0.51mA at 0.054s before final regaining its initial value at about 0.08s (E). The dielectric probe response to the probe current flow between 0.036s and 0.046s (C-D) may indicate that the

heat from the arc is mixing with the dry air in the chamber and may also result in thermal turbulence as shown in the rising and falling from the probe current flow response from the dielectric probe, followed by a recovery period into the post-current zero periods between 0.046s and 0.08s (D-E). The response of the probe to changes in the gas is similar to that of nitrogen with a possible difference in the recovery period after current (D). Between D-E, in the post-current zero periods, the probe response shows the same probe current flow value before the arcing fault current; this may signify that the heat energy was not retained in the dry air after current zero periods as observed in nitrogen gas, implying immediate dielectric recovery at this period. The dielectric weakness in dry air as in figure 5.18a was obtained when the dielectric probe gap was adjusted to 1.5mm at atmospheric pressure after several attempts in probing the dry air in 1mm of gap length. The tests were repeated for 0.5 to 2.0 bars at the increment of 0.5 bars of dry air as shown in the typical figure 5.19a and figure 5.19b. The calculated probe current and gap resistance for dry air at atmospheric pressure during weakened dielectric strength of the probe set at 1.5mm gap are -51.37μA and 84.39MΩ.

6.3.3 Probe Current at 3.2kA and 18.4kA in SF_6 Gas

The result of SF_6 gas behaviour during the passing of positive half-cycle fault current of about 3.2kA and 18.5kA are reported in section 5.3.3, with the intention to determine the weakened effect of arcing on the dielectric strength of SF_6. Figures 5.20c and 5.22c are magnified Excel file waveforms of the fault current, probe current, arc voltage and negative voltage (V1 and V2) from the limiting resistor with time. Both figures show a similar trend in behaviour except in the magnitude of the probe current flows and the probe voltages. Prior to dielectric breakdown as shown in figure 5.20c, the probe current is about 0.195mA with probe voltage set at about -4480V at approximate time of 0.0316s, followed by dielectric breakdown period that lasted for

0.8ms with increase in maximum negative probe current of about -4mA at 0.0318s. At this instance, the probe voltage starts decreasing from about -4480V to -1818V with a probe current of 2.4mA at 0.0326s to the point where the current flow cannot sustain the dielectric breakdown, followed the recovery period that lasted for 47.4ms.

As seen in the gases, before the arcing current beginning shows that leakage current flow but at different magnitude of current values (figures 5.7b for nitrogen gas, 5.18a for dry air and 5.20a for SF_6 gas). The weakened dielectric strength of nitrogen gas and dry air shows the same trend at different amplitudes obtained at 1mm gap for nitrogen gas and 1.5mm for dry air, but this proved difficult to achieve in SF_6 gas even after reducing of the gap to about 0.5mm. During the post-current period in nitrogen gas (figure 5.7b) and SF_6 gas (figure 5.20c), an increasing and decaying behaviour is shown when compared to dry air (figure 5.18c) that recovered immediately at this period.

6.4 Results Discussion

6.4.1 Introduction

Section 6.4 discusses and correlates the results of the probe current flow investigated in chapters five and six for dry air, nitrogen and sulphur hexafluoride gases. It relates the characteristics and behaviour of gases under investigation when heat energy from the arc passes through these gases.

6.4.2 Leakage Current in Dry Air

The investigation of compressed dry air in section 5.2 identifies the flow of probe current in current interrupter. A typical illustration is shown in figure 5.4, when a dielectric probe biased

with negative DC voltage is coupled in a circuit breaker filled with dry air. The interrupter behaviours are affected by physical conditions of the gas, namely pressure, temperature, electrode field configuration, the nature of electrode surfaces and availability of initial conducting governing the ionisation processes [53, 55].The dielectric probe response to arcing is consistent in its trend as the pressure is increased.

6.4.3 Probe Current

The results of the investigation on probe current flow were carried out for nitrogen gas (section 5.4.1), compressed dry air (section 5.4.2) and sulphur hexafluoride gas (section 5.4.3) with applied negative DC voltage on dielectric probe when an arc is present inside the breaker for various gases. The three gases under investigation before the arc shows leakage current flow; these are shown in figure 5.6 for nitrogen gas (section 5.4.1), in figure 5.18 for dry air (section 5.4.2) and in figure 5.22 for SF_6 (section 5.4.3). These investigations confirm that the current flow is an inherent characteristic in interrupters as presented in sections 5.2 and 6.2. The dielectric probe is negatively biased while the biasing voltage is set just a bit below the breakdown voltage of the probe in the test gas and the positive side is grounded to earth. Applying a positive half-fault current creates an arc voltage that stresses the gap of the parting electrodes carrying the fault current. The arc's electromagnetic force with ions (positive and negative) and electrons will create heat in the test gas. The test gas will absorb the heat and dissociate into ionized particles which will be attracted by the dielectric probe to neutralise; these movements of the charges may result in a small current flow. The type of current flow will be determined by the discharging fault current, the mode of the biased probe and the nature of the test. In this case, the fault current is a positive half-AC current and the dielectric probe is negatively biased in the three types of gases mentioned above. During the arcing periods,

nitrogen gas shows dielectric strength weakness when the dielectric probe tips were set into a 1mm gap. The probe currents were achieved from atmospheric pressure of nitrogen gas up to 2 bars of pressure as shown in section 5.4.1. Moreover, the dielectric probe response to probe current flow after current zero indicates the retention of the heat from the arc voltage when the fault current has been extinguished, resulting in a gradual dielectric strength recovery time (section 5.4.1). Similarly, the same procedure was applied to the compressed dry air but could achieve the probe current only when the dielectric probe gap was adjusted to 1.5mm and in an atmospheric pressure of the dry air wherein the weakened dielectric strength was obtained as shown in section 5.4.2 and in figure 5.18. The dielectric recovery period shows quick recovery which signified that the dry air did not retain the heat energy, unlike in nitrogen gas where the hot gas from the arc was retained after the fault current zero periods. Subsequent increments in the pressure for dry air following the same procedure and condition could not detect a pronounced weakened dielectric strength of the probe (sub-section 5.4.2.2 and figure 5.19a), rather showing a change in the probe current flow in the dielectric probe from its previous varying positive and negative values to a positive one. However, the increasing and decaying trends show similar current flow during the post-current zero periods.

The obtained probe current and gap resistance for dry air at 1.5mm and for nitrogen gas at 1mm under the identical experimental conditions are shown below. Normalising the gap resistance indicates that dry air is six times higher than that of the nitrogen gas under this test condition as shown in table 6.3.

Gas	Pressure	Probe current	Gap resistance	Normalising	Gap length
Dry air	Atmospheric	-51.3µA	84.39MΩ	6	1.5mm
Nitrogen gas	Atmospheric	0.274mA	13.57MΩ	1	1.0mm

Table 6.3 shows calculated probe current I_{2w} and gap resistance R_{gw} during dielectric weakened period at atmospheric pressure and same experimental condition.

Also, in SF_6 gas, the weak dielectric strength proved difficult to achieve with the dielectric probe within the same conditions and experimental limits. The dielectric probe tips were also adjusted to 0.5mm from 1mm gap. This was done to reduce the negative DC voltage to suit the test condition. To induce an effect, the positive half-cycle of fault current was varied as presented in section 5.4.3, in figures 5.20 and 5.22. The experiment varies between dielectric strength breakdown (as in figures 5.20 and 5.22) and no breakdown (as in figures 5.21 and 5.23) but has a gradual recovering characteristic as in nitrogen gas. In separate investigations carried out where the fault current was made constant while varying the applied negative voltage to the dielectric probe, it was observed that reduction in voltage difference of -23V will result in no breakdown from the dielectric strength. The voltage difference was about 0.5% of the input voltage of -4463V at no breakdown. This indicates that the breakdown in SF_6 may be partially due to decomposed ionic particles of sulphur-fluoride gases and metal-fluorides (the by-products of white powdery substance as seen in figure 5.24). With the present configuration, probing the weakened dielectric strength of SF_6 might also be difficult due to SF_6 having a higher molecular weight, density and the pronounced tendency to capture free electrons, forming heavy ions with low mobility, making the development of electron avalanches very difficult. The dielectric strength of SF_6 is higher than that of dry air and N_2 gas under the same condition [55]. To achieve the reduced dielectric strength of SF_6 gas, the effect of its higher potential gradient needs to be carefully considered. In the arcing period, the three gases under investigation show that, at weakened dielectric strength, the probe current flow rises while the applied negative DC voltage reduces.

Section 5.4.1.2 investigates the direction of probe current flow before and during arcing periods in nitrogen gas. The probe response to the arc indicates the present of thermal energy in the

circuit breaker at post-current zero periods. Tables 6.1 and 6.2, and figures 6.3 and 6.4 presents summaries of data and results of probe voltages from the limiting resistor into the dielectric probe. In both cases, the results show an increase in probe voltage as the pressure rises. However, the voltages obtained during the arcing period shows lower values than for no arc. The results were also compared in terms of probe current flow against the pressure of nitrogen gas at these periods as in figure 6.5. Figure 6.5 show more probe current flowing during dielectrically weakened periods when compared to no dielectric strength weakened periods.

The circuit condition before the arcing may also influence the direction of the current flow since the probe circuit is operated below the breakdown voltage of the dielectric probe. This might result in more positive ions at the tips and the surrounding gas before the arc. When the arc current is passed through the gas, this may causes the positive ions being repelled and the recombination of the negative ions at the tips and the surrounding gas thereby setting in motion the ions and electrons in the dielectric medium. The pre-set negative DC voltage is set below the breakdown point of the dielectric probe. Applying the positive half cycle AC current will definitely repel the +ve charges and neutralise the –ve charges, resulting in +ve charge to flow, i.e., in figure 6.2d; the probe current is in a counter-clockwise direction during the arc. Also, the directions of probe current flow may be determined and influenced by the potential polarities of the input and the output of voltages, whose the input or output is more negative than other (see figure 6.2c to figure 6.2e) since current flow is conventionally from negative to positive. In figure 6.2b, the probe current flow shows a clockwise direction but the calculated current flow is negative, meaning the current flow will be as shown in figure 6.2c at no arc condition.

Section 5.4.1.3.5 deals with the orientations of the dielectric probe in nitrogen gas. The change is to understand the effect the orientation has on the dielectric probe response to the probe current

flow during the arcing fault current. Figures 6.6 to 6.10 show the results of the behaviour of nitrogen gas in terms of probe current flow response from the probe at various incremented pressures when the arcing fault current were passed through individually. In either position, the dielectric probe orientation shows similar trends since the probe current flows during the passage of the fault current in the vicinity of the gas. The difference in magnitude of the probe current detected may be due to fault current, shot-to-shot variation during setting and triggering from the synthetic circuit. The shield at 0^0 orientations has a relatively low effect on current flow during the fault current passed in the nitrogen gas.

In summary, this chapter analysed and discussed the experimental results generated from the investigation on probe current flow in dry air, nitrogen (N_2) gas and sulphur hexafluoride (SF_6) gas. The chapter commenced with the confirmation of the correct dielectric probe operation in dry air. This was then followed by the analysis of probe current flow in N_2, dielectric probe orientation for 0^0 and 90^0 also in N_2 gas. Furthermore, the analysis and discussions on probe current flow in dry air and SF_6 gas were considered. Finally, the results from N_2, dry air and SF_6 were discussed as a component from which their behaviours with negative voltage applied dielectric probe in a fault current were assessed. The assessment confirms that N_2 gas has a lesser dielectric strength as compared to the dry air and to SF_6 gas, as N_2 gas has shown to exhibit a weaker dielectric potential in relation to dry air and SF_6 within the same experimental conditions.

Chapter 7 Conclusion and Further Work

7.1 Introduction

The conclusion of the research and the implications arising from the results in chapter 5 and the analysis in chapter 6 are presented and discussed considering the techniques and the gases investigated throughout the work. This chapter also provides suggestions for further research.

7.2 Conclusion

The dielectric probe was used during the operation of a circuit breaker filled with dry air, nitrogen and sulphur hexafluoride gas. The probe was connected to a negative DC voltage supply. Initial tests were conducted to verify the operation of the circuit breaker as in sub-section 4.2.4 and the correct operation of the dielectric probe in dry air as in sub-section 5.2 whose gap was set between 4.8-4.9 mm was performed inside the circuit breaker. As seen in section 5.2, consistent patterns of results were obtained which also confirmed by previous researchers [58].

For tests in nitrogen, the dielectric probe tips were set at 1mm gap and positioned approximately 55mm away from the fault current carrying electrodes of the circuit breaker. The tests were undertaken for a range of pressures from near vacuum up to 2 bars of nitrogen gas (5.4.1). Apart from the reduced dielectric strength during the fault current zero periods, the investigation identifies probe current flow before, during and after the arcing fault current in the circuit breaker. The results from the dielectric probe were used to estimate gap resistance. The result shows that, when the fault current is extinguished, the gap resistance gradually increases back to its original form before the arcing current. As in tables 6.1 and 6.2, the gap resistance between 0 and 1.0 bar reduces with pressure rise, but, as the pressure increases above 1.0 bar toward 2.0

bars, the gap resistance starts increasing with pressure rise. This may signify that the dielectric strength increases with the increase in gas pressure. The change in the resistance confirms the present of hot gas in the circuit breaker which is dielectrically weaker than the initial dielectric strength of the gas. The transfer of energy from the arc to the surrounding gas is complex, and this is highlighted by the variation of the probe gap resistance. During the period, before the arcing, the gap resistance remains constant. Then during the arcing period the gap resistance changes rapidly, an indication of non-homogenous hot gas flow. After current zero, the gap resistance commences, gradually regaining its resistance as the hot gas dissipates away from the nitrogen gas.

Also, in nitrogen gas as in sections 5.4.1.2 and 6.3.1.2, the experimental data were used empirically to determine the values and directions of the probe current in the circuit before and during the arcing period of the fault current. Typical examples are illustrated in figures 6.2a to 6.2e, showing the determined probe current values, the direction of probe current and electron flow in the circuit. Typical currents recorded during the test in N_2 indicate that the current flow through the gas is lower before than during the arcing current. This is shown in tables 6.1, 6.2 and in figure 6.5. In both cases, the current flow varies as the pressure upswings but appears that more current flows during the weakened dielectric stages of the gas. During and after the arc, the circuit breaker shows unusual current flow pattern which indicates highly complex conditions in the gap and surrounding gas. Tests indicate that the current flow in the dielectric probe could be into the gap or away from it. These are seen from increases and decreases of the probe current flow with respect to time during and after the arc. Also, the circuit condition at this stage of the arcing may also influence the direction of the probe current flow since the dielectric probing circuit is operated below the breakdown voltage of the dielectric probe. This might result in more

positive ions at the tips and the surrounding gas before the arc. When the arc current is passed in the nitrogen gas environment, this may result in the positive ions being repelled and a recombination of the negative ions at the tips and the surrounding gas thereby influencing the movement of the ions and electrons in the dielectric medium. However, the direction of current flow may likewise be determined by the polarity of the terminal voltages (V1 and V2). Section 6.4.3 discussed and explained the possible influential factors and direction of the probe current flow with negative voltage applied dielectric probe. The movement of the charges may weaken the dielectric strength of the probe in the gas, invariably weakening the dielectric strength of the gas under study.

In compressed dry air, the dielectric probe gap was adjusted to 1.5mm, and only in atmospheric pressure of the dry air (in section 5.4.2 and in figure 5.18) was the weakened dielectric strength detected. When a half cycle of fault current was passed through the circuit breaker, the weakened dielectric strength and low probe current were detected. The compressed dry air proves to be more resistive to the fault current as compared to the nitrogen gas. Table 6.3 confirms that, under this test condition, dry air is six time higher than nitrogen gas at the same circumstance. The probe response to the current flow after fault current zeroed under the similar settings shows quicker recovery as compared to nitrogen. The implications of the dry air behaviour of the fault current suggests that dry air may have better insulation capability as compared to the nitrogen gas.

The tests in sulphur hexafluoride gas (SF_6) proved difficult to achieve the SF_6 dielectric weakness due to the superior arc-quenching ability of the gas. The investigations were carried out when the dielectric probe electrode tips were set to 0.5mm. The study shows SF_6 is more or less affected by the fault current as in dry air. This was evident by the lack of any reduction in

dielectric strength by the probe as discussed in section 6.3.3 and in section 6.4.3. These characteristics of the SF_6 gas might be linked to the physical and chemical properties of SF_6 gas, including its higher molecular weight and density and pronounced tendency to capture free electrons forming heavy ions with low mobility, making the development of electron avalanches very difficult. With this, a SF_6 dielectric medium indicates better insulation properties to the fault current as compared to dry air and N_2 gas mediums under the same experimental conditions.

7.3 Further Work

The detection of probe current flow through gas during the arcing period of fault current has proved successful over a relatively small area using low pressure and limited applied negative DC voltage to the dielectric probe. This could be done, but was not within the scope of this study. The methodologies used with this project could be used to run long-term tests in gas-insulated switchgear and in circuit breakers, but the dielectric probe will need to be checked regularly for the decomposed solid by-products deposited from the gases, for this may cover and reduce the sensitivity of the gap of the probe as shown in figure 5.24b. It may cause frequent breakdown in the probing circuit of the dielectric probe. The arcing contacts are not nozzled, so the arc voltage will spread round the circuit breaker. The dielectric probe depends on the discharge from the gas while the gas depends on the heat from the arc, meaning the circuit breaker needs to be insulated so as not to absorb the heat from the arc internally and externally. Thermal absorption of the metallic steel body of the circuit may cause a loss of heat energy to the test gas under investigation. These may affect repeatability of probe current detected and subject the current flow to the circuit breaker's experimental conditions. For the monitoring and control of the fault current discharges, the electrodes carrying the fault current electrodes need be

nozzled so as to direct the hot gas from the arc to a specific direction (i.e., in the dielectric probe direction in the test gas). This may increase the dielectric probe response effectiveness to the probe current flow during the arcing periods. During such arcing periods, the gases decompose, forming solid by-products. For instance, the SF6 gas decomposes to form sulphur-fluoride gases and metal-fluorides which are toxic, dry air forms corrosive nitrogen oxides and other compounds, and nitrogen gas forms nitric oxide (NO), a colourless gas formed in the electric-arc process and nitrogen dioxide. These by-products will cover the dielectric probe tips while reducing the dielectric probe's chances of establishing contact with ions and electrons. The probe needs to be checked regularly and the deposited cleaned for better response. The by-products will lessen the quality of the gas in use for the arc monitor, and the circuit breaker needs to be pump down and refilled with fresh gas after long-term usage as to maintain the value of the interrupter.

References

[1] Rene P, van der Linden WA. Current-zero measurements of vacuum circuit breakers interrupting short-line faults. In: IEEE Transactions on Plasma Science, 2003, pp. 852-858.

[2] Jones GR. High pressure arcs in industrial devices: diagnostic and monitoring techniques. Cambridge University Press Cambridge, 1988.

[3] Ryan HM, editor. High voltage engineering and testing. In: IEE power series: 17, Stevenage, Herts., U.K, 1994.

[4] Yanabu S, Homma M, Kaneko E, Tamagawa T. Post-arc current of vacuum interrupters. IEEE Power Engineering Review, 1984. (4): 42.

[5] Barrault M, Bernard G, Maftoul J, Rowe S. Post-arc current measurement down to the ten milliamperes range. IEEE Transactions on Power Delivery. 1993, (8): 1782-1788.

[6] Kranling, SK, Electrical supply using SF6 technology life cycle assessment. Solvay Germany, May 1999.

[7] Hoshina Y, Sato M, Shiiki M, Hanai M, Kaneko E. Lightning impulse breakdown characteristics of SF6 alternative gases for gas-insulated switchgear. IEE Proceedings -- Science, Measurement & Technology, 2006. (153): 1-6.

[8] Ackermann DW. Current transformer measurements of distorted current waveforms with secondary load impedance. In IEEE, 1999, 765-768.

[9] Makky ARAM, Abo-Zied H, Abdelbar FN, Mutschler P. Design of the instrument current transformer for high frequency high power applications, 2008, 230-233.

[10] Warnes LAAA. Electronic and electrical engineering: principles and practice. Basingstoke : Palgrave Macmillan, 2003. 3rd ed., 2003.

[11] Tap wound cores, magnetics design manual TWC-500. Spang & Company, 2000.

[12] Rashtchi V, Bagheri A, Shabani A. Optimal design of measurement-type current transformer using particle swarm optimization. 2008, pp. 68-74.

[13] Hrabliuk JDP. PP interfacing optical current sensors in a substation. In IEEE, 2001: pp. 147-155.

[14] Maffetone TD, McClelland TM. 345 kV substation optical current measurement system for revenue metering and protective relaying. IEEE Transactions on Power Delivery, 1991 (6): 1430-1437.

[15] Day G, Hale P, Deeter M, Milner T, Conrad D, Etzel S. Optical power line voltage and current measurement systems. Volume 1: Limits to the precision of electro-optic and magneto-optic sensors, Final Report National Bureau of Standards, Washington, DC., 1 (1987).

[16] Li G. Faraday current sensing using chromatic modulation, Liverpool University: Thesis Ph.D., 1997.

[17] 'Optical current sensor using the Faraday effect', Patent, Netherlands NL-8700679-A, 1987.

[18] Pilling NA, Holmes R, Jones GR. Low-power optical current measurement system employing a hybrid transmitter. In: IEE Proceedings: Science, Measurement and Technology, 1994 (141): 129-134.

[19] Chu BCB, Ning YN, Jackson DA. An optical current comparator for absolute current measurement. Sensors and Actuators: A. Physical, 1993 (37-38): 571-576.

[20] Fowles GR. Introduction to modern optics. New York: Holt, Rinehart & Winston, 1975.

[21] Chen J, Li H, Liu Y, Wang X. A novel optical current transformer based on comparative measurement, 2006, pp. 837-840.

[22] Electric current transformers, International Electrotechnical Commission, 1-10 July (2002).

[23] Kumai T, Nakabayashi H, Hirata Y, Takahashi M, Terai K, Kaminishi T, Uehara K, Ieee I. Field trial of optical current transformer using optical fiber as Faraday sensor.

[24] Liu Y, You S, Lu F, Wan Q. Optical electric current transformer error measuring system based on virtual instrument, 2007, pp. 3278-3282.

[25] Shang Q, Yang Y, Yu W, et al. Test and calibration of optical electric current transformer. Automation of Electric Power Systems (2005)

[26] Microbridge Technologies. Rejustors., Microbridge Technologies, Inc., 1980.

[27] Ward D. Measurement of current using Rogowski coils. In: Instrumentation in the Electrical Supply Industry, IEE Colloquium on, IET, 1993, pp. 1/1-1/3.

[28] U.S. Patent A planar Rogowski current sensor. In: Patent for a planar Rogowski Current Sensor U.S. Patent 6,414,475, 2002.

[29] Tumanski S. Induction coil sensors-A review. Measurement Science and Technology, 2007 (18): R31-R46.

[30] Chattock AP. On a magnetic potentiometer. In: Proceedings of the Physical Society of London, 1886 (9): 23-26.

[31] Rogowski W, Steinhaus W. Die Messung der magnetischen Spannung - Messung des Linienintegrals der magnetischen Feldstärke, Archiv für Elektrotechnik, 1 (1912) 141-150.

[32] Shirkoohi GH, Kontopoulos AS. Computation of magnetic field in Rogowski-Chattock potentiometer (RCP) compensated magnetic testers. Journal of Magnetism and Magnetic Materials, 1994 (133): 587.

[33] Murgatroyd PN, Chu AKY, Richardson GK, West D, Yearley GA, Spencer AJ. Making Rogowski coils. Measurement Science and Technology, 1991 (2): 1218-1219.

[34] Wikipedia, 2010.

[35] Jingsheng L, Xiaohua G, Cheng L, Mingjun Z, Zefu Y. Studies of Rogowski coil current transducer for low amplitude current (100A) measurement. 2003, pp. 463-466.

[36] Koon W., Current sensing for energy metering, Application Engineering. Analog Devices, (2002).

[37] Dickinson R. Using allegro current sensors in current divider configurations for extended measurement range. In: Allegro microsystems and applications, 2005.

[38] Chen K, Chen N. A new method for power current measurement using a coreless Hall effect current transformer. IEEE Transactions on Instrumentation & Measurement, 2011 (): 158-169.

[39] Honeywell, MICRO SWITCH Sensing and Control. Honeywell 1 MICRO SWITCH Sensing and Control, 2010.

[40] Popović RS. Hall effect devices.. Bristol : Institute of Physics, 2004.

[41] Cummings J, Friedrich A. Recent trends in Hall effect current sensing. In: Recent Trends in Hall Effect Current Sensing. Allegro Micro Systems, Inc., 2006.

[42] National Instruments. Shunt resistor current sensor. National Instruments Corporation, 2009.

[43] Johnson CM, Palmer PR. Current measurement using compensated coaxial shunts. IEE Proceedings: Science, Measurement and Technology, 1994 (141): 471-480.

[44] Matthaei GL, Young L. Microwave filters, impedance-matching networks, and coupling structures. Dedham, MA: Artech House, 1980.

[45] Burr Brown Product, Low side and high-side measurement current shunt monitor. Texas Instruments, 1995.

[46] Uchii T, Nishiwaki S, Boggs S. Effects of hot SF 6 on post-arc circuit breaker design. IEEE Transactions on Power Delivery, 2004 (19): 124-130.

[47] Matsumura T, Yokomizu Y, Almiron PC, Yamamoto K, Ohta D, Shibuya M. Breakdown voltage of CO2 at temperatures around 4000 K and in range from 300 to 700 K. IEEJ Transactions on Power and Energy, 2005 (125): 1063-1069.

[48] Bobrow LS. Elementary linear circuit analysis. New York: Rinehart and Winston, 1981.

[49] Donald HWB, Fink G. Standard handbook for electrical engineers, 2000.

[50] Nilsson JW, Riedel SA. Electric circuits. Upper Saddle River, NJ: Pearson/Prentice Hall, 2008.

[51] Air-Liquid. In: Gas encyclopaedias; http://encyclopedia.airliquide.com/encyclopedia.asp. Accessed 26/07/12, 2012.

[52] Flurscheim CH, editor. Power circuit breaker theory and design. Stevenage: Peregrinus for the Institution of Electrical Engineers, 1977.

[53] Reece BS, Eng, C. Physics of circuit breaker arcs. London: Peregrinus, 1982.

[54] Brookes RJ. Exploration of polymer replacements for SF6 in circuit breakers. Liverpool University: PhD Thesis, 2010.

[55] Naidu MS, Kamaraju V. High voltage engineering. New York: McGraw-Hill, 1995.

[56] Rodrigo H. Impulse breakdown of a point-plane gap in SF6 and SF6/N2 mixtures. Liverpool University: PhD Thesis, 1982.

[57] Sölver, C. Electric arcs and arc interruption. Chalmers University of Technology, Götenburg, Sweden, EEK, 2006 (195).

[58] Meek JM, Craggs JD. Electrical breakdown of gases. Oxford: Clarendon Press, 1953.

[59] Kuffel E, Zaengl WS, Kuffel J. High voltage engineering: fundamentals. Oxford: Butterworth-Heinemann, 2000.

[60] Little P. Secondary effects. In: Electron-Emission Gas Discharges I/Elektronen-Emission Gasentladungen I, Springer, 1956: 574-662.

[61] Bouziane A, Hartmann G, Hidaka K, Taplamacioglu M, Waters R. Linear-geometry electric-field probe for DC corona measurements. IEE Proceedings-Science, Measurement and Technology, 1994 (141): 111-117.

[62] Fukuchi T, Yamaguchi Y, Nayuki T, Nemoto K, Uchino K. Development of a laser wavefront sensor for measurement of discharges in air. Electrical Engineering in Japan. 2004 (146): 10-17.

[63] Kumada A, Chiba M, Hidaka K, OkabeS. Residual charge distribution measurement of positive surface streamer with high spatial resolution. In: Papers of Technical Meeting on Electrical Discharges, IEE Japan, 2003, 63-68.

[64] Grundy J. Sinusoidal response of coaxial current shunts. Proceedings of the Institution of Electrical Engineers. 1997 (124): 499-504.

[65] Ono R, Oda T. Dynamics and density estimation of hydroxyl radicals in a pulsed corona discharge. Journal of Physics D: Applied Physics, 2002 (35): 2133.

[66] Ono R, Oda T. Dynamics of ozone and OH radicals generated by pulsed corona discharge in humid-air flow reactor measured by laser spectroscopy, Journal of Applied Physics, 2003 (93): 5876-5882.

[67] Park JH. Journal of Research of the National Bureau of Standards. 191-122.

[68] Silsbee F. Notes on the design of four-terminal resistance standards for alternating current. Bureau of Standards Journal of Research, 1930 (4): 73-83.

[69] Spencer J. Some investigations of the behaviour of a rotating arc discharge. Liverpool University: PhD Thesis, 1987.

[70] M.P.R. Ltd., Power resistor. http://www.mf-powerresistor.com/cement.htm.

71] TE connectivity. In: TE connectivity, Tyco Electronics. www.tycoelectronics.com, 2008.

[72] Tektronix, Oscilloscopes. DPO2000 Series Oscilloscopes, User Manual., 2nd edition, 2004. www.tektronix.com

[73] Tektronix. High voltage probe Tektronix instruction manual, P6015A 1000X (2004).

[74] Hunka G. Typical earth electrode. . University of Pennsylvania, 2010.

[75] Loeb LB. Fundamental processes of electrical discharge in gases. New York: Wiley, 1939.

[76] Blower RW, Reeves EA. Distribution switchgear: Construction, performance, selection and installation. Collins, 1986.

[77] MF Power Resistor Ltd. Power resistor. http://www.mf-powerresistor.com/cement.htm

[78] Clark FM. Insulating materials for design and engineering practice. New York: Wiley, 1962.

[79] National Institute of Standard and Technology (NIST). www.NIST/Chemistry, , 2013.

Appendix A

Let probe 1 output be A ± ạ Volts

And probe 2 output is B ± ḅ Volts, where ạ and ḅ are the error voltage.

Equation 4.1 is used to obtain the voltage difference between Probe 1 and Probe 2 as shown in table A1. Table A1 is used to obtain figure 4.2, figure 4.3 and figure 4.4.

	Recorded voltage		Voltage difference (Q)
Input voltage (kV)	Probe 1 (Output voltage) volt	Probe 2 (Output voltage) volt	(Probe 1- Probe 2) volt
0	1280±80	1200±80	80±113.14
2	1920±80	1840±80	80±113.14
3	2960±40	2720±80	240±113.14
4	3920±80	3780±80	160±89.44
5	4960±40	4640±80	320±89.44
6	5920±40	5600±40	320±56.57
7	6960±40	6560±40	400±113.14
8	7920±80	7520±80	400±113.14
9	8960±40	8480±40	480±56.57
10	9920±80	9360±80	560±89.44
11	10920±80	10320±80	600±113.14
12	11920±80V	11280±80	640±113.14

Table A1 shows probe voltage (V1 and V2) from the Brandenburg HV power supply and voltage difference from both probes at the same point.

For example, to obtain the voltage difference for input voltage at zero output of the Brandenburg is illustrated as follows:

Probe 1- Probe 2 = $Q = (\mathrm{A} \pm \mathrm{a}) - (\mathrm{B} \pm \mathrm{b}) = \mathrm{A} - \mathrm{B} \pm \sqrt{\mathrm{a}^2 + \mathrm{b}^2}$ 4.1

$$Q = (1280 \pm 80) - (1200 \pm 80) = 1280 - 1200 \pm \sqrt{80^2 + 80^2}$$

$$Q = 80 \pm 113.4\mathrm{V}$$

Appendix B

In order to normalize the voltage drop from probe 1 and 2 at the same potential, a correction factor was determined. The value of the correction factor k is obtained from the linear trend line equation from figure 5.2 (sub-section 5.1.1) and as presented in equation 5.1 below. The voltage difference between probe 1 and 2 is drawn as against the input voltage V_1 as presented in the tableA1 (appendix A) and in figure 5.2. The example below illustrates how the correction factor k and leakage current I_2 were obtained.

$$k = 0.0532V_1 - 12.52 \qquad 5.1$$

From table 5.1B, the input voltage V_1 equal to -6204.78V is obtained.

Therefore, k is calculated as:

$$k = 0.0532(-6204.78) - 12.52 = -3422.61V$$

where k is the voltage difference between probe 1 and 2 probe at atmospheric dry air of input voltage of -6204.78V. The k value is added to the output voltage value V2 as to correct the voltage difference between both probes and presented in the tables (5.1B, 5.2B and 5.3B).

The leakage current I_2 is determined for 0 bar pressure as illustrated below.

$$I_2 = \frac{\Delta V}{R_L} = \frac{V_1 - V_2}{R_L} = \frac{(-6204.780 - -6209.81)V}{58400\Omega} = \frac{5.03\text{V}}{58400\Omega} = 0.086mA$$

Tables 5.1B, 5.2B and 5.B presents the data obtained in various pressure ranges in bars, probe voltage 1 (input V_1) and probe voltage 2 (output V_2) and the leakage current in milliamperes while the result is shown in figure 5.4.

Pressure	Probe voltage		Voltage difference	Probe current
(bar)	Input V1(V)	Output V2(V)	V_1-V_2	ΔV/R (mA)
0	-6252.5	-6263.9	11.47	0.196
0.5	-6402.7	-6405.3	2.58	0.0442
1	-7532.4	-7573.9	41.48	0.71
1.5	-8479.9	-8506.6	26.72	0.46
2	-9656.2	-9686	29.81	0.5104

Table 5.1B

Pressure	Probe voltage		Voltage difference	Probe current
(bar)	Input V1(V)	Input V1(V)	V_1-V_2	ΔV/R (mA)
0	-6204.8	-6209.8	5.03	0.086
0.5	-6395.6	-6378	-17.62	-0.31
1	-7431.7	-7453.6	21.88	0.375
1.5	-8389.8	-8394.9	5.12	0.0877
2	-9670.2	-9677.5	7.25	0.124

Table 5.2B

Pressure	Probe voltage		Voltage difference	Probe current
bar	Input V1 (V)	Output V2(V)	V1-V2	ΔV/R (mA
0	-6268.15	-6270.1	1.95	0.033
0.5	-6466.1	-6438.6	-27.48	-0.471
1	-7504	-7533.8	29.75	0.509
1.5	-8466.2	-8472.5	6.3	0.108
2	-9670.2	-9677	6.71	0.115

Table 5.3B

The below figures (1B, 2B, 3B, 4B and 5B) shows typical graphs of probe voltage and probe current versus time determined at various pressures in dry air when the high voltage is set at no dielectric breakdown while figure 6B and 7B shows a typical results of probe voltage (input V1 and output V2) from the limiting resistor (from table 5.1B) and results of leakage current variation with rise in pressure in dry air (from tables 5.1B, 5.2B and 5.3B).

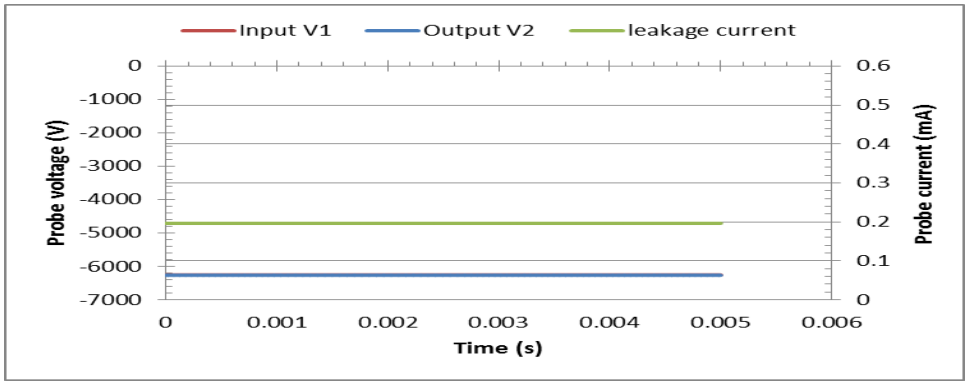

Figure 1B in atmospheric pressure of dry air.

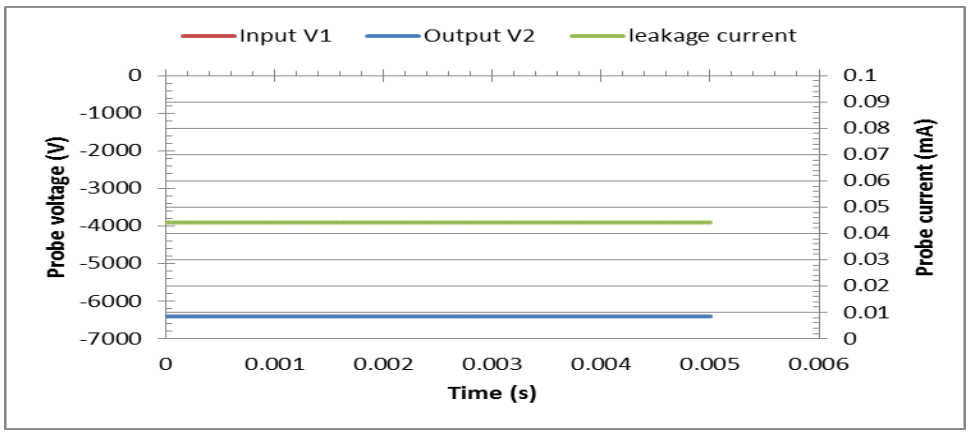

Figure 2B in 0.5bar of dry air

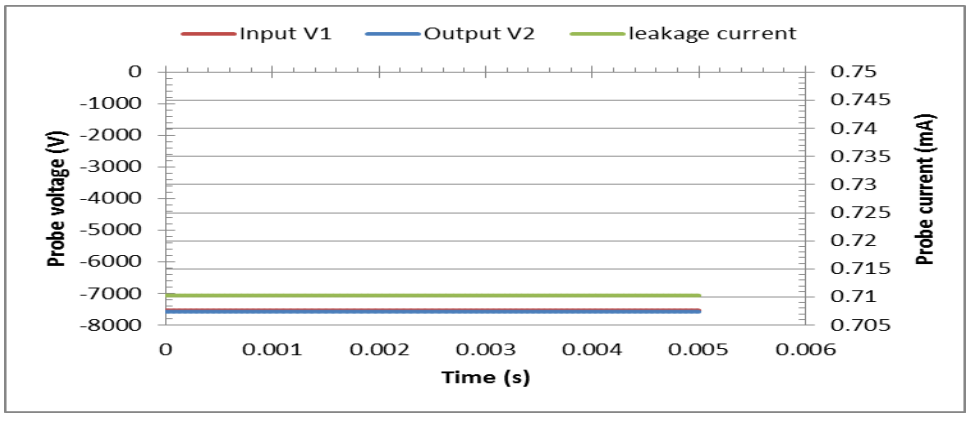

Figure 3B in 1.0bar of dry air

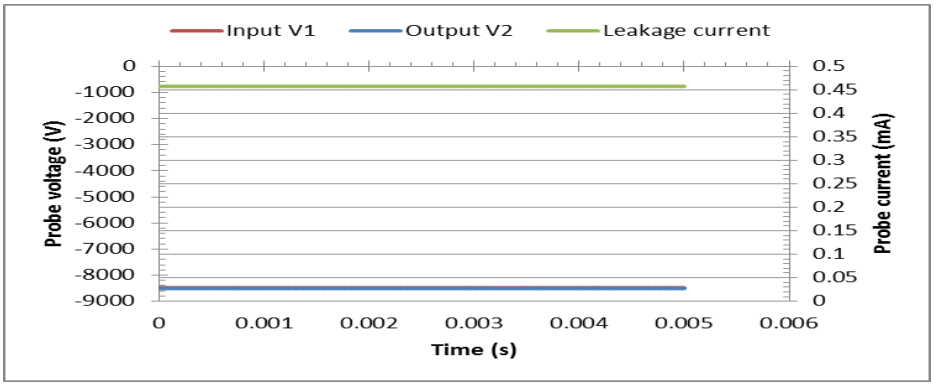

Figure 4B in 1.5bar of dry air

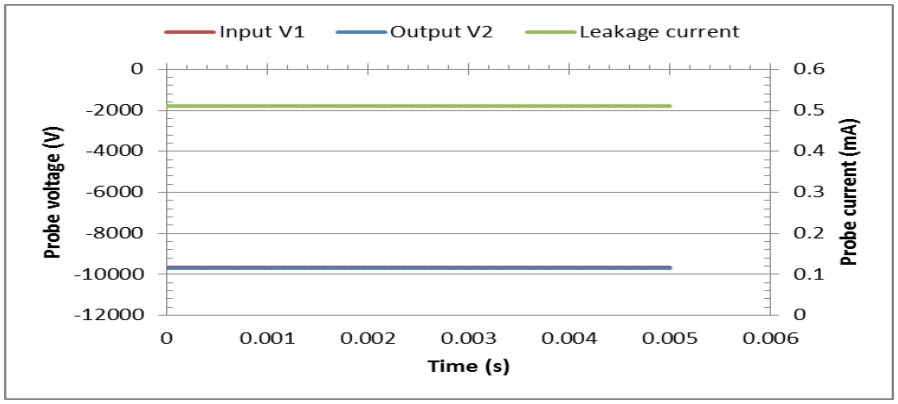

Figure 5B in 2.0bar of dry air

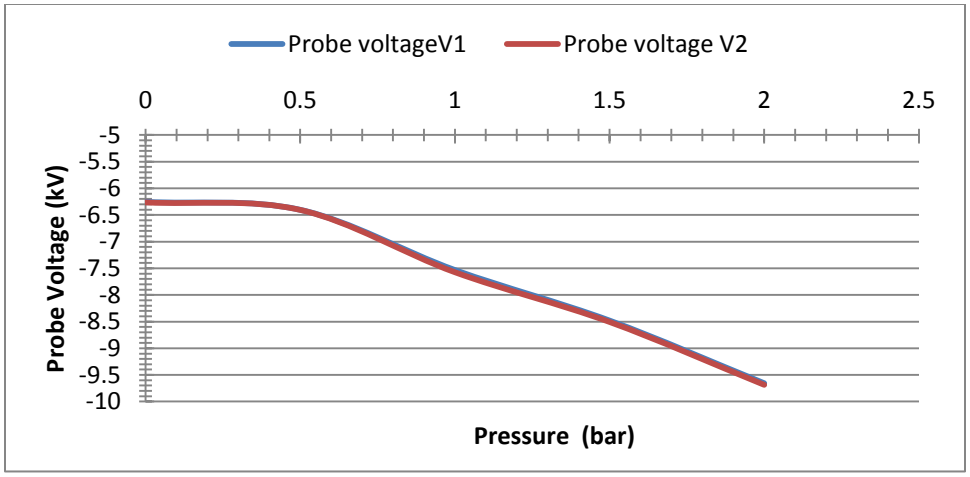

Fig 6B shows typical result of probe voltage (input V1 and output V2) from the limiting resistor in dry air.

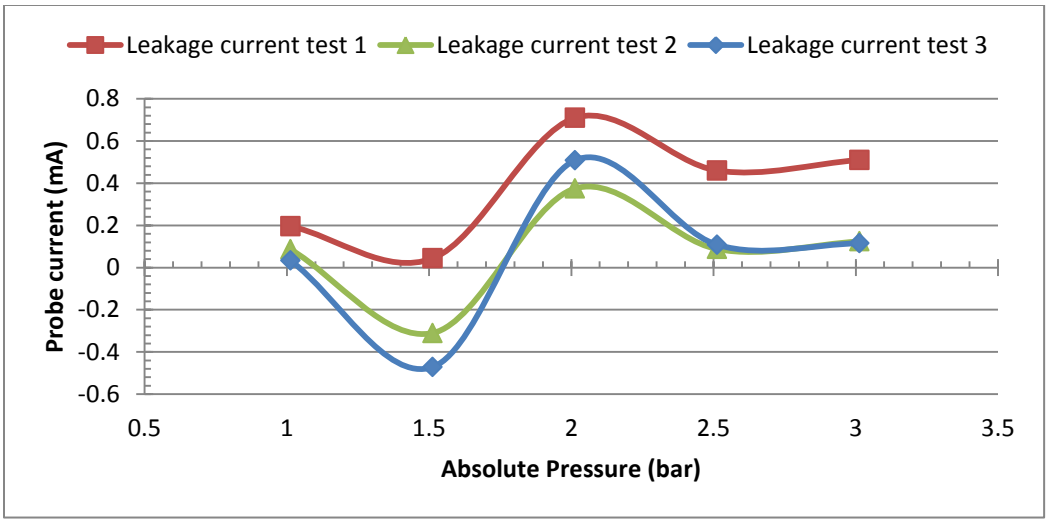

Fig 7B shows variation in leakage current in dry air at atmospheric pressure (table 4.1)